

HYGROTHERMAL EFFECTS ON CFRP: TESTING, ANALYSIS AND STRUCTURAL OPTIMIZATION

Lorena Marín Hernández

Per citar o enllaçar aquest document:
Para citar o enlazar este documento:
Use this url to cite or link to this publication:
<http://hdl.handle.net/10803/398412>



<http://creativecommons.org/licenses/by-nc-nd/4.0/deed.ca>

Aquesta obra està subjecta a una llicència Creative Commons Reconeixement-
NoComercial-SenseObraDerivada

Esta obra está bajo una licencia Creative Commons Reconocimiento-NoComercial-
SinObraDerivada

This work is licensed under a Creative Commons Attribution-NonCommercial-
NoDerivatives licence

Doctoral Thesis

Hygrothermal effects on CFRP testing, analysis and structural optimization

Lorena Marín Hernández



Escola Politècnica Superior
Dept. d'Enginyeria Mecànica i de la Construcció Industrial

Doctoral Thesis

Hygrothermal effects on CFRP testing, analysis and structural optimization

Lorena Marín Hernández

2015

Doctoral Program in Technology

Advisor:

Dr. Daniel Trias Mansilla

Universitat de Girona, Spain

Thesis submitted for the degree of Doctor by University of Girona

Lorena Marín Hernández

Hygrothermal effects on CFRP: testing, analysis and structural optimization

Doctoral Thesis, 2015

Doctoral Program in Technology

Advisor: Dr. Daniel Trias Mansilla

Universitat de Girona

Escola Politècnica Superior

Dept. d'Enginyeria Mecànica i de la Construcció Industrial

AMADE Research Group

Campus Montilivi s/n

17071 Girona

A mis padres,
Arsenio y M^aAntonia
y a mi marido, Emilio

“

Caminante, son tus huellas
el camino y nada más;
caminante no hay camino,
se hace camino al andar.

A. Machado
Campos de Castilla, Soria

Acknowledgements

agradecimientos

'...son tus huellas el camino...'

A lo largo de la vida, todo paso es importante pero las huellas que nos deje el camino serán lo que nos forme en lo que somos en cada instante.

Éste es otro paso nuevo en mi andadura y, por ello, quisiera empezar por el principio del camino, expresando mi gratitud a quienes me han acompañado en cada paso desde el gateo, mis padres y hermanos, que siempre me han apoyado, a menudo desde la distancia pero con la cercanía que les caracteriza.

A aquellos que un día me acogieron en tierras extrañas con una pila de libros amenazantes a mi llegada: gracias Joan Andreu y Dani. Quizá no recordéis aquel día como yo pero vuestro entusiasmo hizo que tomase la decisión de emprender este viaje. Eso dejó una gran huella.

Durante unos meses tuve la oportunidad de realizar una estancia de investigación. Me gustaría agradecer a Pedro por acogerme al otro lado del Duero y a Giussepe por su humor y su paciencia para entendernos.

Al runner, o biker, (en todos los sentidos) del grupo, Pere M. que hace fácil lo difícil, casi rodado (aunque le falte un poco de mano alzada arquitectónica). Y a mis compañeros de AMADE, los grandes y pequeños runners, que han hecho más ameno cada paso, sobre todo, cuando parece que van hacia atrás. En especial, a Carlos y a Piedra, a dos pasos de mí, aunque a veces parezcan zancadas... gracias por acompañarme (hasta las tantas y tantos cafés con brownie).

Y, por último, al que da los pasos junto a mí desde hace un tiempo, Emilio, quien con su dualidad paciencia-impaciencia me ha apoyado y ayudado en cada pequeño gran paso.

Gracias a todos por estos años. Estas páginas significarán muy poco en el *todo* científico, pero para mí ha supuesto mucho más que eso.

Para aquellos que leen estas líneas y están comenzando esta andadura (o cualquier otra), os dejo con ese último y sencillo verso de Machado:

'... se hace camino al andar'

The work contained in this Ph.D. thesis was conducted in the AMADE research group (Department of Mechanical Engineering and Industrial Construction, University of Girona, Spain). The thesis was carried out under the grant BES-2010-042387 from the FPI program from the Spanish *Ministerio de Economía y Competitividad* and is within the framework of the EVISER2 (*Ensayo Virtual y Supervisión Estructural de Revestimientos de CFRP*) under the code DPI2009-08048.

Part of the research presented in this thesis was developed during the Ph.D. candidate's stay at the Universidade do Porto, which was funded by the Spanish *Ministerio de Economía y Competitividad* through the grant EEBB-I-13-06186.

Publications

The present Ph.D. thesis has been prepared as a compendium of peer-reviewed journal papers, according to the regulations of Universitat de Girona. The thesis is comprised of the following three papers:

- L. Marín, D. Trias, P.Badalló, G. Rus, J. A. Mayugo. Optimization of composite stiffened panels under mechanical and hygrothermal loads using neural networks and genetic algorithms. *Composites Structures* 2012; 94(11):3321-6.
doi:10.1016/j.compstruct.2012.04.024
ISSN: 0263-8223, Impact factor: 2.231, ranked 4/24 in category *Materials science, composites* (1st quartile) ¹.
- L. Marín, E. V. González, P.Maimí, D. Trias, P.P.Camanho. Hygrothermal effects on the translaminar fracture toughness of cross-ply carbon/epoxy laminates with: failure mechanisms. *Submitted to Composite Science and Technology*; 2015.
ISSN: 0266-3538, Impact factor: 3.633, ranked 1/24 in category *Mechanics* (1st quartile) ².
- L. Marín, D. Trias, P.Maimí, E. V. González, G. Catalanotti. Hygrothermal effects on the fracture toughness of quasi-isotropic carbon/epoxy laminates. *Submitted to Composites Part A-Applied Science and Manufacturing*; 2015.
ISSN: 1359-835X, Impact factor: 3.071, ranked 2/24 in category *Engineering, Manufacturing* and 4/24 in category *Materials science, composites* (1st quartile) ².

¹ According to the 2012 Journal Citation Reports

² According to the 2014 Journal Citation Reports

Other publications that have been derived from this thesis but are not included in this document are listed below:

Journal articles

- P. Badalló, D. Trias, L. Marín, J. A. Mayugo. A comparative study of genetic algorithms for the multi-objective optimization of composite stringers under compression loads. *Composites Part B: Engineering* 2012; 47:130-136.
doi:10.1016/j.compositesb.2012.10.037
ISSN: 1359-8368, Impact factor: 2.602, ranked 5/24 in category *Materials science, composites* and 5/83 in category *Engineering, Multidisciplinary* (1st quartile) ¹.
- Yi Liv, G. Guillet, E. V. González, L. Marín, J. Costa, J. A. Mayugo. Experimental study into compression after impact strength of tailored non-conventional laminates. *Submitted to Composites Part A-Applied Science and Manufacturing*; 2015.
ISSN: 1359-835X, Impact factor: 3.071, ranked 2/24 in category *Engineering, Manufacturing* and 4/24 in category *Materials science, composites* (1st quartile) ².

Publications without external review

- L. Marín, D. Trias, G. Rus, P. Badalló, E. Martín. Optimización de paneles rigidizados de materiales compuestos sometidos a cargas termomecánicas. *Actas del IX Congreso Nacional de Materiales Compuestos 2011*; 663-668.
ISBN: 978-84-8458-352-3.
- P. Badalló, D. Trias, L. Marín, J.A. Mayugo. Comparación de algoritmos genéticos en rigidizadores de material compuesto sometidos a cargas de compresión. *Actas del IX Congreso Nacional de Materiales Compuestos 2011*; 675-678.
ISBN: 978-84-8458-352-3.

¹ According to the 2013 *Journal Citation Reports*

² According to the 2014 *Journal Citation Reports*

- E. Martin, P. Maimí, A. Turon, E.V. González, L. Marín. Generación de modelos de elementos finitos parametrizados de probetas con agujero descubierto. Actas del IX Congreso Nacional de Materiales Compuestos 2011; 625-630.
ISBN: 978-84-8458-352-3
- G. Guillamet, Y. Liv, A. Turon, L. Marín, E.V. González, J.A. Mayugo, J. Costa. Design of non-conventional CFRP laminates for improved damage resistance and damage tolerance. 16th European Conference on Composite Materials, ECCM 2014.
ISBN: 978-000000000-2.
- L. Marín, D. Trias, P. Maimí, E.V. González, G. Guillamet. Efectos higrotérmicos en la tenacidad intra y trans laminar. Actas del XI Congreso Nacional de Materiales Compuestos 2015; 1159-648.
ISBN: 978-84-697-0406-6.

Attended Conferences

- L. Marín, D. Trias, G. Rus, P. Badalló, E. Martin. Optimización de paneles rigidizados de materiales compuestos sometidos a cargas termomecánicas. IX Congreso Nacional de Materiales Compuestos, 2011. Girona (Spain).
National Conference. Oral presentation.
- P. Badalló, D. Trias, L. Marín, J.A. Mayugo. Comparación de algoritmos genéticos en rigidizadores de material compuesto sometidos a cargas de compresión. IX Congreso Nacional de Materiales Compuestos, 2011. Girona (Spain).
National Conference. Poster.
- E. Martin, P. Maimí, A. Turon, E.V. González, L. Marín. Generación de modelos de elementos finitos parametrizados de probetas con agujero descubierto. IX Congreso Nacional de Materiales Compuestos, 2011. Girona (Spain).
National Conference. Poster

- L. Marín, D. Trias, P.Badalló, G. Rus, J. A. Mayugo. Optimization of composite stiffened panels under mechanical and hygrothermal loads using neural networks and genetic algorithms. SAMPE Student Conference, 2012. Paris (France).
International Conference. Oral presentation.
- L. Marín, D. Trias, P.Badalló, J.A. Mayugo. On how tough testing toughness can be: fracture toughness of quasi-isotropic carbon/epoxy laminates. 17th International Conference on Composite Structures (ICCS17), 2013. Porto (Portugal).
International Conference. Oral presentation.
- G. Guillaumet, Y. Liv, A. Turon, L. Marín, E.V. González, J.A. Mayugo, J. Costa. Design of non-conventional CFRP laminates for improved damage resistance and damage tolerance. 16th European Conference on Composite Materials, ECCM 2014. Sevilla (Spain).
International Conference. Oral presentation.
- L. Marín, D. Trias, P.Maimí, E.V. González, G. Guillaumet. Efectos higrotérmicos en la tenacidad intra y translaminar. XI Congreso Nacional de Materiales Compuestos, 2015. Móstoles-Madrid (Spain).
National Conference. Oral presentation.



Dr. Daniel Trias Mansilla, Associate Professor at University of Girona,

hereby CERTIFY that

The work entitled *Hygrothermal effects on CFRP: testing, analysis and structural optimization*, submitted for the doctoral degree by Lorena Marín Hernández, has been conducted under his supervision and that it fulfills the requirements to aim for the *International Mention*.

Girona, September 2015.

Daniel Trias Mansilla
Universitat de Girona, Spain

List of Figures

FIGURE 1.1	10
SEM fractography of poor matrix/fiber adhesion [34]	
FIGURE 1.2	11
SEM image with a broom-like tension failure of a GFRP laminate [46]	
FIGURE 1.3	12
SEM micrographs of the fracture surface of dry specimens: (a) the fracture surface (x30); (b) the slow crack growth zone (x200); (c) the fast crack growth zone (x200); (d) the rapid crack growth zone (x400) [52]	
FIGURE 1.4	12
SEM micrographs of the fracture surface of wet specimens: (a) the fracture surface (x30); (b) the slow crack growth zone (x400); (c) the fast crack growth zone (x100); (d) the rapid crack growth zone (x400) [52]	
FIGURE 1.5	14
SEM inspection for delamination failure with moisture and temperature [21]	
FIGURE 1.6	15
Effect of high temperature on static mode II toughness of a carbon/epoxy material [56]	

LIST OF FIGURES

FIGURE 1.7	17
Terms related to failure modes from the literature	
FIGURE 1.8	18
Planes of fracture. Definition of intralaminar, interlaminar and translaminar failures	
FIGURE 1.9	19
Failure mechanism comparison [75]	
FIGURE 1.10	20
CT specimen with a T800S/M21 quasi-isotropic laminate [82] (a) C-Scan inspection with compression failure at the back part of the $[(90/45/0/-45)_2]_s$ laminate, (b) C-San inspection for $[90_2/45_2/0_2/-45_2]_s$ laminate, (c) buckling of the $[90_2/45_2/0_2/-45_2]_s$ laminate. Test performed by the PhD candidate	
FIGURE 1.11	21
Micro-cuts drill along the crack path by laser system [70], where the desired fracture is described by bundles of fibers	
FIGURE 1.12	21
SEM inspection of the highest-energy failure pattern studied by Bullegas et al. [70]	
FIGURE 1.13	22
Failure modes for T-shape stiffened panels [88]: (1) delamination failure in the laminate at the skin-stiffener junction, (2) failure in the stiffener blade, (3) failure between skin and stringer and (4) failure at core	
FIGURE 1.14	24
Topology optimization of a fuselage [95]	

LIST OF FIGURES

FIGURE 1.15 Geometric design variables	25
FIGURE 2.1 Stiffened panel (dimensions in mm)	39
FIGURE 2.2 Optimization scheme	44
FIGURE 2.3 Neural Network scheme	46
FIGURE 2.4 Comparison between reference and optimal panels	49
FIGURE 3.1 Ultimate and nominal stress-size	61
FIGURE 3.2 Linear regression II of the CP laminate for each conditioning	63
FIGURE 3.3 Fiber R-curve comparison for CP laminate	63
FIGURE 3.4 Size effects graphics for CP laminate	64
FIGURE 3.5 SEM fractography comparison between the three conditionings	66
FIGURE 3.6 SEM fractography explanation between the three conditionings	67

LIST OF FIGURES

FIGURE 3.7	70
Comparison of failure mechanisms for each conditioning	
FIGURE 4.1	83
Ultimate and nominal stress-size for QI laminates	
FIGURE 4.2	84
Delamination damage mechanism in L2-CV-PC and L4-nCV laminates	
FIGURE 4.3	85
Linear regression II of the L1-CV laminate for each conditioning	
FIGURE 4.4	85
R-curve comparison for the L1-CV laminate	
FIGURE 4.5	86
Size effects charts for L1-CV laminate	
FIGURE 4.6	88
SEM fractography comparison between the three conditionings of L1-CV laminate	
FIGURE 4.7	90
Longitudinal section of a laminate under tension with the presence of a matrix crack	

List of Tables

TABLE 1.1	5
Glass transition temperature (T_g), elastic properties and strength under hydrothermal effect on the literature	
TABLE 1.2	6
Fracture toughness properties under hydrothermal effect on the literature	
TABLE 1.3	27
Classification of optimization of mono-stiffened panels	
TABLE 1.4	28
Classification of optimization of multi-stiffened panels	
TABLE 2.1	39
T800/M21 UD CFRP properties [135]	
TABLE 2.2	40
Geometric variables domain	
TABLE 2.3	42
Loading conditions for each subproblem	

LIST OF TABLES

TABLE 2.4	48
Objectives and constraints values by each subproblem	
TABLE 2.5	49
Objectives and constraints values by each subproblem	
TABLE 3.1	57
T800S/M21 UD CFRP properties	
TABLE 3.2	58
Specimen geometry	
TABLE 3.3	61
Laminate properties	
TABLE 4.1	79
T800S/M21 mismatch angles	
TABLE 4.2	82
Properties for QI laminates and each conditioning	

Contents

| Abstract

1 | CHAPTER 1 Introduction

1.1	Background	1
1.1.1	Governing laws and physical phenomena	7
1.1.2	Translaminar fracture toughness	16
1.1.3	Stiffened panels	22
1.2	Motivation	29
1.3	Objectives	30
1.4	Thesis structure	30

I | OPTIMIZATION OF COMPOSITE STIFFENED PANELS UNDER MECHANICAL AND HYGROTHERMAL LOADS

2 | CHAPTER 2 Optimization of composite stiffened panels

2.1	Introduction	36
2.2	Definition of the multi-objective problem	38
2.2.1	Stiffened panel design	38

CONTENTS

2.2.2	Model of the panel: finite element modeling	40
2.2.3	Definition of subproblems	42
2.2.4	Formulation of the multi-objective opt. problem	43
2.3	Optimization procedure	43
2.3.1	Model of the panel: neural network modeling	44
2.3.2	Genetic algorithm	46
2.4	Results and discussion	47
2.5	Conclusions	50

II HYGROTHERMAL EFFECTS ON THE TRANSLAMINAR FRACTURE TOUGHNESS

3

CHAPTER 3

Hygrothermal effects on the translaminar fracture toughness: CP laminates

3.1	Introduction	54
3.2	Material, hygrothermal conditions and test set-up	56
3.2.1	Hygrothermal conditions	58
3.2.2	Fractography	59
3.3	Data reduction and results	59
3.3.1	DEN-T test and data reduction	59
3.3.2	R-curve results	60
3.3.3	Fractography	64

3.4	Discussion	68
3.4.1	Fractography	68
3.4.2	Characterization of translaminar failure mechanisms	71
3.5	Conclusions	72

4

CHAPTER 4

Hygrothermal effects on the translaminar fracture toughness: QI laminates

4.1	Introduction	76
4.2	Material, test set-up and hygrothermal conditions	78
4.2.1	Material and stacking sequences	78
4.2.2	Hygrothermal conditioning	79
4.2.3	Fractography	80
4.3	Data reduction and results	80
4.3.1	DEN-T tests and data reduction	80
4.3.2	R-curve	82
4.3.3	Fractography	87
4.4	Discussion	89
4.4.1	Influence of ply clustering	89
4.4.2	Fractography	91
4.4.3	Cross-ply and quasi-isotropic laminates comparison	92
4.5	Conclusions	93

CONTENTS

III CONCLUDING REMARKS

5 | CHAPTER 5 Conclusions

5.1	Optimization of stiffened panels	97
5.2	Translaminar fracture toughness	98
5.3	General conclusions	101

6 | CHAPTER 6 Suggestions for future research

6.1	Translaminar fracture toughness characterization	103
6.2	Constitutive model for FE simulations	105
6.3	Stiffened panels	105

IV BIBLIOGRAPHY

| Bibliography

V APPENDICES

A | APPENDIX A Published paper

Abstract

Structural aircraft components are expected to be exposed to a wide range of changes in the environmental conditions during their service. In the common design and certification process, a large number of experimental tests, going from simple small specimens to the full structure, are performed. In these tests, all the environmental conditions, especially temperature and humidity, which the structural component will be submitted are considered. This multiplies the number of tests to be performed. With the aim of reducing the economic cost and the time needed for the design and the certification of components, numerical tools that allow a reduction of experimental tests and help in the analysis of results, are developed. In this framework, the present doctoral thesis tackles the topic of hygrothermal effects in composite materials in both fields: experimental tests and numerical tools. Specifically, the thesis focuses its attention on two analysis levels which are seldom present in the scientific literature: the optimization of structural components considering environmental changes and the experimental characterization of the translaminar failure of the material under different environmental conditions.

With respect to the structural components, an optimization methodology for stiffened panels is presented. This methodology is based on genetic algorithms and uses a neural network as a metamodel. The proposed methodology is able to find the optimal panel geometry, for a set of different environmental changes together with mechanical loads, in a short time.

On the other hand, the experimental characterization with hygrothermal effects is considered for the translaminar toughness. A test campaign is performed using the Double Edge Notched Tensile specimen. The broken specimens are observed by means of Scanning Electron Microscopy in order to analyse how temperature and moisture effects influence the failure mechanisms. The general conclusion is that the quality of the fibre/matrix interface plays a key role in the translaminar toughness since it is linked to failure mechanisms such as constituent debonding and fiber pull-out. With moisture, a slight weakening of the fiber/matrix interface and small fiber pull-out are produced but humidity reduces the friction coefficient between constituents, which reduces the amount of energy needed to produce slippage between fiber and matrix and, consequently, the material toughness. Conversely, elevated temperature and humidity cause a weakening in the interface in a way that in the failure process a large number of long fiber pull outs are produced, which dissipate an important amount of energy. In this way, translaminar fracture toughness is slightly reduced because of humidity but its value grows under high humidity and temperature conditions.

Resumen

Los elementos estructurales de aeronaves se ven sometidos a una gran diversidad de cambios en las condiciones ambientales durante su servicio. En el proceso habitual de diseño y certificación de componentes aeronáuticos se realiza un elevado número de ensayos experimentales que van desde pequeñas probetas hasta la estructura final. En estos ensayos se consideran también las condiciones ambientales, especialmente temperatura y humedad, a las que el componente se verá sometido, hecho que multiplica el número de ensayos a realizar. Con el propósito de disminuir el elevado coste y el tiempo de diseño y certificación de los componentes se desarrollan herramientas numéricas que permiten substituir parte de los ensayos en laboratorio y facilitan el análisis de resultados. En este ámbito, la presente tesis enfoca la problemática de la consideración de los efectos ambientales tanto en los ensayos de laboratorio como en el desarrollo de herramientas numéricas. Concretamente, la tesis se centra en dos niveles de análisis con escasa o nula presencia en la literatura científica sobre efectos higrotérmicos: optimización de elementos estructurales considerando cambios ambientales y la caracterización experimental del fallo translaminar del material en diferentes condiciones ambientales.

Con respecto a los elementos estructurales, se presenta una metodología de optimización de paneles rigidizados, basada en algoritmos genéticos y que usa una red neuronal como metamodelo. La metodología utilizada propuesta es capaz de obtener la geometría óptima del panel, para un conjunto de situaciones ambientales distintas junto con cargas mecánicas, en un tiempo reducido.

En cuanto a la caracterización experimental con efectos higrotérmicos, la tesis se centra en la tenacidad a la fractura translaminar. Se lleva a cabo una campaña de ensayos basados en la probeta *Double Edge Notched Tensile*. Una vez ensayadas, el plano de rotura de las probetas es observado mediante microscopía electrónica de rastreo, realizando un análisis sobre cómo varían los mecanismos de fallo a causa de la temperatura y la humedad. Se concluye que la calidad de la intercara matriz/fibra juega un papel crucial en la tenacidad translaminar, ya que está ligada a mecanismos de fallo como la separación entre constituyentes y el *pull-out* de la fibra. La humedad provoca cierto debilitamiento en la intercara matriz/fibra lo que conduce a una rotura con pequeños *pull-outs* pero, a su vez, reduce el coeficiente de fricción entre fibra y matriz, hecho que reduce la energía necesaria para producir el deslizamiento fibra/matriz y en consecuencia, la tenacidad del material. En cambio, en presencia de humedad y temperatura elevadas, la intercara se debilita considerablemente de manera

que en el plano de rotura se producen numerosos *pull-out* de longitud importante que disipan elevada cantidad de energía. De esta manera, la tenacidad translaminar del material se reduce ligeramente en presencia de humedad, pero en cambio aumenta notablemente en presencia de humedad y temperatura elevadas.

Resum

Els elements estructurals de les aereoaus es veuen sotmesos a una gran diversitat de canvis en les condicions ambientals durant el seu servei. En el procés habitual de disseny i certificació de components aeronàutics es realitza un elevat nombre d'assaigs experimentals que van de petites provetes fins a l'estructura final. En aquests assaigs es consideren també les condicions ambientals (temperatura i humitat) a les que el component es veurà sotmès, fet que multiplica el nombre d'assaigs a realitzar. Per tal de disminuir l'alt cost econòmic i el temps de desenvolupament de components que implica aquesta campanya experimental, s'intenta produir eines computacionals que permeten substituir part dels assaigs a laboratori i faciliten l'anàlisi de resultats. En aquest àmbit, la present tesi enfoca la problemàtica de la consideració dels condicions ambientals tant en els assaigs a laboratori com en el desenvolupament d'eines computacionals. Concretament, la tesi es centra en dos nivells d'anàlisi amb poca o nul·la presència en la literatura científica sobre efectes higrotèrmics: optimització d'elements estructurals considerant canvis ambientals i la caracterització experimental de la fallada translaminar del material a diferents condicions ambientals.

Pel que fa als elements estructurals, es presenta una metodologia per a l'optimització de panells rigiditzats, basada en algorismes genètics i que usa una xarxa neuronal com a metamodel. La metodologia proposada es capaç d'obtenir la geometria òptima del panell per a un conjunt de situacions ambientals diferents juntament amb càrregues mecàniques, en un temps reduït.

Quant a la caracterització experimental amb efectes higrotèrmics, la tesi es centra en la tenacitat translaminar. En el treball es duu a terme una campanya d'assaigs en diferents condicions de temperatura i humitat usant el procediment basat en la proveta *Double Edge Notched Tensile*. En les provetes trencades s'observen els mecanismes de fallada que es donen en aquest tipus de fractura emprant microscòpia electrònica de rastreig i s'analitza com varien aquests mecanismes a causa de la temperatura i humitat. Es conclou que la qualitat de la intercara matriu/fibra juga un paper crucial en la tenacitat translaminar, ja que està lligada a mecanismes de fallada com la separació entre constituents i el *pull-out* de la fibra. La humitat redueix el coeficient de freg entre fibra i matriu, fet que redueix l'energia requerida per produir el lliscament fibra/matriu i conseqüentment, la tenacitat del material. En canvi, en presència d'humitat i temperatura elevades la intercara es debilita considerablement de manera que, en el moment de la fallada, es produeixen nombrosos *pull-out* de longitud important que dissipen molta energia. D'aquesta manera, la tenacitat del material es redueix lleugerament en presència d'humitat, però en canvi augmenta notablement en presència d'humitat i temperatura elevades.

1 | Introduction

1.1 Background

Technological advances are allowing to use the knowledge acquired from the behavior of natural materials into the design of structural components which nowadays can be manufactured with advanced (composite) materials. An understandable example of these natural or traditional materials is the structure of a tree, which is made up of cellulose fibers and lignite matrix. The main advantage of these natural materials is that the shape of the structure is able to adapt itself the mechanical loads given by both the environmental conditions, such as the wind actions. The fibers bear the loads while the lignite transfers the stresses and binds the fibers together. The resulting material from two or more constituents or phases such as cellulose-lignite is known as composite material. Generally, the combination of two or more constituents produces better mechanical properties than its mere individual components. The macroscale material properties will depend not only on the nature of its constituents, but also on the geometry and the behavior of the interface between them.

The industry has achieved an evolution of these materials by improving the material properties through the analysis of the geometry and the composition of each material. For instance, from using the mud bricks (straw-clay) to reinforced concrete (steel-concrete), where the brittleness of the concrete is improved by adding steel.

Composite materials are usually classified according to the reinforcement geometry or to the matrix material. Related to the geometry of the reinforcement, composites can

be reinforced by long continuous fibers, short fibers or particles. In addition, related to the matrix material, three sets of materials can be found: materials composed by Polymeric Matrix Composites (PMC), Metal Matrix Composites (MMC) and Ceramic Matrix Composites (CMC). On the other hand, when long fibers are used to reinforce PMC, the composite is known as Fiber Reinforced Plastic (FRP), using, for instance, Glass fibers (GFRP) or carbon fibers (CFRP). They are often fabricated in the form of laminates, i.e. a combination of thin plies stacked together with a suitable fiber orientation in order to achieve the mechanical design requirements.

CFRP components offer higher strength-to-weight and stiffness-to-weight ratios than metallic ones, thereby their use in aerospace industry is increasing, mainly because of the capacity of producing lightweight structures.

The increasing use of these materials in elements with higher structural responsibility requires thick laminates, so one of the concerns of the aeronautical industry is how these composite materials are affected by changes in the environmental conditions. Some structural components of a plane can be subjected to high temperatures and humidity in the take-off phase and, minutes later, to below-zero temperature in regular flight conditions. In spite of that, environmental conditions have been seldom considered in the optimization of structural design neither on thin nor thicker laminates and generally buckling is the main type of analysis considered.

Although some analytical approaches of simple structures are possible, the optimization of composite structures is generally based on the use of Finite Element (FE) codes. When a composite material is modeled in a FE code, a considerable number of material properties are required. For example, to model a composite ply at the mesoscale level, commonly considered as a transversally isotropic material, the elastic properties required are: longitudinal (E_{xx}) and transverse (E_{yy}) elastic moduli at tension ($E_{xx,T}$ and $E_{yy,T}$) and compression ($E_{xx,C}$ and $E_{yy,C}$); shear elastic modulus (G_{xy}); Poisson's coefficients (out-of-plane ν_{yz} and in-plane ν_{xy}); longitudinal and transverse strengths at tension and compression (X_T and X_C , Y_T and Y_C) and longitudinal in-plane shear strength (S_L). Concerning the fracture toughness properties in order to simulate delamination, the required properties are, at least: mode I ($G_{c,I}^{del}$), mode II ($G_{c,II}^{del}$) and mixed-mode ($G_{c,I,II}^{del}$) fracture energies. Finally, other fracture properties are the longitudinal

tensile fracture energy ($\mathcal{G}_c^{X_T}$) and the longitudinal compression fracture energy ($\mathcal{G}_c^{X_C}$). The thorough characterization of all these properties is essential to design composite structures and so most of these properties can be obtained following standards.

It is worth noting that some of the commented properties are strongly affected by environmental conditions. To illustrate that, Tables 1.1 and 1.2 present the values of some properties found from the literature, which have been obtained considering moisture and/or temperature conditions. In these tables, matrix-dominant properties, as $E_{yy,T}$, $E_{yy,C}$, Y_C , Y_T and S_L , suffer a decrease with moisture [1–4], temperature [5] and the combination of both [5, 6], whereas the fiber-dominant properties such as $E_{xx,C}$ and $E_{xx,T}$ are generally stable [2, 4]. $E_{xx,C}$ and $E_{xx,T}$ would only change when temperature is near the glass transition temperature, T_g .

As X_T is also a fiber-dominant property, it suffers a decrease in the case of GFRP [3]. However, for CFRP is not clear because the variation is very small and depends on the kind of matrix [4], increasing for the regular matrix and decreasing for the tougher matrix. This is due to the fact that carbon fibers do not absorb moisture and have a very small negative Coefficient of Thermal Expansion (CTE) in their longitudinal direction. However, matrix has high Coefficient of Moisture Expansion (CME) and CTE [7, 8], so the moisture absorption capacity and the expansion at high temperature are very large in comparison with those of carbon fibers [9]. Therefore, some types of matrix can slightly influence fiber-dominant properties as well.

Regarding the interlaminar fracture toughness, moisture and temperature have influence in all the propagation modes. It is specially relevant the increment with both moisture and high temperature for $\mathcal{G}_{c,I}^{del}$ [10–12]. This phenomenon can be explained by means of the plasticity of the matrix, which causes a tougher behavior.

Nevertheless, from the authors knowledge, there are no experimental data available in the scientific literature under hygrothermal conditions concerning the $\mathcal{G}_c^{X_T}$. Only a brief fractography description of failure mechanisms through Four-Point Bend Test specimens is presented in [13]. In this study, it is relevant the evidences of fiber pull-out with less resin under WET/HOT conditions close to T_g .

The lack of experimental data in this field is probably related to the fact that there are only a standardized Single-Edge-Notched (SEN) specimen configuration for composite

Chapter 1 Introduction

materials [14, 15] and standardized Compact Tension (CT) for metals. SEN only covers fracture energy determination for damage initiation and the specimen configuration proposed recently [16–19] showed larger fracture process zone. Moreover, $G_c^{X_T}$ has usually been considered a fiber-dominant property, so the environment conditions were thought not to have a relevant influence on these properties. However, as it was observed in [13], the matrix-dominant properties and matrix/fiber interface properties could be damaged by environment and this could have a significant influence on the translaminar behavior significantly. In addition, if matrix/fiber interface properties are relevant for translaminar fracture, moisture could affect considerably its behavior since moisture exploits the capillaries of the interface, besides the cracks and voids, to get in the composite.

The achievement of good mechanical properties in a composite material depends crucially upon the efficiency of stress transfer between fibers through the matrix, which requires a proper adhesion of the constituents. In order to gain an understanding of how hygrothermal conditions can affect composite structures, a study about what these conditions are and an analysis about the behavior of these materials from the microscale level have to be carried out.

ref	Material	Type	Conditioning ¹	Elastic properties							Strengths					T_g [°C]
				$E_{res,T}$ [GPa]	$E_{res,C}$ [GPa]	ν_{xy} [-]	$E_{yp,T}$ [GPa]	$E_{yp,C}$ [GPa]	G_{xy} [GPa]	X_T [MPa]	X_C [MPa]	Y_T [MPa]	Y_C [MPa]	S_L [MPa]		
[1]	CF ² /5228	UD	AR/RT	-	-	-	-	-	-	-	-	-	-	-	-	97.9
			WET (0.99% water)/RT	-	-	-	-	-	-	-	-	-	-	-	-	87.5
[5]	CF/EP ³	UD	AR/HOT(60°)	-	-	-	-	-	-	-	-	-	-	-	-	108
			WET(1.3% water)/HOT(60°)	-	-	-	-	-	-	-	-	-	-	-	-	92
			AR/HOT(70°)	-	-	-	-	-	-	-	-	-	-	-	-	109
			WET(1.3% water)/HOT(70°)	-	-	-	-	-	-	-	-	-	-	-	-	79
[20]	CF/EP	UD	DRY/-	-	-	-	-	-	-	-	-	-	-	-	-	209
			WET(1% water)/-	-	-	-	-	-	-	-	-	-	-	-	-	176
			WET(1.7% water)/-	-	-	-	-	-	-	-	-	-	-	-	-	160
[2]	GL ⁴ /EP	UD-QI	AR/RT	49.7	-	0.25	22.0	-	6.28	1212	-	54.8	-	84	-	-
			WET(0.53% water)/RT	50.7	-	0.27	19.8	-	6.02	1162	-	48.5	-	79.6	-	-
			WET(0.87% water)/RT	47.5	-	0.26	14.8	-	5.42	762	-	36.4	-	52.7	-	-
			WET(1.46% water)/RT	51.4	-	0.26	13.4	-	4.68	474	-	26.7	-	43.1	-	-
[3]	CF/EP	UD [0/0] _s	AR/RT	-	-	-	-	-	-	-	-	-	-	-	-	84.5
			WET(1.8% water)/RT	-	-	-	-	-	-	-	-	-	-	-	-	60.8
			AR/RT	-	-	-	-	-	-	-	-	-	-	-	-	66.4
			WET(1.4% water)/RT	-	-	-	-	-	-	-	-	-	-	-	-	49.6
[6]	IM7/8552	UD	AR/RT	-	-	-	-	-	-	-	-	-	-	-	-	-
			WET(1.4% water)/RT	-	-	-	-	-	-	-	-	-	-	-	-	-
			AR/HOT(35°)	-	-	-	-	-	-	-	-	-	-	-	-	-
			WET(0.4% water)/HOT(35°)	-	-	-	-	-	-	-	-	-	-	-	-	-
[4]	CF/EP ⁵	UD	DRY/-	-	-	-	-	-	-	-	-	-	-	-	-	258
			WET/-	-	-	-	-	-	-	-	-	-	-	-	-	220
			DRY/RT	152	80	-	11	22	-	1600	1870	51	297	-	-	-
			WET(1% water)/RT	155	83	-	8.5	12	-	1670	1400	21	210	-	-	-
[4]	CF/EP ⁶	UD	DRY/-	-	-	-	-	-	-	-	-	-	-	-	-	197
			WET/-	-	-	-	-	-	-	-	-	-	-	-	-	120
			DRY/RT	149	83	-	10	22	-	1900	1510	71	230	-	-	-
			WET(1% water)/RT	149	83	-	8	15	-	1850	1010	21.5	150	-	-	-

Table 1.1: Glass transition temperature (T_g), elastic properties and strength under hygrothermal effect on the literature.

1 Humidity conditioning at equilibrium state/temperature during test.
 2 CF: carbon fiber. Unspecified nomenclature.
 3 EP: epoxy. Unspecified nomenclature.
 4 GL: glass fiber. Unspecified nomenclature.
 5 First generation matrix
 6 Tougher matrix than *

ref	Material	Type	Conditioning ¹	Interlaminar fract. toughness [J/m ²]			Test method	T _g [°C]
				G _{c,I} ^{del}	G _{c,I} ^{del}	G _{c,I,II} ^{del}		
[10]	T300/934	UD [0] ₁₆	DRY/RT	103	-	-	DCB ²	-
			WET(0.56%water)/RT	106	-	-	DCB	-
			WET(2.1%water)/RT	129	-	-	DCB	-
			DRY/RT	103	-	-	DCB	-
			DRY/HOT(127°)	121	-	-	DCB	-
[11]	AS 3501-6	UD	DRY/RT	121	-	-	DCB	-
			WET(1.5%water)/RT	138	-	-	DCB	-
			DRY/RT	-	272	-	CLS ³	-
			WET/RT	-	239	-	CLS	-
			DRY/RT	130	322	-	DCB/CLS	-
[12]	HTA/6376C	UD [0] ₁₂ / [(±5/0) ₁] _s]	DRY/RT	152	297	-	DCB/CLS	-
			DRY/RT	149	181	-	DCB/CLS	-
			WET/RT	152	149	-	DCB/CLS	-
			DRY/COLD(-50°)	251.1	997.5	517.5	DCB/ENF ⁴ /MMB ⁴	-
			DRY/RT	229.4	883.1	452	DCB/ENF/MMB	-
[21]	T300/M10	UD	DRY/HOT(100°)	263.5	701.8	514.5	DCB/ENF/MMB	-
			WET/COLD(-50°)	243.9	586.6	445.6	DCB/ENF/MMB	-
			WET/RT	248.3	698.4	425.4	DCB/ENF/MMB	-
			WET/HOT(100°)	313.7	375.1	397.8	DCB/ENF/MMB	-
			DRY/HOT(90°)	-	413.3	-	ENF	222
[21]	T300/M10	UD	WET(0.94%water)/HOT(90°)	-	427.4	-	ENF	165
			WETsaturated(2.53%water)/HOT(90°)	-	390.8	-	ENF	129
			DRY/HOT(90°)	-	931.3	-	ENF	141
			WET(0.74%water)/HOT(90°)	-	770.6	-	ENF	118
			WETsaturated(2.02%water)/HOT(90°)	-	578.6	-	ENF	-

Table 1.2: Fracture toughness properties under hygrothermal effect on the literature. From the author knowledge, there are no data for translaminar fracture toughness under hygrothermal effects.

- 1 Humidity conditioning at equilibrium state/temperature during test
- 2 Double Cantilever Beam test
- 3 Cracked-Lap-Shear test
- 4 End Notched Flexure test
- 5 Mixed-Mode Bending test

1.1.1 Governing laws and physical phenomena

The heterogeneity of polymer-based composite materials generates the usual but complex failure mechanisms, with an interaction of several damage modes (delamination, matrix microcracking, debonding and fiber breakage). The way, the sequence of apparition and the interaction of these mechanisms could be modified by the influence of the hydrothermal effects. Most polymeric materials can absorb relatively small moisture content from the surrounding environment along the service life of the structure. However, this is a continuous process, which can lead to substantial effects on the material properties.

The uptake of moisture is usually measured by weight gain, Eq. (1.1):

$$M = \frac{W_i - W_0}{W_0} 100(\%) \quad (1.1)$$

where W_i [g] and W_0 [g] are the initial (*as-received* or dry condition) and the post-absorption specimen mass, respectively.

The physical mechanism for moisture gain is often assumed to be mass diffusion, following Fick's Law [20, 22, 23] (Eq. 1.2), which was firstly proposed in 1855 [24] and then confirmed by Whitaker et al. [25] for neat epoxy and carbon/epoxy composites (some polymers have a non-Ficklian behavior [26]):

$$\frac{\partial c}{\partial t} = D_z \frac{\partial^2 c}{\partial z^2} \quad (1.2)$$

being c the moisture content [ML^{-3}]¹, t is the time [T], z is the point (at the thickness or the length) [L]. D_z is the moisture diffusivity constant [L^2T^{-1}], which is a material property that describes the rate at which the material absorbs/desorbs moisture, and is defined as [23]:

$$D_z = \pi \left(\frac{h}{4M} \right)^2 \left(\frac{M_2 - M_1}{\sqrt{t_2} - \sqrt{t_1}} \right)^2 \quad (1.3)$$

¹[M]: unit of mass, [T]: unit of time, [L]: unit of length

where h is the specimen thickness [L], M is the effective moisture equilibrium content [M] (see Eq. 1.1), M_2 and M_1 [M] allow to describe the slope of moisture absorption and t_1 and t_2 [T] are respectively the initial and final time of a portion of the time curve.

The Fick's Law equation is useful to determine the strain due to the moisture and the moisture content until achieving the equilibrium state for a given moisture exposure level, normally expressed by the Relative Humidity (RH). For a determined RH, the moisture content increases gradually with the time until an *effective* equilibrium, established when the variation of the moisture content is smaller than 0.01% in a determined t_2-t_1 time period [23]. If this equilibrium state has been achieved, the higher the RH is, higher moisture content will be. The *effective* equilibrium moisture content can change slightly; only when moisture content requires no measurable change, the moisture equilibrium is *absolute*. In the same way, moisture saturation content is defined as the moisture equilibrium content at the maximum possible moisture exposure level [23], 100% of RH, normally achieved by immersion.

Temperature may affect moisture absorption in polymers. Diffusion is a thermally activated process and its temperature dependence is defined by the Arrhenius exponential relation with inverse absolute temperature [27–29]:

$$D_z = \frac{D_0}{e^{E_A/(kT)}} \quad (1.4)$$

in which E_A is the activation energy of diffusion, D_0 the pre-exponential factor, T is the absolute temperature (°K) and k is the Boltzmann constant.

The moisture flow through-the-thickness occurs relatively slowly, so the temperature influence (from 10° to 85°C) is normally used in experimental tests to accelerate the uptake of moisture inside a climatic chamber [23] and to achieve the equilibrium state for a given RH in a reduced time. Only when the moisture equilibrium content is reached, the local moisture content is uniform through-the-thickness of the specimen [30].

This process causes: dimensional changes known as *swelling* (measured by CME), a plasticizer effect of the matrix [30, 31], a decrease of the T_g of the polymer and the composite [20, 30], and reduces the matrix and matrix/fiber interface dependent mechanical properties of the composite [30]. Moreover, moisture can also penetrate into

the polymeric by the capillary process [32]. The microcracks act as capillary channels for moisture with a faster process [32] than diffusion and swelling and plasticity mechanisms can increase the capillarity in polymeric composites [33].

Consequently, the material service temperature or Material Operation Limit (MOL), which is normally established as equivalent to T_g [30], decreases. This effect is usually reversible when water is desorbed and temperature is below T_g , but an interaction with high temperature can cause irreversible effects, due to a chemical degradation of the matrix and a weakening of the matrix/fiber interface [30, 31, 34]. This phenomenon causes an increment of voids and microcracks into the polymer matrix and this is one of the reasons why hot-wet conditioning is recommended to evaluate as the worst-case effects of moisture content [30]. To determine a cold MOL, the moisture conditioning is not required below room temperature, being -55°C the coldest design service temperature generally considered [30]. However, it is worth noting for a given moisture content, under negative temperature, water freezes and expands in the solidification process and thus increases internal strains [35], which generates new cracks.

Therefore, in addition to the areas rich in resin, moisture exploits microcracks, voids and the capillaries of the material [34, 36], being the matrix/fiber interface and the surfaces between plies or structural elements the most sensitive paths for penetrating into the material. Consequently, these regions become weakened by moisture presence and they are strongly weakened by the combination of high temperature and moisture.

In composite materials, residual stresses are caused during manufacturing process but damage due to initial thermal residual stresses by the shrinkage of the matrix is rarely observed [37]. Therefore, capillarity occurs when water gets into the material along the matrix/fiber interface by intermolecular forces between the liquid and the surfaces. On the other hand, hygrothermal stresses induced by the mismatch CTE and CME of each constituent, are mainly located at the matrix/fiber interface. Swelling is a reversible effect, but a significant swelling could cause cracks, which is, of course, irreversible.

Constituent level

In a constituent level (microscale), fibers practically do not absorb moisture and matrix has a high capacity of absorption (it can be five times higher than that of fibers [9]).

Chapter 1 Introduction

And concerning the temperature effects, there is a large mismatch between both constituents (carbon fibers have a negative CTE), so this effect may contribute to increase or reduce the internal stresses [38]. During the manufacturing process, which depends on the type of matrix and fibers [7], residual stresses are generated between matrix and fibers. For instance, following the Hexcel manufacturer recommendations [39], for an epoxy resin, a curing process of 120 minutes at 180° has to be applied for curing a panel with a thickness smaller than 15 mm. After the curing process, there is a cooling down process until room temperature, when the residual stresses take place. These stresses can be reduced by swelling during the moisture absorption process or by dilatation during a positive temperature variation. By contrast, they increase with a drying process or a negative temperature variation.

These effects can trigger or increase the lack of adhesion between constituents and the apparition of failure mechanisms such as debonding or fiber pull-out, which were studied without considering the hygrothermal effects around the 90s [40–43].

A good tool to observe and to understand the physical mechanisms of composite materials and the influence of the environment, is fractography analysis. As an example, Fig. 1.1 shows two Scanning Electronic Microscope (SEM) images of a poor matrix/fiber adhesion, with bare fibers (1.1(a)) or the imprints of the fibers on the matrix surface (1.1(b)) [34].

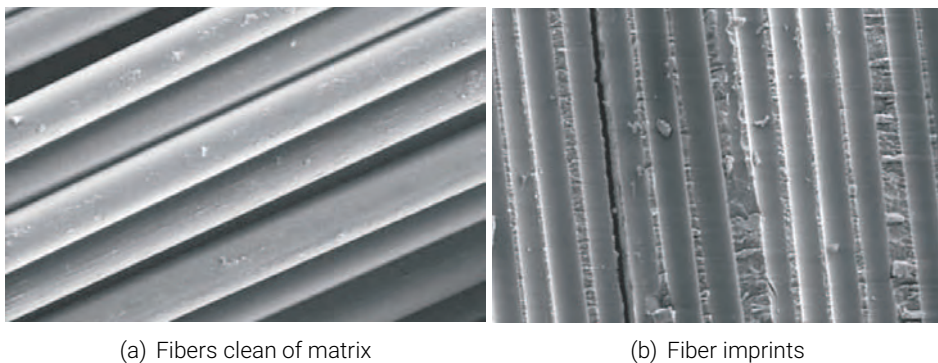


Figure 1.1: SEM fractography of poor matrix/fiber adhesion [34].

In a longitudinal tensile failure, a very weak matrix/fiber interface can increase the fiber debonding before fiber failure occurs and can cause long fiber pull-outs, as shown in Fig. 1.2. Therefore *broom-like* failures and the lack of matrix on the surface of the fibers is commonly a general characteristic of a weak matrix/fiber adhesion [44, 45].



Figure 1.2: SEM image with a broom-like tension failure of a GFRP laminate [46].

Regarding the matrix constituent (transverse tensile failure), normally epoxy has been mostly used for polymer composites because of the high elastic modulus and its good behavior under thermal conditions [38]. The main drawback of epoxy resin is the poor resistance to crack propagation, which leads a small absorption of energy during fracture [47]. In order to improve this, modified epoxy resin are being studied for commercially available materials [48]. The most recurrent methods involve the use of rubber-modified epoxy [48, 49] or thermoplastic particles on the matrix and on the surfaces of the plies [50], which improve the interfacial adhesion and produces a tougher matrix with a slight reduction of the elastic modulus and T_g [51]. In fractography inspections, this rubbery behavior can be showed by small wrinkles, which will have more presence with moisture content. Lin and Chen [52] performed an experimental comparison with dry (Fig. 1.3) and wet (Fig. 1.4) epoxy specimens. In addition, to the clear increment of these wrinkles, they obtained different behavior from a slow to a fast propagation of the crack.

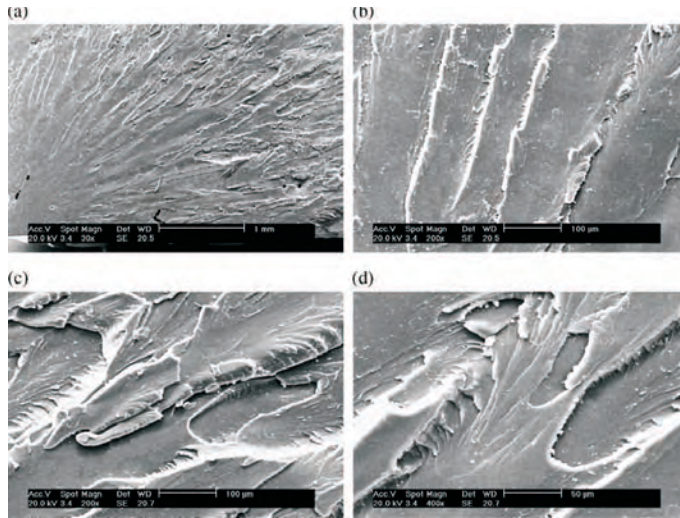


Figure 1.3: SEM micrographs of the fracture surface of dry specimens: (a) the fracture surface (x30); (b) the slow crack growth zone (x200); (c) the fast crack growth zone (x200); (d) the rapid crack growth zone (x400) [52].

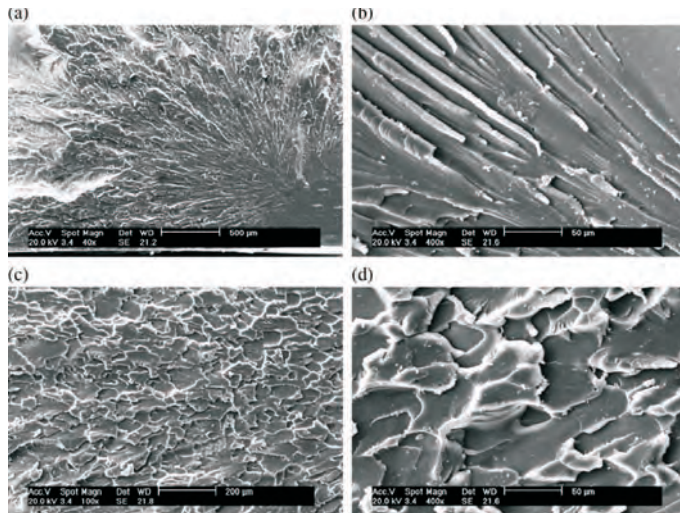
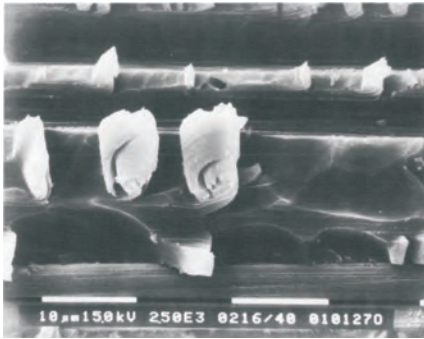


Figure 1.4: SEM micrographs of the fracture surface of wet specimens: (a) the fracture surface (x30); (b) the slow crack growth zone (x400); (c) the fast crack growth zone (x100); (d) the rapid crack growth zone (x400) [52].

Laminate level

In a laminate level (mesoscale), the residual stresses between plies will depend on the orientation and the thickness of each ply due to the mismatch in CTE between longitudinal and transverse direction of a unidirectional ply [53]. The effect of residual stresses is visually appreciated with non-symmetric layups because the thermal and chemical expansion mismatch, between plies with different angle, leads to curvature development. These out-of-plane strains are compensated in symmetric laminates [54], but internal residual stresses keep existing.

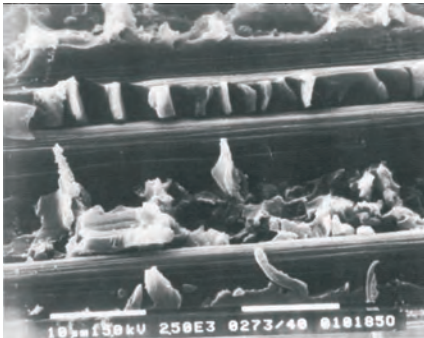
Ogi et al. [55] determined that both moisture and high temperature relax the residual stresses between plies. However, moisture increases the critical stresses for transverse cracking and delamination but with high temperature these stresses decrease. This comparison could be justified by a plasticity of the matrix with moisture content, which is possible to analyze with fractography image taken between plies. In this field, a study of hygrothermal effects on mode II delamination was developed by Zhao and Gaedke [21], using SEM inspections. Two different moisture contents at equilibrium state were chosen with high temperature for two carbon/epoxy composites, T300/M10 and T300/914C, the latter with a better modified matrix/fiber adhesion. Fig. 1.5 and Table 1.2 depict the effect of moisture on interlaminar toughness for different values of the moisture content. For the first material, $\mathcal{G}_{c,II}^{del}$ decreases with moisture content in spite of increasing the toughness with the plasticity of the matrix, which indicates a gradual deterioration of the quality of the matrix/fiber interface. For the second material, the middle moisture content shows a higher delamination toughness, while at the highest moisture content, it presents the lowest toughness. This can be explained by an interfacial strength high enough to resist the crack propagation because of the quality of the interface, shown in Fig. 1.5(c) and 1.5(d). On the other hand, a study of high temperature effect, without moisture, was developed by Greenhalgh and Singh [56]. In Fig. 1.6, an increment of bare fibers is shown, resulting in a reduction of $\mathcal{G}_{c,II}^{del}$.



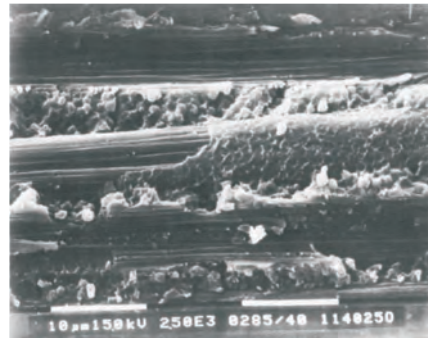
(a) Mode II delamination in dry specimen of T300/M21. Moisture content is 0%



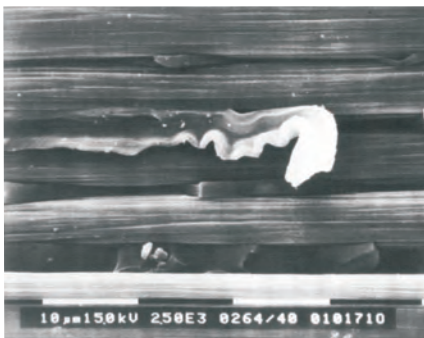
(b) Mode II delamination in wet specimen of T300/M21. Moisture content is 0%



(c) Mode II delamination in wet specimen of T300/M21. Moisture content is 0.74%



(d) Mode II delamination in dry specimen of T300/914C. Moisture content is 0.94%



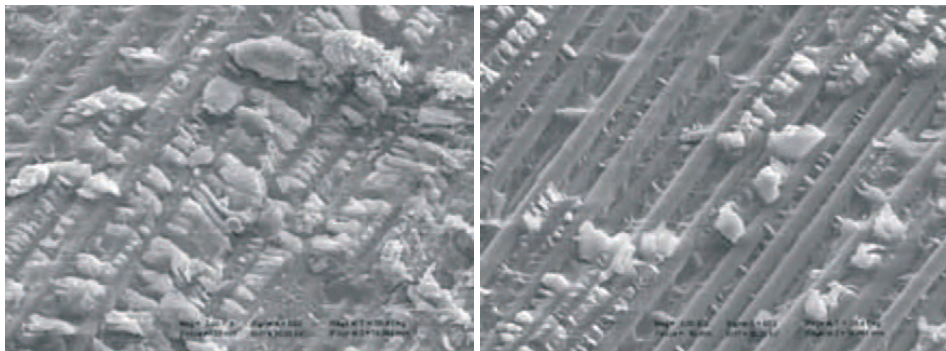
(e) Mode II delamination in wet specimen of T300/914C. Moisture content is 2.02%



(f) Mode II delamination in wet specimen of T300/914C. Moisture content is 2.53%

Figure 1.5: SEM inspection for delamination failure with moisture and temperature [21].

On the other hand, the performance of a multidirectional laminate under hygrothermal loads is strongly dependent on its stacking sequence [57]. Moisture could reduce the thermal residual stresses and the diffusion process could be slowed by the multidirectionality of the lay-up. However, the mismatch angle between plies and the ply thickness affect the residual stresses, so the hygrothermal loads could have special influence for larger mismatch angle and thicker plies.



(a) SEM fractography at room temperature

(b) SEM fractography at 100°

Figure 1.6: Effect of high temperature on static mode II toughness of a carbon/epoxy material [56].

Structural level

In a substructural or structural element level (macroscale), for the author's knowledge in the scientific literature there are no published studies about hygrothermal effects on the laminate composite structures such as stiffened panels. A common process is the strategy for structural design, known as *building block approach*, which analyzes these effects at each level from the selection of the material and stacking sequences to the structural component.

However, composite joints can be affected by hygrothermal conditions and these effects depend on the residual stresses caused during the manufacturing process. A joint can be manufactured by using adhesive bonds or by co-curing process [58]. In the case of composite joints bonded with adhesive, the presence of moisture could weaken

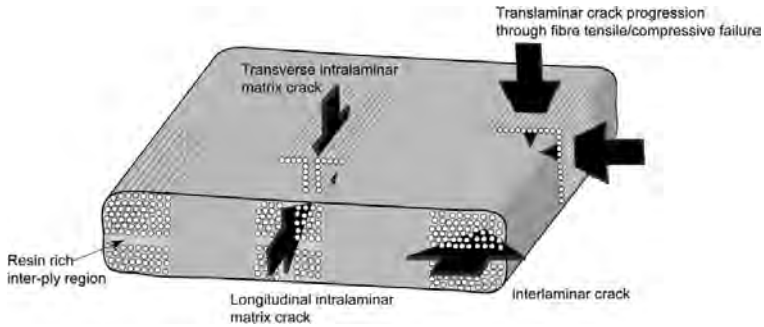
the physical and chemical properties of the adhesive and the interface between adhesive and surface [59]. The process can be performed at elevated temperature (one-part epoxies cure) or at room temperature (two-part epoxies cure), which can be accelerated with temperature. The advantage of curing at room temperature is the no existence of residual stresses between elements. The MOL depends not only on the characteristic of the composite, but also on the adhesive, so the service temperature is from -40°C to $100/180^{\circ}\text{C}$ and combinations between high-temperature adhesives with low-temperature adhesives increase the range from -55°C to 200°C [60]. In both cases, adhesives or co-curing processes, the interlaminar stresses between the joined elements should be analyzed. Further relevance should have the hygrothermal effects when other kind of 3D-reinforcements are used [61, 62], such as a thread (glass, aramid or carbon) for stitching or tufting [63], and stiff carbon fiber rod in the case of Z-pins [64], which produces an improvement in the behavior of the joint but allows the moisture absorption through the new voids.

Therefore, the matrix/fiber interface, the interface between plies and the surfaces between structural elements are the more affected zones by the hygrothermal effects and, however, they have not been considered in optimization of stiffened panels nor in the analysis of the translaminar fracture. A wider description about prior work related to these issues is given below in the following subsections.

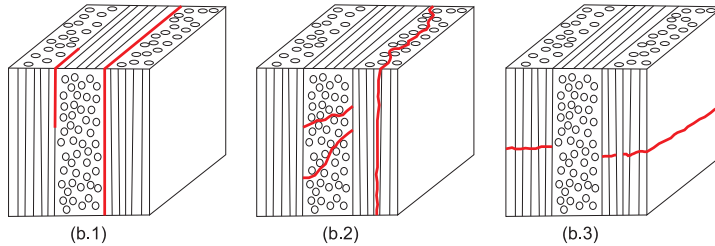
1.1.2 Translaminar fracture toughness

The failure of a laminate is governed by one or a combination of ply-level failure mechanisms, initially defined as [65] (see Fig. 1.7(a)):

- Translaminar crack progression through fiber tensile/compression failure.
- Transverse/longitudinal intralaminar matrix crack.
- Interlaminar crack. Failure occurs between plies.



(a) Ply-level failure modes [65].



(b) Planes of fracture: (1) interlaminar fracture (2) intralaminar fracture (3) translaminar fracture (after [66])

Figure 1.7: Terms related to failure modes from the literature.

This description is in accordance with the definition given by Kessler [66] (Fig. 1.7(b)), where remarks the difference of the dominance of matrix failure for inter/intralaminar fracture surfaces. By contrast, the so-called *translaminar fracture* is governed by fiber failure.

According to the ASTM E1922 [14] in a laminate-level, the fracture toughness of the laminate is known as translaminar. However, in the existent literature, this definition is not clear. Some authors define the intralaminar fracture as the combination of any failure *inside* the laminate (e. g. [16, 67]). Other authors assume the dominance of the fiber fracture referring the term translaminar fracture as the combination of any failure *through* the laminate (e. g. [34, 68–73]).

To unify these terms, along the present document, translaminar fracture is considered as the failure of the laminate caused by the combination of any failure through the laminate with a fiber-dominant failure. Consequently, the main terminology for a multidirectional or unidirectional laminate is stated as follows (see Fig. 1.8):

- Translaminar fracture of the laminate, which depends on the stacking sequence or the architecture of the laminate. It combines matrix, fiber and matrix/fiber interface failures.
- Translaminar fracture of plies at 0° , which occurs in a perpendicular plane to the fibers and is mainly affected by fiber breakage and fiber pull-out. It is equivalent to the translaminar fracture toughness studied in [68–72].
- Transverse/longitudinal intralaminar fracture along the fiber, which refers to a matrix-dominant failure and/or a matrix/fiber interface failure.
- Interlaminar fracture, which refers to failure between plies.

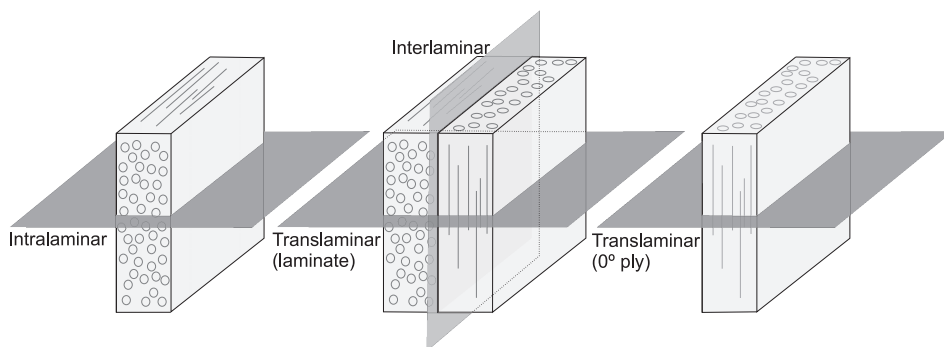
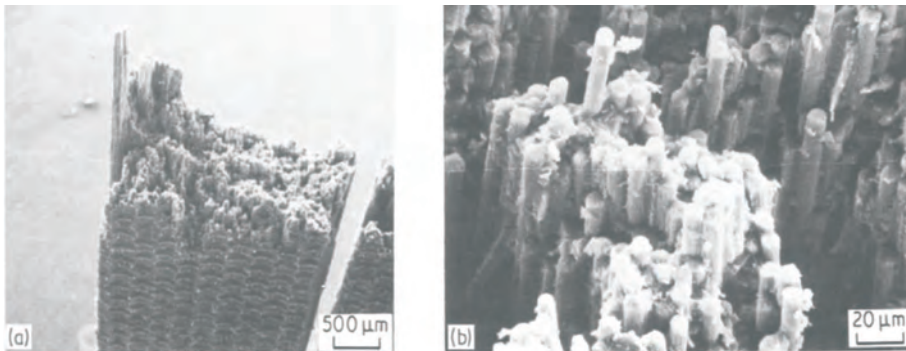


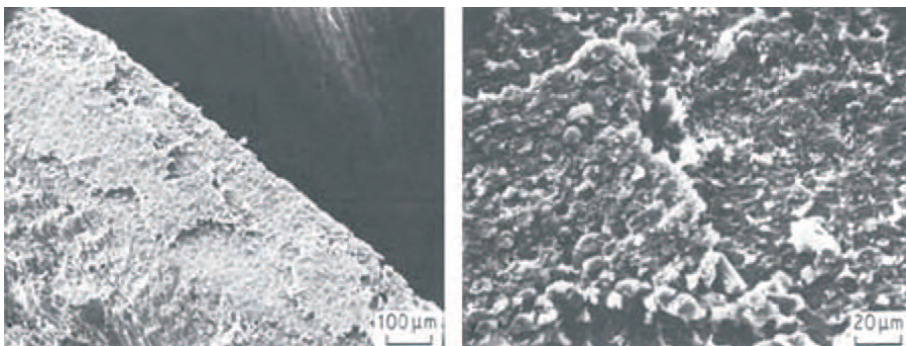
Figure 1.8: Planes of fracture. Definition of intralaminar, interlaminar and translaminar failures.

The translaminar fracture toughness can be obtained by the critical Energy Release Rate (cERR) [74], $\mathcal{G}_{c,I}^{X_T}$, also known as fracture energy, associated to translaminar fracture. Consequently, the translaminar cERR, or fracture toughness, is the energy required to fracture the material in a perpendicular plane to the loading direction. The dissipated energy is the result of the combination of complex failure mechanisms such as the fiber

breakage, matrix cracking, fiber pull-out and debonding, among which the fiber breakage is the most dissipative damage mechanism. However, the breakage in bundles of fibers and fiber pull-outs may contribute to alter the value of the fracture toughness as well. Clements [75] and Greenhalgh [34] described these two failure mechanisms as high-energy failure morphology (see Fig. 1.9(a)), while the failure characterized by a compact bundle of fibers (see Fig. 1.9(b)) is described as a low-energy failure morphology.



(a) Failure mechanism with high energy dissipated: breakage in bundles of fibers (left) and fiber pull-outs (right) [75].



(b) Failure mechanism with low energy dissipated: breakage in compact bundle of fibers [34, 75].

Figure 1.9: Failure mechanism comparison [75].

Chapter 1 Introduction

These morphologies are directly related to the quality of the matrix/fiber interface [76], which may be affected by the environmental conditions. Therefore, a detailed study accounting the exposure environmental conditions should be performed.

Although there is a standardized test to obtain the cERR [14], the proposed data reduction does not consider the orthotropy of the laminate. Therefore, the cERR of a wide range of laminates should not be obtained by this method [65]. In this field, the different specimens considered to obtain this property are explained in [65]. Compact Tension (CT) [19, 68, 69, 77], Over-Height Compact Tension (OCT) [78–80] and Double Edge Notched Tensile (DEN-T) [16] specimens are being the specimens more frequently used in recent works. CT and OCT have been successfully used for materials with not very high fracture toughness. However, for a tougher material, these specimens presented buckling or compression failures at the back part of the specimens [81, 82] (see Fig. 1.10). Catalanotti et al. [16] obtained the fracture toughness by using DEN-T specimens with a methodology based on size effect law [83–85], which is able to consider a wider range of material orthotropies. The goodness of [16] is that these undesirable failures of CT tests are avoided, although the fracture is unstable.

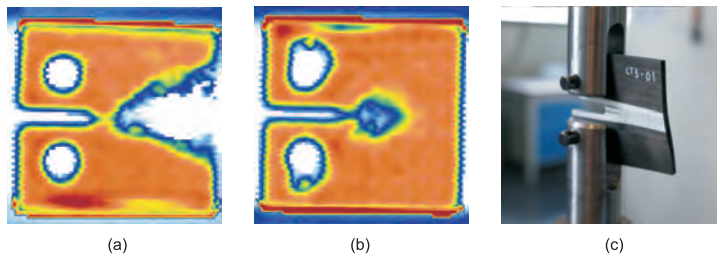


Figure 1.10: CT specimen with a T800S/M21 quasi-isotropic laminate [82] (a) C-Scan inspection with compression failure at the back part of the $[(90/45/0/-45)_2]_s$ laminate, (b) C-Scan inspection for $[90_2/45_2/0_2/-45_2]_s$ laminate, (c) buckling of the $[90_2/45_2/0_2/-45_2]_s$ laminate. Test performed by the PhD candidate

Recently, Bullegas et al. [70] developed a study using modified CT specimens at which is triggered the failure morphologies in bundles of fibers to dissipate more energy. The procedure consists of drilling micro-cuts at different heights close to the crack path as

shown in Fig. 1.11. Fig. 1.12 depicts one of the patterns, which increased the fracture toughness by 60% of the baseline without micro-cuts.

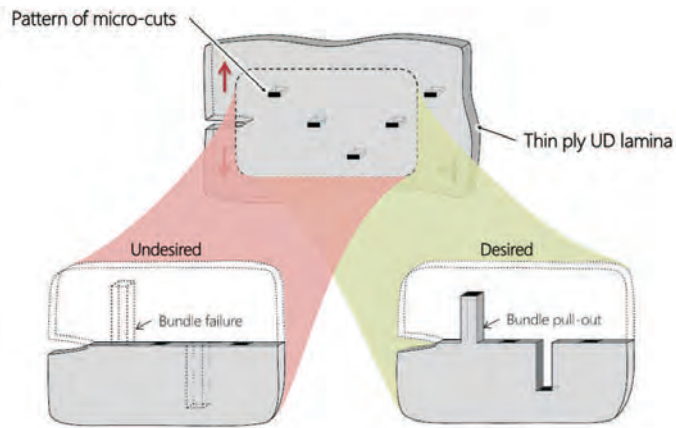


Figure 1.11: Micro-cuts drill along the crack path by laser system [70], where the desired fracture is described by bundles of fibers.

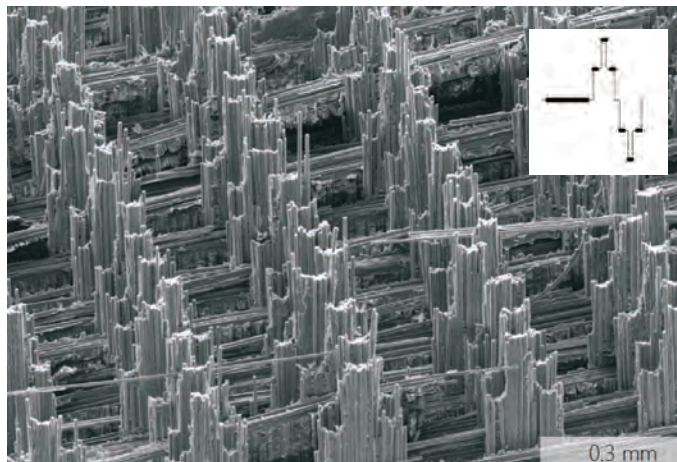


Figure 1.12: SEM inspection of the highest-energy failure pattern studied by Bullegas et al. [70].

Therefore, these mechanisms observed in translaminar fracture have to be analyzed taking into account hygrothermal effects, since the energy dissipated due to pull-out process can be affected significantly.

1.1.3 Stiffened panels

Many composite components in aerospace structures are made of flat or curved panels with co-cured or adhesively-bonded frames and stiffeners. Although hygrothermal effects are not commonly considered on experimental tests of stiffened panels due to the cost of each test, the failure mechanisms showed by Orifici et al. [86–88] (see Fig. 1.13), for a T-shape joint at laboratory conditions, match those described previously with hygrothermal effects for composite joints. Hence, for both mechanical and hygrothermal loads, the weakest zones are generally the interfaces between elements and the areas rich of matrix. Additionally, all the combinations between mechanical and hygrothermal loads increase considerably the cost for experimental tests, so a tool able to find an optimum panel for a given range of combination would be important to develop.

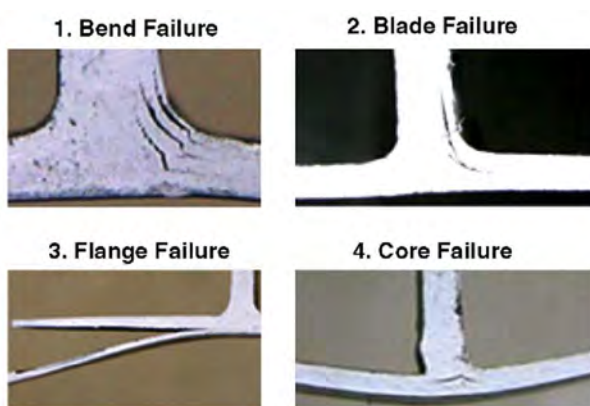


Figure 1.13: Failure modes for T-shape stiffened panels [88]: (1) delamination failure in the laminate at the skin-stiffener junction, (2) failure in the stiffener blade, (3) failure between skin and stringer and (4) failure at core.

In this field, optimization processes could be useful, where the stiffened panels has been already analyzed taking into account mono- or multi- stiffened geometries and considering one or more objectives and constraints depending on the complexity of the problem (Tables 1.3 and 1.4). However, to the author's knowledge, hygrothermal loads have never been considered in such optimization procedures. The standard formulation for an optimization problem is:

$$\min F(x_i) = [f_1(x_i), f_2(x_i), \dots, f_m(x_i)] \quad (1.5)$$

subject to

$$\begin{aligned} g(x_i) &< 0 \\ h &= 0 \\ x_i^l &\leq x_i \leq x_i^u \end{aligned}$$

where $F(x)$ is the objective function, m the number of objectives, x_i is the set of i design variables with x_i^l and x_i^u as the lower and upper bounds. g and h are the constraints. When $m = 1$ the expression indicates a mono-objective optimization problem and, by contrast, for $m \neq 1$ the problem is multiobjective.

Optimization methods are generally classified in two main categories: classic and heuristic. Generally, classic methods explore the objective functions locally by iteratively computing gradients, which is generally computationally expensive but guarantees fast convergence even for large number of variables [89]. They tend to have issues with problems which are not continuous or not differentiable, which is a common fact in engineering problems. To overcome this drawback, during the last century different families of heuristic methods were proposed. They avoid the computation of gradients and explore the objective function globally. They tend to be more effective for multi-objective problems. The most popular families of heuristic methods for mechanical engineering problems are Ant Colony Optimization (ACO) methods [90] and Genetic Algorithms [91, 92].

Furthermore, for engineering optimization problems where the structure has to be defined to generally minimize a multiobjective function, there is a second classification: parametric and topology optimization [93]. Parametric optimization defines the final

size of each design variable with an initial shape of the element. It is the most used in optimization of composite stiffened panels. By contrast, topology optimization optimizes material layout within a given design space, an area [93–95]. For instance, a stringer shape (1.15) could be found by a specific section (e.g. T-shape) by parametric study, while topology procedure could find the optimal stringer for any kind of section from an initial area. For composite structures, Fig. 1.14 shows the optimal stiffener layout for the fuselage obtained by topology optimization [95].

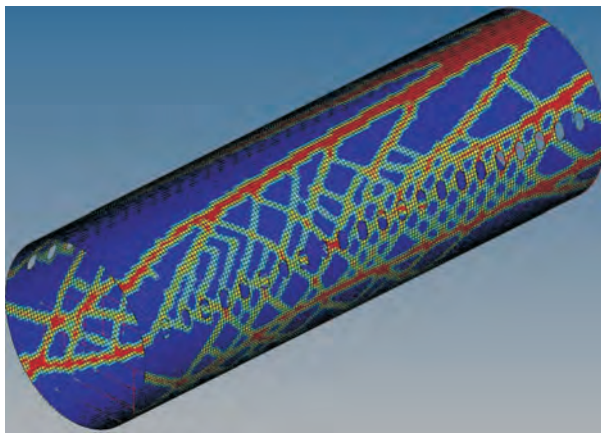


Figure 1.14: Topology optimization of a fuselage [95].

Additionally to the complexity of the optimization problem, the number of design variables x_i considered can often be very high. In Fig. 1.15, the geometric variables for each kind of stiffened are identified. Moreover, in order to reduce the stresses at the tip of the stringer and to avoid the interlaminar damage, geometric *run-out* configurations can be studied [96, 97]. On the other hand, the stacking sequence design is a special issue in optimization procedures [89].

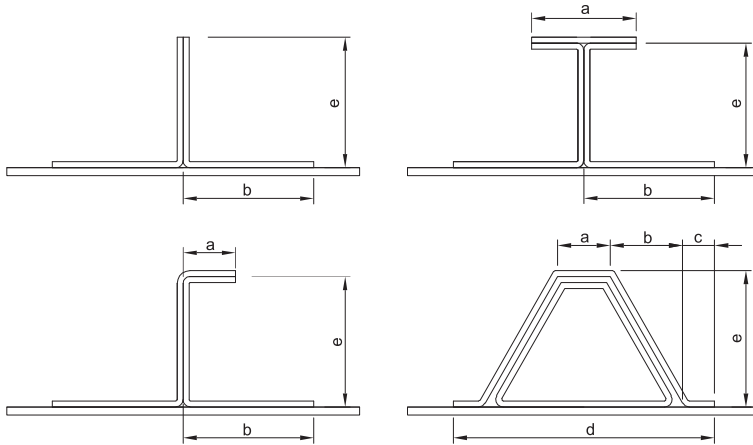


Figure 1.15: Geometric design variables.

Different strategies have been used to simplify the optimization processes: global approximation techniques, fragmentation in sub-problems and multi-level optimization problem.

- Global approximation techniques, known as surrogate models, response surface models or metamodels [98], are able to have similar behavior than Finite Element models, in terms of input and output patterns, and to get the required parameters in a faster process. The most extended techniques are:
 - Artificial Neural Network (ANN). This method is based on biological system by a training process [99]. They are able to reproduce characteristic typical from the human brain, such as the capacity of memorize and associate dates from the knowledge and experience. This system needs a training pattern. Bisagni and Lanzi [100] and Lanzi et al. [101] used this method with several networks with an optimum behavior by comparing to FE results.
 - Radial Basis Functions (RBF) consist of a interpolation technique able to describe non-linear functions and are suitable for interpolation of scattered data.

Chapter 1 Introduction

- Kriging models approximates non-linear functions as linear combination of known regression model and a stochastic process.
Lanzi and Giavotto [102] compared three of these methods: ANN, RBF and Kriging models. All of them obtained closed results with similar behaviors in comparison to FE analysis.
- Other response surface models: Todoroki et al. [103–105] developed a method based on *branch-and-bound* to obtain the constraints for the optimization process. Polynomial regression functions were also performed by Rikards et al. [106, 107] and Badran et al. [108].
- Fragmentation in sub-problems. To simplify the global optimization problem, some authors break up the general problem in several subproblems, reducing the computational cost. For instance, Irrisarri et al [109] optimized the stacking sequence of the skin in a first sub-problem and of the stringer in a second sub-problem.
- Multi-level optimization. Similar to the sub-problem fragmentation, a multi-level optimization process is usually used to consider different objectives or constraints for each level [110]. Also, Herencia et al [111] used two-level strategy, corresponding to different sets of variables.

Regarding the objectives $F(x_i)$, as previously noted, the most common objective used in optimization of stiffened panels is the weight of the panel. However, additional objectives to minimize the influence of hygrothermal effects on the joints of any composite structure could be included in the study. Therefore, a multiobjective optimization procedure with the capacity to afford different load conditions should be considered.





ref	Strategy		Variables	Objective function		Loading	Stringer shape
	Classification	Type		Objectives	Constraints		
[111]	Multi-level	MMA ¹ +GA ²	1 st level: Geometrical 2 nd level: Stacking sequence	$min W^3$ $min W$	P_{cr}^4 and resistance max No. of plies plies at same orientation	local-global buckling local-global buckling	
[112]	Approximation technique	ANN ⁵ +GA	Geometrical	$min W$		buckling (static)	
[104]	Approximation technique	Branch-and-bound	Stacking sequence	P_{cr}		buckling	
[113]	Multilevel	GA	1 st level(panel): Geometrical 2 nd level(laminate): Stacking sequence	$min W$ P_{cr}	Design variables $g(\theta)$ ⁶	buckling buckling	

Table 1.3: Classification of optimization of mono-stiffened panels.

- 1 Method of Moving asymptotas
- 2 Genetic Algorithms
- 3 Weight of the panel
- 4 Buckling critical load
- 5 Artificial Neural Networks
- 6 Stacking sequence conditions

















ref	Strategy		Variables	Objectives	Obj. function		Loading	Stringer shape
	Classification	Type			Constraints			
[100]	Approximation technique	ANN+GA ²	Stacking sequence Geometrical	$minW^3$	$P_{cr}^4, P_{cr}^5, S_{pb}^6$	post-buckling		
[102]	Approximation technique	(ANN,RBF ⁷ ,Kriging) +GA	Geometrical+ Stacking sequence	$minW$	P_{cr}, P_{co} and S_{pb}	post-buckling		
[109]	Approximation technique	(RBF,Kriging)+AE ⁸	Stacking sequence	$maxP_{cr}, maxP_{co}$		buckling and post-buckling		
[110]	Multi-level	AE	Stacking sequence	min No. of plies, $maxP_{cr}$		buckling		
[114]	Direct method	Reduce Mono-obj (GA)	Geometrical	DOC ⁹	Design variables	buckling		
[103]	Approximation technique	Branch-and-bound	Stacking sequence	$maxP_{cr}$	calculated per RSA	buckling		
[115]	Direct method	ACO ¹⁰	Stacking sequence	$maxP_{cr}$	W	buckling		
[106] [107]	Approximation technique	Polynomial regression	Geometrical	$minW$		post-buckling		
[106] [107]	Approximation technique	Polynomial regression	Geometrical	$minW$	P_{cr} and S_{pb} and S_{p2b} ¹¹	post-buckling		
[108]	Direct method+	GA+	Geometrical	$minW$ and $maxP_{cr}$	Design variables	buckling		
[116]	Approximation technique Direct method	Polynomial regression GA	Stacking sequence	$minW$		buckling and Damage resistance		
[117]	Direct method	GA	Stacking sequence			Damage resistance		
[117]	Direct method	GA	Topologic optimization Geometrical	$minW$		buckling		
[118]	Direct method	BMOGA ¹²	Stringer shape Geometrical	mono-obj $minW$	P_{cr} and damage resistance	buckling and damage resistance		
[119]	Direct method	GA	Stacking sequence	Multi-Objective: $minW$	$minW$ and min cost	damage resistance		
[119]	Direct method	GA	Stacking sequence	$minW$	$P_{cr}, g(\theta)$ ¹³	buckling		

Table 1.4: Classification of optimization of multi-stiffened panels.

- 1 Artificial Neural Networks
- 2 Genetic Algorithms
- 3 Weight of the panel
- 4 Buckling critical load
- 5 Buckling collapse load

- 6 Pre-buckling stiffness
- 7 Radial Basis Function
- 8 Evolutionary Algorithm
- 9 Direct Operating Cost manufacturing, production and inspection+constraint

- 10 Ant Colony Optimization
- 11 Post-buckling stiffness
- 12 Bit-Masking-Oriented GA
- 13 Stacking sequence conditions

1.2 Motivation

The present thesis has been developed in the framework of the project called *Ensayo Virtual y Supervisión Estructural de Revestimientos de CFRP: EVISER2* (funded by the *Ministerio de Economía y Competitividad-Gobierno de España* with reference: DPI2009-08048), which is focused on the virtual testing of stiffened panels of CFRP subjected to different hygrothermal conditions.

The aeronautical industry is clearly concerned in reducing the weight of aircraft structures. Regarding the greenhouse effect, one of the main issues is the gas emissions and, in aircraft, a reduction of the fuel consumption can be obtained by a decrease of the weight of each element. This supposes that a wide study where both mechanical and environmental loading has to be analyzed for structural elements and optimization techniques can be a good tool for structural designing.

However, as presented in the previous sections, despite of the growing use of FRP in structural elements, the behavior of composite panels under hygrothermal conditions is still difficult to predict due to the lack of understanding of the failure mechanisms.

To access to the highest level of the building block approach, expensive experimental tests are required, so a combination of testing and virtual analysis techniques is usually employed to reduce certification costs.

Developing a numerical tool able to account the combination of both mechanical and hygrothermal loads is essential for the numerical analysis. A constitutive model based on the micromechanical behavior under hygrothermal understanding is needed. Nevertheless, the material characterization under hygrothermal effects is not enough to feed up a virtual tool. Experimental tests have to be performed and analyzed in order to build an understanding of the failure mechanisms under hygrothermal conditions, from the first level of the building block approach.

Over all, for the translaminar fracture behavior where an analysis of the behavior of the matrix/fiber interface could be performed. Hygrothermal conditions could affect directly the quality of this interface and the efficiency of stress transfer between fibers by the matrix may be reduced and, so changes the global behavior of the material.

1.3 Objectives

The present thesis aims is to provide a wider understanding about the hygrothermal effects on composite materials. For that, two principal objectives have been considered:

In a first part, at developing the optimization procedure for composite stiffened panels under combination of hygrothermal and mechanical loadings. In this procedure, an optimum structure with a combination of the lowest weight, lowest tension between skin-stiffeners and minimum strain is developed under several different environment and mechanical loadings.

Throughout this first part of the thesis, the deficiencies of the material characterization under hygrothermal effects have been detected, thereby a suitable procedure able to involve hygrothermal conditions is needed. An experimental test campaign is proposed to analyze part of the properties that could feed up a virtual tool and could increase the knowledge about the hygrothermal effects on composite materials.

Therefore, a second objective in the first level of the building blocking approach is considered, where the translaminar fracture toughness of plies at 0° and translaminar fracture toughness of quasi-isotropic laminates are analyzed experimentally considering moisture and temperature effects. This part delves into the goal of experimentally obtaining the translaminar fracture toughness, and the analysis of the failure mechanisms involved in the failure processes for different hygrothermal conditionings.

1.4 Thesis structure

In order to achieve the objectives described in Section 1.3, the thesis has been divided into two main research blocks that are reflected in this document as two parts. Part I includes Chapter 2 and contains the work related to the optimization procedure for stiffened panels. Part II encompasses Chapters 3 and 4, containing the experimental investigations conducted to determine and analyze the intra- and trans- laminar fracture toughness in CFRP considering hygrothermal effects in a cross-ply and quasi-isotropic laminates.

1.4 Thesis structure

In Chapter 2 an optimization tool based on neural networks and genetic algorithms able to reach an optimum stiffened panel under several hygrothermal and mechanical loading is developed. This work has been published on the journal *Composite Structures* [120] and also yielded two contributions to the National Conference *MATCOMP2011* [121] and the International Student Conference *SAMPE* [122]. In Appendix A, is presented a reproduction of the manuscript published.

In Chapter 3, experimental tests of a cross-ply laminate for obtaining the translaminar fracture toughness have been performed. An in-depth research about the failure mechanisms for this kind of fracture is conducted for different hygrothermal conditions.

In Chapter 4, specimens of three quasi-isotropic laminates are tested for several conditionings in order to find a suitable standard for the translaminar fracture toughness.

The second part of the thesis have been presented in the National Conference *MATCOMP 2015* [123] and in the *International Conference on Composite Structures (ICCS17)* [82]. The work corresponding to Chapter 3 have been submitted to *Composite Science and Technology* [124] and the corresponding to Chapter 4 to *Composite Part A - Applied Science and Manufacturing* [125].

The thesis is concluded in Chapter 5 and 6, where general concluding remarks and recommendations for future research are given, respectively.

Part I

Optimization of composite stiffened panels
under mechanical and hygrothermal loads

2 | Optimization of composite stiffened panels under mechanical and hygrothermal loads using neural networks and genetic algorithms

Abstract. The present work develops an optimization procedure for a geometric design of a composite material stiffened panel with conventional stacking sequence using static analysis and hygrothermal effects. The procedure is based on a global approach strategy, composed by two steps: first, the response of the panel is obtained by a neural network system using the results of finite element analyses and, in a second step, a multi-objective optimization problem is solved using a genetic algorithm. The neural network implemented in the first step uses a sub-problem approach which allows to consider different temperature ranges. The compression load and relative humidity of the air are assumed to be constants throughout the considered temperature range.

The mass, the hygrothermal expansion and the stresses between the skin and the stiffeners are defined as the optimality criteria. The presented optimization procedure is shown to yield the optimal structure design without compromising the computational efficiency.

2.1 Introduction

Fibre reinforced polymer (FRP) composite materials have been used in the aerospace industry because of their high strength-to-weight and stiffness-to-weight ratios, and good behavior under elevated temperature environments. However, the major drawback of these materials is its high cost, so a suitable design and optimization process is essential in order to improve their structural behavior to cost ratio.

This has led several authors to study the optimization of composite panels, considering frequently as an objective the minimum mass, by geometric [107, 108, 114] and stacking sequence design [103–105, 109, 110, 115, 116, 119]. On the other hand, these studies have focused on buckling or post-buckling dynamic analysis, without considering environmental effects. Nevertheless, these structures are exposed to extreme environmental conditions and some researchers have studied optimization problems of laminated composite plates with thermal effects to maximize the critical temperature capacity with uniform [126, 127] or nonuniform temperature distribution [128]. In addition, Ijsselmuiden et al. [129] carried out a thermomechanical design optimization of composite panels and Cho [130] studied the hygrothermal effects in optimization problems of dynamic behavior, where temperature and moisture are assumed to be uniform once they have reached equilibrium.

Moisture and temperature changes affect the stiffness and strength of composites, and generate tensions between bonded sub-components. Their static and dynamic behaviors can depend significantly on such hygrothermal conditions. The combination of both phenomena is usually known as hot-wet (H/W) conditions. This state is characterized by moisture absorption by the matrix due its exposure to humid air and high temperature, which reduces the mechanical properties of the laminate. Additionally, this absorption causes a volume increase and consequently internal tensions between elements and interfaces. Experimental results show the influence of the temperature in moisture absorption [57, 131–133], so this phenomenon should be analyzed for different thermal load cases and hygrothermal effects should be considered in any design and optimization process. On the other hand, Orifici et al. [86, 88] analyzed the post-buckling

failure of T-shaped stringers classifying in four failure modes: bend, blade, flange and core failure. The authors also found that delamination arises under the edges of stiffeners and the triangular resin-rich area.

The solution of the optimization problem is generally obtained with genetic algorithms (GA) which have become one of the most employed solution method in engineering problems since they can handle integer, zero-one, discrete and continuous variables and are effective with nonlinear functions and non-convex design spaces. Due to this, both geometric and stacking sequence variables can be introduced. These methods are based on Darwin's theory of natural adaptation and biological evolution [91, 92], which is translated into algorithmic terms through the computational operators of selection, crossover and mutation. In engineering applications, the evaluation of the objective function may be performed by means of an analytical function or, frequently, a numerical model (a finite element model, for instance). Since a large number of evaluations is generally required to obtain the optimal solution, the whole solution process implies a high computational cost. Some authors have used global approximation techniques to reduce function evaluation computational time by using data previously obtained with analytical or numerical methods. In this direction, Bisagni et al. [100] developed an optimization procedure with a global approximation strategy based on obtaining the structure response by means of a system of artificial neural networks (ANN) and GA. Lanzi et al. [101] performed a comparative study between three different global approximation techniques: ANN, kriging method and radial basis functions. All the techniques showed a similar behavior that the dynamic finite element (FE) analysis and computational time was satisfactorily reduced.

The aim of the present work is the definition of a fast multi-objective optimization procedure for the geometric design of stiffened panels under mechanical and hygrothermal loads, which minimizes the mass, the stresses between elements and the strain due to hygrothermal effects. The optimization problem is subject, in turn, to the corresponding constraints of tensions between stiffener-skin, provided by a failure criterion. The

Chapter 2 Optimization of composite stiffened panels

optimization procedure is carried out under different thermal load cases. A global approximation technique based on ANN is used to reduce computational cost.

This paper is structured as follows: firstly, in Section 2, a standard panel is analyzed to set up the model that will compute the objective functions and to define suitable constraints; the optimization process is described in Section 3; next, results are shown in Section 4 and finally, conclusions are presented in Section 5.

2.2 Definition of the multi-objective problem

2.2.1 Stiffened panel design

The considered structure is a compression loaded stiffened composite panel with three stringers, as shown in Figure 2.1. This kind of panels represents a flat and partial idealization of the wings and fuselage structures of commercial aircrafts and so is frequently used in analysis and testing as a subcomponent. It is made of carbon fiber reinforced polymer (CFRP) and is symmetric in x - z and y - z planes. The stiffener sections are double-L shaped¹ showing rounded corners with a mean radius of 4 mm for construction reasons. No run-outs are present. The different stacking sequences corresponding to each part of the geometry are shown in Figure 2.1. Ply thickness is 0.184mm.

The specimen studied in this work is made with Hexcel T800/M21 prepreg ribbon of epoxy matrix reinforced with unidirectional carbon fibers. Its properties are shown in Table 2.1.

¹ Cure process: The panel and stringers are manufactured independently according the manufacturer recommendations [39] and they are joined by using of high-temperature and low-temperature adhesives.

2.2 Definition of the multi-objective problem

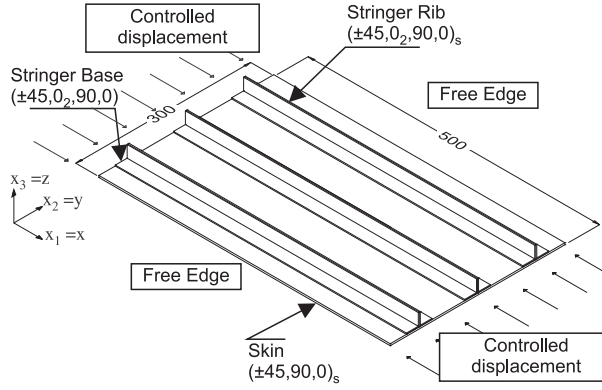


Figure 2.1: Stiffened panel (dimensions in mm).

Property	Value	Description
E_{xx} [GPa]	134.7	Young's modulus
$E_{yy} = E_{zz}$ [GPa]	7.7	Young's modulus
$\nu_{xy} = \nu_{xz}$	0.369	Poisson's ratio
ν_{yz}	0.5	Poisson's ratio
$G_{xy} = G_{xz}$ [GPa]	4.2	Shear modulus
G_{yz} [GPa]	2.5	Shear modulus
α_{xx} [$^{\circ}\text{C}^{-1}$]	$-3.08 \cdot 10^{-7}$	Coefficient of thermal expansion ¹
$\alpha_{yy} = \alpha_{zz}$ [$^{\circ}\text{C}^{-1}$]	$3.18 \cdot 10^{-5}$	Coefficient of thermal expansion ¹
ρ [Kg/m ³]	1590	Density
X_T [MPa]	2290.5	Longitudinal tensile strength
X_C [MPa]	1051	Longitudinal compression strength
Y_T [MPa]	41.43	Transverse tensile strength
Y_C [MPa]	210	Transverse compression strength
S_L [MPa]	69.4	Shear strength
S_{IS} [MPa]	106.48	Shear strength <i>in situ</i>
α [$^{\circ}$]	53.5	Transverse compression fracture angle
β	$5.10 \cdot 10^{-8}$	Shear response factor
g	0.5769	Toughness ratio (G_I/G_{II})

¹ Values obtained using the relations described in [134].

Table 2.1: T800/M21 UD CFRP properties [135].

Chapter 2 Optimization of composite stiffened panels

The parametric analysis of the stiffened panel is performed in function of three geometric design variables $\mathbf{x} = (\mathbf{x}_1, \mathbf{x}_2, \mathbf{x}_3)$ where x_1 is the stringer base width, x_2 is the stringer rib and x_3 is the distance between stringers with domains set forth in Table 2.2 and $\mathbf{x} \in \Omega_d$, where Ω_d is the decision space.

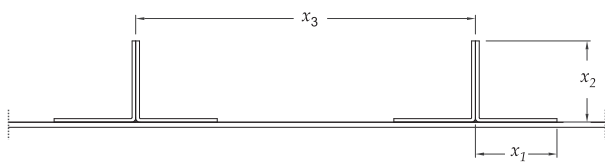
Geometric variables: \mathbf{x}	Lower bound: $\mathbf{x}^{(l)}$	Upper bound: $\mathbf{x}^{(u)}$
		
x_1 : Stringers base width	20	30
x_2 : Stringers rib	20	30
x_3 : Stringers separation	70	110

Table 2.2: Geometric variables domain (mm).

2.2.2 Model of the panel: finite element modeling

For the automatic parametric generation of panels, a *python* code is used together with the commercial software ABAQUS [136]. The stiffened panels are modeled by 4-node shells S4R, with six degree of freedom at each node, three integration points along the thickness for each ply. A compressive controlled displacement is applied to each transverse edge, while the longitudinal edges are free, as shown in Figure 2.1. On the other hand, different temperature states are considered with a constant moisture.

The temperature and moisture are assumed to be in equilibrium state. The thermal strain is defined as $\epsilon^T = \alpha \Delta T$ and the moisture strain has been computed by the formulation proposed by Chang et al. [133] which considers the influence that temperature has in moisture strain for HTA1200A/ACD8801 material:

$$\epsilon^H = \frac{0.591R}{T + 273} \quad (2.1)$$

2.2 Definition of the multi-objective problem

where T is considered as the final temperature of the ΔT and R is the relative humidity. This approach is used for transverse and out-of-plane direction, while the longitudinal moisture strain is considered negligible [7]. So the general form of stress-strain relationship for a transversely isotropic ply in which temperature and moisture effects are considered is $\epsilon^{\text{Tot}} = \epsilon^{\text{T}} + \epsilon^{\text{H}} + \epsilon$, where the components are:

$$\begin{pmatrix} \epsilon_{xx}^{\text{Tot}} \\ \epsilon_{yy}^{\text{Tot}} \\ \epsilon_{zz}^{\text{Tot}} \end{pmatrix} = \begin{pmatrix} \alpha_{xx} \\ \alpha_{yy} \\ \alpha_{zz} \end{pmatrix} \Delta T + \begin{pmatrix} \approx 0 \\ \frac{0.591R}{T+273} \\ \frac{0.591R}{T+273} \end{pmatrix} + \begin{pmatrix} \epsilon_{xx} \\ \epsilon_{yy} \\ \epsilon_{zz} \end{pmatrix} \quad (2.2)$$

A standard stiffened-panel, analyzed in a previous project [135], is taken as the reference panel with the following dimensions: $x_1 = 24$ mm, $x_2 = 24$ mm and $x_3 = 100$ mm. The behavior of the reference panel under different compressive and hygrothermal loads is studied in depth, using LaRC-03 failure criterion [137], which defines the following variables: failure indexes for transverse tensile failure (FI_{TT}), transverse compressive failure (FI_{TC}), longitudinal tensile failure (FI_{LT}), and longitudinal compression failure (FI_{LC}).

For temperature rising cases, the strains in the perpendicular direction are higher than the temperature decreasing cases, and localized in the stiffener bases, so the tensions between stringers and skin also increase. However, FI_{TC} and FI_{LC} indicate that the panel is capable of supporting larger temperature increases without breaking up to 1.45 mm compressive controlled displacement.

For decreasing thermal variations, the panel shows lower tensions, breaking with variations between -50° and -125° and compressive moderated displacement, depending on the final temperature. In these cases, FI_{TT} and FI_{LC} are the most important failure indexes. The interaction between moisture and thermal effects helps to the behavior of the panel but the matrix is damaged after the moisture absorption. Different environmental conditions with decreasing and rising thermal variations have been considered in the optimization problem.

Chapter 2 Optimization of composite stiffened panels

2.2.3 Definition of subproblems

The behavior of the panel under a wide range of temperatures leading to different failure modes is analyzed. For this purpose, the initial problem has been decomposed into seven sub-problems so that, for each one, different ranges of temperature are considered. Initial temperatures correspond to the most significant values used in experimental analysis (generally -55°C, ambient temperature, 70°C, 90°C and 120°C) and temperature variations are chosen by the most important cases within the considered temperature range from -55°C to 120°C [138], where the minimum and the maximum service temperature commercial transport aircraft are considered as -54°C and 71°C respectively and the design ultimate loads at temperature up during takeoff and landing is 93°C; the temperatures higher than 100°C are considered only for special cases, such as supersonic transport, fighter, and bomber aircraft. So the different subproblems described in Table 2.3 were considered. The variables T_I (initial temperature) and ΔT (temperature variation) form the vectors $\mathbf{y}_n = (\mathbf{y}_{1n}, \mathbf{y}_{2n})$ where n is the number of each subproblem.

Subproblem (n)	Loading conditions		
	Mechanical	Hygro (H [%])	Thermal (T [°C])
	Compression (Controlled displacement)		$T_I^1(y_1)$ T_F^2 $\Delta T^3(y_2)$
SP1			-55 120 175
SP2			20 120 100
SP3			70 90 20
SP4	1.9mm	70	20 -55 -75
SP5			70 20 -50
SP6			90 -55 -145
SP7			120 -70 -190

¹Initial temperature

²Final temperature

³Temperature variation

Table 2.3: Loading conditions for each subproblem.

2.2.4 Formulation of the multi-objective optimization problem

A multi-objective problem is established, which seeks to minimize the weight of the panel $f_1(\mathbf{x}, \mathbf{y}_n)$, the local strain in direction perpendicular $f_2(\mathbf{x}, \mathbf{y}_n)$ and the tension between skin and stiffeners $f_3(\mathbf{x}, \mathbf{y}_n)$. All three objective functions are considered to be equally important.

In this way, the optimization problem can be formulated as:

$$\begin{aligned}
 &\text{Minimize} && Y(f_1(\mathbf{x}, \mathbf{y}_n), \mathbf{f}_2(\mathbf{x}, \mathbf{y}_n), \mathbf{f}_3(\mathbf{x}, \mathbf{y}_n)) && Y \in \Omega_o \\
 &\text{Subject to} && g_k(\mathbf{x}, \mathbf{y}_n) > \mathbf{0} && k = 1, 2 \\
 & && x_j^{(l)} \leq x_j \leq x_j^{(u)} && (2.3) \\
 &\text{where} && \mathbf{y}_n = (\mathbf{y}_{1n}, \mathbf{y}_{2n}) \\
 & && \mathbf{x} = (\mathbf{x}_1, \mathbf{x}_2, \mathbf{x}_3)
 \end{aligned}$$

where Ω_o is the objective space. The constraints $g_k(\mathbf{x}, \mathbf{y}_n)$ are defined as:

$$\begin{aligned}
 & \left. \begin{aligned} g_1(\mathbf{x}, \mathbf{y}_n) &= \mathbf{1} - \mathbf{FI}_{TC}(\mathbf{x}, \mathbf{y}_n) \\ g_2(\mathbf{x}, \mathbf{y}_n) &= \mathbf{1} - \mathbf{FI}_{LC}(\mathbf{x}, \mathbf{y}_n) \end{aligned} \right\} \text{if } \Delta T > 0, && (2.4) \\
 & \left. \begin{aligned} g_1(\mathbf{x}, \mathbf{y}_n) &= \mathbf{1} - \mathbf{FI}_{TT}(\mathbf{x}, \mathbf{y}_n) \\ g_2(\mathbf{x}, \mathbf{y}_n) &= \mathbf{1} - \mathbf{FI}_{LC}(\mathbf{x}, \mathbf{y}_n) \end{aligned} \right\} \text{if } \Delta T < 0
 \end{aligned}$$

2.3 Optimization procedure

The solution of the problem, displayed in Eq. 2.3 and 2.2.4, implies a high computational cost for the optimization process since the values of the objective functions and the constraints are obtained from a parametrized FE model. For this reason, the procedure shown in Figure 2.2 based on a global approximation technique is used to reduce the computational time. This procedure is composed by two steps:

1. A system of ANN that is partially capable to reproduce the solution of the FE model is developed. To the seven inputs corresponding to each subproblem

Chapter 2 Optimization of composite stiffened panels

$E_n(I_n)$ it delivers the different outputs composed of the objectives and constraints $E_n(O_n)$.

2. A GA obtains to get the optimal value for the design variables previously described.

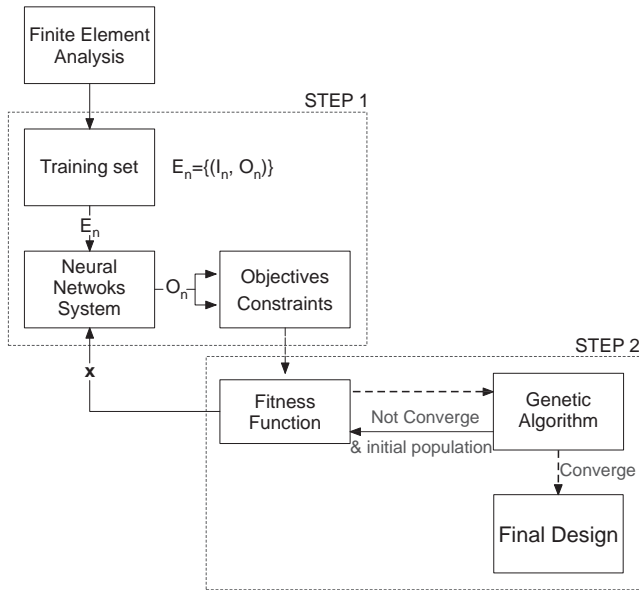


Figure 2.2: Optimization scheme.

2.3.1 Model of the panel: neural network modeling

An ANN is a system used for information processing whose basic unit is inspired by the fundamental cell of the human nervous system: the neuron. This system is capable of acquiring knowledge and resolve situations that can not be expressed mathematically by the experience [99].

The ANN needs a learning process and a training set, composed of input-output patterns, as known examples. The input signals of an artificial neuron are continuous variables instead of discrete pulses, as presented in a biological neuron. Each input

2.3 Optimization procedure

signal passes through a *weight or gain*, known *synaptic weight* or strength of the connection whose function is analogous to the synaptic function of the biological neuron. An other term, called *bias*, supposes a reinforcement of these connections. The summation node accumulates all input signals multiplied by the weights and bias and output passes through a *transfer function* or, where appropriate, *activation function*. The result of this sum is known as *propagation function*, which obtains the output vector.

A commercial software, Matlab [139], was applied for developing an ANN procedure that includes the following process:

- Choice of data set. The training data set is composed by seven subsets that correspond to the different sub-problems displayed in Table 2.3. The set consists of an input-output pattern-pairs obtained through FE analysis.

The input pattern forms a vector I_n , composed of the geometrical parameters \mathbf{x} and the vector \mathbf{y}_n , and the output pattern O_n , composed of the corresponding responses of the panel for each sub-problem (objectives and constraints).

- Architecture of the ANN. The complexity of the problem is solved by using by a suitable architecture to implement the information of the input-output pattern for each sub-problems discussed that, once inside the network will be merged.

This architecture, shown in Figure 2.3, is defined by multilayer perceptron (MLP) that consists of an input layer with a vector dimensions I_n , two hidden layers with *compet* and *tansig* functions as *activation and transfer functions* respectively, and Levenberg-Marquardt [140] backpropagation learning rule and an output layer, with *tansig* function, that obtains the vector O_n , calculated from the bias and weights are adapted after training in the network.

- Training of the ANN. The ANN is taught to form the relationship between input and output variables by the training data set of known input-output patterns. This set is composed by the response of 120 FE analysis for each sub-problem to achieve a good performance of the system. A data processing MSE of about 10^{-4} is obtained.

Chapter 2 Optimization of composite stiffened panels

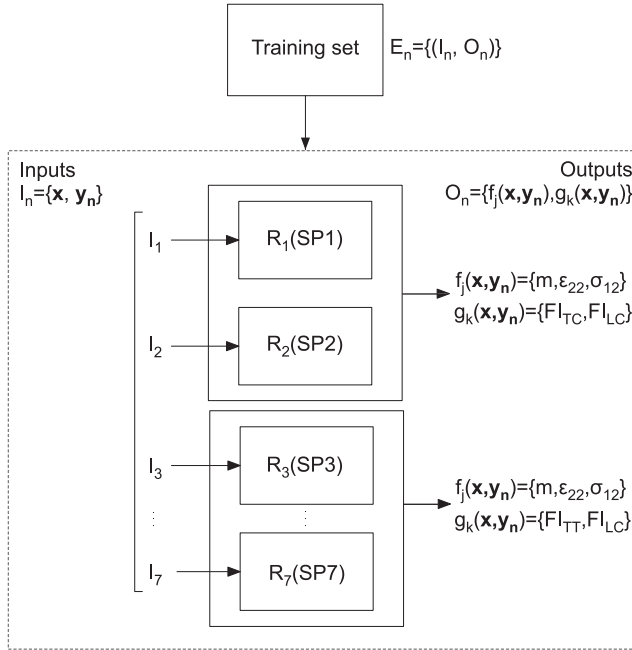


Figure 2.3: Neural Network scheme

2.3.2 Genetic algorithm

A variant of the algorithm Non-dominated Sorting Genetic Algorithm II (NSGA-II) [141] is used to solve the formulated problem by the Toolbox for Matlab (Global Optimization). It is one of the results of the evolution of the GA and is based on the application of elitism preserving the use of Pareto front. This elitism is controlled by two options: the *Pareto fraction* and *crowding distance measure* functions. The first, limits the number of individuals on the Pareto front and the distance function helps to maintain diversity on a front by favoring individuals that are relatively far away on the front.

The fitness function, which measures the genetic informations of each individual, is composed of the different objectives and the constraints. A penalty method is used to describe the constraints, reported in Eq.2.2.4. The individuals with better characteristics survive during the evaluation process.

The genetic search is performed with a population size of 75 members, generated randomly, with a 'genotype' function as crowding distance measure and the value of the Pareto fraction is set as 0.5.

2.4 Results and discussion

The GA converged after 33 generations and required 1701 fitness function evaluations. A considerable reduction of the computational cost is achieved with the optimization procedure proposed. In fact, to obtain the optimal configuration, 120 FE analysis for each subproblem were performed in a total computational time of about 35 h. The used computer is a DELL Precision T1500 with an Intel® Core™ i5 CPU with 2.67GHz, 4GB of RAM, Windows 7 x64 Edition. The CPU time required by the ANN training process was approximately 25 min, while the computational cost for optimization was about 8 min. However, a direct optimization using GA coupled with FE analysis supposes about 1701 different simulations for each subproblem, which means roughly 500 h of computational time.

The optimal panel has been selected between all those solutions of the Pareto front such as each objective function has the same weight. This panel is characterized by a mass of 378 g and the following dimensions: $x_1=26.397$ mm, $x_2=21.404$ mm and $x_3=90.23$ mm.

The solution obtained using the ANN modeling is compared with the FE modeling for each subproblem as shown in Table 2.4.

In turn, all the failure indexes of LaRC criterion are verified to be lower than 1. For this parameters, the most restrictive problems have been the SP1 for temperature increase and SP3 and SP6 for temperature decrease. In comparison with the reference panel, the reduction in mass is 0.54%, and the hygrothermal strain and the tensions between the stiffeners and the skin are reduced about 6.48-3.43% and 7.55-4.99% respectively depending on the subproblem (Table 2.5).

Positive and negative temperature increments of five degrees are considered for each interval in Figure 2.4, where the comparison between these panels is shown for the extreme temperature cases. In both cases, the reference panel breaks as failure indexes

Chapter 2 Optimization of composite stiffened panels

		Method	SP1	SP2	SP3	SP4	SP5	SP6	SP7
Objectives	m (g)					378			
	σ_{xy} (MPa)	FE Analysis	32.84	28.79	25.43	24.85	23.90	22.08	22.49
		NN System	33.15	29.89	26.50	24.66	24.16	21.80	22.05
		error (%)	0.9	3.1	4.2	0.7	1.1	1.2	1.9
	ϵ_{yy}	FE Analysis	4.76	4.46	4.24	4.23	4.22	4.22	4.21
		NN System	4.78	4.57	4.16	4.17	4.17	4.35	4.23
error (%)		0.4	2.5	1.9	1.4	1.2	3.0	0.5	
Constraints	FI_{TT}	FE Analysis	-	-	-	0.32	0.42	0.948	0.784
		NN System	-	-	-	0.31	0.45	0.93	0.81
		error (%)				6	7.1	1.9	3.3
	FI_{LC}	FE Analysis	0.996	0.64	0.61	0.58	0.47	0.996	0.87
		NN System	0.97	0.68	0.65	0.54	0.49	0.98	0.89
		error (%)	2.6	6.2	6.5	6.9	4.2	1.6	2.3
	FI_{TC}	FE Analysis	0.978	0.80	0.36	-	-	-	-
		NN System	0.98	0.82	0.38	-	-	-	-
		error (%)	0.2	2.5	5.6				

Table 2.4: Objectives and constraints values by each subproblem.

values indicate in Figures 2.4(a) 2.4(d) while the optimal panel shows a good performance and the strain and the tension between the stiffeners and the skin are considerably reduced.

2.4 Results and discussion

		Panel	SP1	SP3	SP6
Objectives	$m(\text{g})$	reference panel		379	
		optimum panel		378	
		reduction (%)		0.54	
$\sigma_{xy}(\text{MPa})$	reference panel	35.52	27.06	23.24	
	optimum panel	32.84	25.43	22.08	
	reduction (%)	7.55	6.02	4.99	
ϵ_{yy}	reference panel	5.09	4.46	4.37	
	optimum panel	4.76	4.24	4.22	
	reduction (%)	6.48	4.93	3.43	

Table 2.5: Comparison of the reference and optimal panels for the most restrictive subproblems.

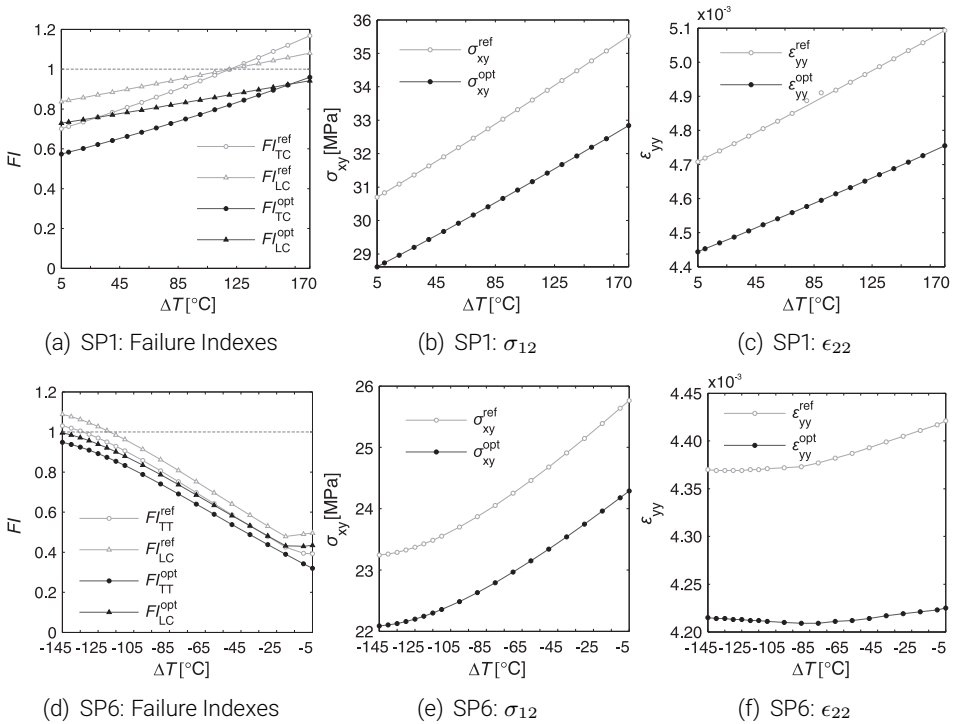


Figure 2.4: Comparison between reference and optimal panels

2.5 Conclusions

An optimization procedure for stiffened panels under mechanical and hygrothermal loads has been developed. This procedure consists of the interaction between an ANN system and a GA with the purpose of reducing the computational cost that could reach a direct optimization using FE analysis to obtain the response of the panel. For the correct definition of the optimization problem, the behavior of a reference panel has been analyzed by means of FE with the aim of selecting the most significant objectives and constraints for the possible load states.

A set of seven subproblems characterized by different temperature ranges and moisture presence was considered in the optimization procedure. This decomposition of the initial problem in several subproblems helps to analyze the hygrothermal effects with negative or positive thermal variations and to find the optimal panel for the maximum number of load cases at which these structural elements can be subject. However, the implementation of different subproblems increases the computational cost in the optimization problem.

The use of ANN systems can increase the speed of the optimization processes, reducing the computational cost about 92.8%. The drawback of these tools is the time required to design its architecture to obtain the suitable learning, which can be higher in specific terms and affect the optimization results. However, comparing the optimal panel behavior calculated with FE analysis and ANN system, it can be observed that it is suitable for all subproblems and is able to reduce the several objectives satisfying the considered constraints. Comparing the optimal and reference panels, the mass is reduced about 0.54% and the hygrothermal strain and tension between stringers and skin are decreased until 6.48% and 7.55% respectively in specific load cases.

In conclusion, ANN and GA reduce the computational cost with suitable accuracy and can help to implement several load states to minimize the global problem. These tools can be used in engineering applications with a unique or various ANN systems. On the other hand, to reduce the time required to train the ANN and replace the problematic trial-and-error approach, a GA system could be used to find the optimal internal architecture.

Part II

Hygrothermal effects on the
translaminar fracture toughness

3 | Hygrothermal effects on the translaminar fracture toughness of cross-ply carbon-epoxy laminates: failure mechanisms

Abstract. The present work addresses the damage mechanisms of polymer-based laminated composite materials under different hygrothermal conditions by means of the translaminar fracture toughness using Double Edge Notched Tensile tests of a cross-ply laminate manufactured with T800S/M21 carbon/epoxy material.

Three different conditionings were considered: as received-room temperature (AR/RT), wet-room temperature (WET/RT), and wet-high temperature (WET/HOT). The highest fracture toughness was for WET/HOT and the lowest for WET/RT. To observe the corresponding failure mechanisms, Scanning Electronic Microscopy (SEM) analysis was performed. The SEM inspections show that the pull-out length and the frictional coefficient are the most significant parameters that best explain the differences observed in the crack propagation and the fracture toughness. For AR/RT, the suitable adhesion between components allows stresses to be transferred from the matrix to the fibers, so the crack is practically continuous in the same failure plane and the pull-out is barely visible. However, higher pull-out lengths can be observed in WET/RT and WET/HOT, especially in the second one. For WET/RT, the crack surface shows fiber bundles at different pull-out lengths, while for WET/HOT fibers are broken individually at longer pull-out lengths. According to the moisture absorption in WET/RT and WET/HOT, a lower frictional coefficient is thought to slightly reduce the fracture toughness, which can be compared between AR/RT and WET/RT. Nevertheless, the highest fracture toughness is caused by the large pull-out lengths in WET/HOT tests, despite the reduction of the frictional coefficient.

3.1 Introduction

The heterogeneity of polymer-based composite materials generates complex failure mechanisms where several damage modes (delamination, matrix microcracking, debonding and fiber breakage) interact. In multidirectional laminates under tension or compression loading, fiber breakage can be considered the most significant failure mechanism. That is because fibers are the principal load-carrying component, while the matrix binds the fibers together and transfers loads between them [142].

Environmental agents can considerably affect the interaction of failure modes, especially by acting on the matrix degradation and the matrix/fiber interface or interlaminar cohesion between plies, which will affect the stress transfer mechanisms.

Following Fick's Law [20, 22], moisture is absorbed by the matrix through a slow diffusion process, which causes dimensional changes known as swelling. Additionally, the glass transition temperature (T_g) decreases and the matrix and matrix/fiber interface mechanical properties are modified. The moisture exploits microcracks, voids and the capillaries along the fiber/matrix interface and between plies [34, 36], and these regions become weakened. On the other hand, fibers do not absorb moisture: therefore the absorption capacity of the matrix can be five times higher than the fiber [9]. The swelling difference between the fiber and the matrix can cause stresses in the interface. Moreover, matrix cracking could appear as a result of expanded frozen water [36].

Concerning the temperature effects, the mismatch between matrix and fibers thermal expansion may cause internal stresses in the interface. In fact, carbon fibers have a negative thermal coefficient in their longitudinal direction, which can magnify this effect. Furthermore, at high temperatures, transverse microcracks occur mainly at the fiber/matrix interface [138].

Combined hygrothermal conditions affect the service performance of composite structures. First, this combination acts on the moisture diffusion velocity since it depends on the temperature [133, 143]. Moreover, with high temperature the presence of microcracks at the interface increases, so the moisture can penetrate into the composite more easily. Another effect, previously mentioned, is that the higher the moisture, the

lower the T_g . The combined effects of moisture and temperature can affect the material strength positively or negatively. For instance, WET/COLD conditions, can cause thermal stresses because of low temperature, but those stresses can be compensated by swelling [34]. On the other hand, the WET/HOT condition is often considered to be the worst scenario. Actually, an extreme Relative Humidity (RH), common in tropical zones [30], is usually taken into consideration together with a high temperature nearby the T_g . A testing temperature of 120°C is considered as extreme and is assumed to be encountered only in supersonic transport, fighters, bomber aircraft or in determined components of the wings, especially on the leading edges of the lifting surfaces or near the engines [120, 138, 144]. The application of an advanced polymer matrix composite is generally limited to a temperature of 120°C [36].

Matrix-dominated mechanical properties, such as compression strength [6, 145] and shear strength [4, 5, 146, 147] or and fiber-dominated mechanical properties like tensile strength [4, 143], have been studied under different hygrothermal conditions. The previous research highlights that there are two zones that are especially weakened because of the moisture and/or temperature: the interlaminar [12, 36, 148] and the matrix/fiber interface regions. Hygrothermal effects on the critical energy release rate for mode I ($G_c^{del,I}$) and mode II ($G_c^{del,II}$) delamination have been studied previously by Asp [12] for dry and wet specimens, where the higher the temperature, the greater the decrease of $G_c^{del,II}$ is in both cases, with lower values for wet specimens. In contrast, $G_c^{del,I}$ seems unaffected by moisture and slightly increases at elevated temperatures.

Regarding to the matrix/fiber interface, some studies were performed in the 90s [40–43], include an exhaustive review published by Kim and Mai [76], in which interface properties are described in terms of fiber debonding, fiber pull-out and stress distribution. The Interfacial Shear Strength (IFSS) [1, 149] is a good measure of the effectiveness of the interactions at the interface. Biro et al. [22] tested the IFSS of two carbon/fiber composites at hygrothermal conditions using microbond tests with two steps of moisture content. They found an IFSS reduction in both cases and an even larger decrease when moisture exposure increases. A microindentation analysis of an IFSS [150], only considering material moisture effects, was performed by Bradley and Grant [149], whose results demonstrated a degradation of the interface.

Chapter 3 Hygrothermal effects on the translaminar fracture toughness: CP laminates

However, although a single-fiber experimental model system can contribute to the understanding of interactions at the interface, it does not show the global behavior in a composite material and it does not provide information about the stress transfer inside the laminate. On that topic, intralaminar fracture (direction along the fibers) and translaminar fracture (perpendicular to the fibers, plies at 0°) and translaminar fracture of the laminate (through the laminate) could result in useful information.

During the propagation of a translaminar crack, energy is dissipated through fiber-matrix interface debonding, fiber fracture and the fiber pull-out [151].

Until now, several different tests have been used to obtain the intra- and translaminar fracture toughness without considering hygrothermal effects by Compact Tension (CT) tests [19, 152] or modified CT tests [78, 151]. But buckling damage appeared for some carbon/epoxy materials and other non-desirable failure types (e.g. bearing, back-end compression), probably because of tougher matrices [78, 81, 151]. However, in a recent study published by Catalanotti et al. [16], Double Edge Notched Tensile (DEN-T) specimens were used to obtain the crack resistance curve (R-curve) and the length of fracture process zone $l_{f_{p_z}}$ based on the size effect law [83].

The aim of the present work is to study how different environmental conditions can affect translaminar fracture toughness and to determine which failure mechanisms appear for each case. Accordingly, this paper is structured as follows. Firstly, Section 2 describes the experimental tests and the different conditionings. Next, Section 3 presents the experimental results and fractographic images and, finally, the results are discussed in Section 4 and conclusions are drawn in Section 5.

3.2 Material, hygrothermal conditions and test set-up

DEN-T tests of a prepreg T800S/M21 cross-ply laminate have been used to measure the translaminar fracture toughness under different hygrothermal conditions. Panels of 300x350 mm were manufactured using hand layup and cured in an autoclave according to the manufacturer Hexcel recommendations (with a curing temperature of 180° for 120 min). A wet saw was used to cut the rectangular plates into the specimen geometry (see Table 3.2).

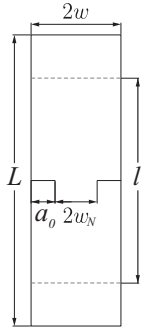
3.2 Material, hygrothermal conditions and test set-up

The stacking sequence is a cross-ply laminate with $[90/0]_{4s}$, where 0° is aligned with the loading axis. The nominal ply thickness is 0.184 mm and the nominal laminate thickness is 2.944 mm. The elastic properties of the ply are shown in Table 3.1.

Property	Value	Description
E_{11} [GPa]	152.8	Young's modulus. ¹
$E_{22} = E_{33}$ [GPa]	8.7	
$\nu_{12} = \nu_{13}$ []	0.335	Poisson's ratio. ¹
ν_{23} []	0.38	Poisson's ratio. ²
$G_{12} = G_{13}$ [GPa]	4.2	Shear modulus [120]
G_{23} [GPa]	3.15	Shear modulus ³
ρ [Kg/m ³]	1590	Density [120]
V_f [%]	56.6	Fiber volume ⁴

Table 3.1: T800S/M21 UD CFRP properties. ¹ Values obtained by tensile test. ² Value approximated using the ν_{23} of the matrix. ³ $\frac{E_{22}}{(2(1+\nu_{23}))}$. ⁴ Value obtained by BS EN 2564:1998[153].

As described in [16], several sizes of the DEN-T specimen are needed in order to obtain the R-curve since the data reduction is based on the size effect law. These sizes are shown in Table 3.2. The geometry is kept constant using the same relation between the crack length, a_0 , and the width, $2w$ keeping the length large enough, i. e. $L=250$ mm [16]. The initial crack of the specimens was performed using a coated diamond thread wire with a diameter of 0.3 mm.



Specimen label	Geometric parameters [mm]				
	$2w$	$2w_N$	a_0	L	l
A	15	6	4.5		
B	20	8	6.0		
C	25	10	7.5	250	170-180
D	30	12	9.0		
E	35	14	10.5		

Table 3.2: Specimen geometry. L is the length of the specimen and l is the free clamping.

Three specimens were tested for each size and each conditioning at a 1 mm/min displacement rate, using an MTS 810 machine with a 250 kN load cell.

Moreover, three tensile specimens for each conditioning have been tested to obtain the elastic properties of the laminate and the ultimate strength, σ_u . The ASTM D3039M standard [154] have been followed and same MTS machine with a 250 kN load cell has been used.

3.2.1 Hygrothermal conditions

The three conditionings considered for this study are: As Received and Room Temperature (AR/RT); 85% RH and RT (WET/RT); and 85% RH and 120°C (WET/HOT).

The choice of both humidity and temperature for the test campaign was based on the results of a previous Dynamic Mechanical Thermal Analysis (DMA). These results show that the T_g is around 173.74°C for AR specimens, while it decreases to 156.71°C for wet specimens. Additionally, DMA reveals that the elastic modulus is constant from RT to HOT (120°C) conditions.

Furthermore, the extreme 85% RH is representative of a tropical area [30]. On the other hand, the testing temperature of 120°C has been chosen, so that the failure mechanisms could be analyzed without achieving a rubbery behavior.

Wet specimens were conditioned according to prEN 2823 [155], in a climatic chamber at 80°C/85% RH during approximately 1700 hours, until achieving the equilibrium state, so the specimens were tested with 1.03 % moisture content.

3.2.2 Fractography

After testing, Scanning Electron Microscopy (SEM) images were taken with a Zeiss DSM 960 scanning electron microscope and the digital images were collected and processed using ESPRIT 1.9 BRUKER program. The samples were sputtered with a 22.5 nm gold layer a 1.5KV, deposition current at 30 mA, deposition time 2 minutes.

3.3 Data reduction and results

3.3.1 DEN-T test and data reduction

The data reduction method is developed in the recent work by Catalanotti et al. [16], which relates the size effect law of DEN-T specimens (strength versus specimen width: $\sigma_u = \sigma_u(w)$), with the crack resistance curve of the composite laminate [83].

The fracture toughness can be measured by the Energy Release Rate (ERR), \mathcal{G} , also known as fracture energy [74]. The ERR for a crack propagation in mode I of any orthotropic planar specimen with its principal directions aligned with the crack can be expressed as:

$$\mathcal{G}_I = \frac{1}{E} \sigma^2 w \kappa^2(\alpha, \rho, \lambda) \quad (3.1)$$

where σ is a stress measure (for DEN-T usually the mean gross or net stress), w a measure of specimen size, in this case the width, E the young modulus (for orthotropic material under plane stress is defined as $\acute{E} = \lambda^{1/4} \left(\frac{1+\rho}{2E_{22}E_{11}} \right)^{-1/2}$, where 1 is the direction normal to the crack), $\alpha = a/w$ is the normalized crack length and ρ and λ are two material properties that accounts form material orthotropy. For plane stress, they are defined as:

$$\lambda = \frac{s_{11}}{s_{22}} \quad \text{and} \quad \rho = \frac{2s_{12} + s_{66}}{2\sqrt{s_{11}s_{22}}} \quad (3.2)$$

Chapter 3 Hygrothermal effects on the translaminar fracture toughness: CP laminates

where s_{ij} are the components of the compliance matrix. The orthotropic rescaling property of planar elasticity allows the elastic stress field of a set of orthotropically rescaled specimens to be defined by changing the material parameter λ [156]. Consequently, for the DEN-T specimen the rescaling depends on the specimen length (l , distance between the grips). Then, if this length is large enough, the parameter κ does not depend on λ : $\kappa(\alpha, \rho)$, the specimens tested are under these circumstances according to Catalanotti's results. Bao [157] presents the parameter κ for $0 < \rho < 4$ and then Catalanotti increases the applicability up to $\rho < 20$, covering the typical values of cross-ply laminates.

The determination of the R-curve from the size effect law results in a curve that depends on the material and on specimen geometry but is independent of the specimen size [84, 85, 158, 159]. The ultimate strength with respect to the specimen size can be expressed as $\frac{1}{w\sigma_u^2} = \dot{A}\frac{1}{w} + \dot{C}$, where \dot{A} and \dot{C} are two parameters fitted with the experimental results and are related with the fracture toughness and the equivalent l_{fpz} as [16, 83]:

$$\mathcal{G}_c = \mathcal{R}_{ss} = \frac{\kappa_0^2}{\dot{E}} \frac{1}{\dot{C}} \quad \text{and} \quad l_{fpz} = \frac{\kappa_0}{2\dot{\kappa}_0} \frac{\dot{A}}{\dot{C}} \quad (3.3)$$

where $\kappa_0 = \kappa |_{\alpha=\alpha_0}$, $\dot{\kappa} = \frac{\partial \kappa}{\partial \alpha}$ and $\dot{\kappa}_0 = \frac{\partial \kappa}{\partial \alpha} |_{\alpha=\alpha_0}$. With these material parameters it is possible to define the R-curve with the following expressions:

$$\mathcal{R} = \mathcal{G}_c \frac{\kappa \dot{\kappa}}{\kappa_0 \dot{\kappa}_0} \frac{\Delta a}{l_{fpz}} \quad \text{and} \quad \Delta a = l_{fpz} \frac{2\dot{\kappa}_0}{\kappa_0} \left[\frac{\kappa}{2\dot{\kappa}} - \alpha + \alpha_0 \right] \quad (3.4)$$

Obviously, this R-curve depends on the geometry but not on specimen size; so it is useful to compare two different materials if the specimen geometry is the same.

3.3.2 R-curve results

The corresponding properties of the laminate without initial notch are reported in Table 3.3.

Tensile test results confirm that the elastic modulus does not change for the considered range of conditionings, which indicates that the testing temperatures do not achieve the T_g .

3.3 Data reduction and results

Conditioning	Laminates properties									
	E_{xx} [GPa]		ν_{xy} [-]		G_{xy} [GPa]	σ_u [MPa]		\dot{E} [GPa]	ρ [-]	λ [-]
	Average	S.D.	Average	S.D.		Average	S.D.			
AR/RT	79.19	1.69	0.041	0.0015	4.2	1580.38	25.51	34.75	9.39	1
WET/RT	80.44	0.70	0.036	0.0150		1582.04	30.34	35.04	9.54	
WET/HOT	80.57	2.78	0.037	0.0066		1546.93	2.75	35.01	9.55	

Table 3.3: Laminate properties. *a* Estimated using Classical Laminate Theory with the UD properties (Table 3.1). *b* S.D.: Standard Deviation.

Results of tensile strength versus specimen width of the DEN-T are shown in Fig. 3.1.

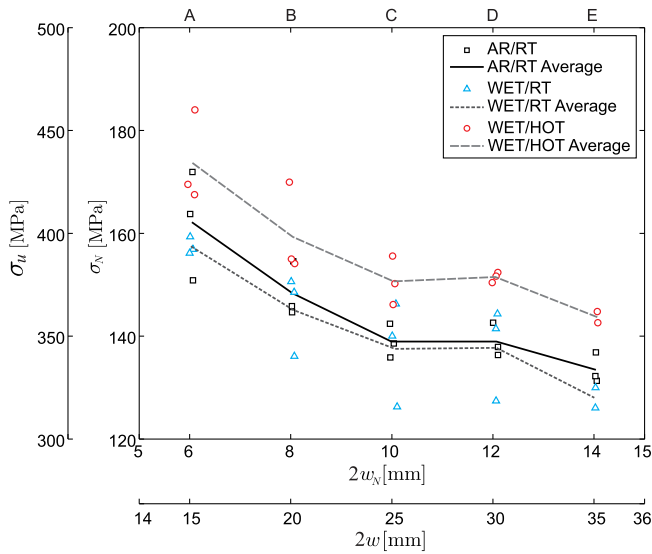


Figure 3.1: Ultimate and nominal stress-size. σ_N and w_u are the nominal stress and the nominal width, while σ_u and w are the ultimate stress and the full width being $\sigma_u = \sigma_N \frac{w}{w_N}$.

As it can be seen, a clear trend of the size effect is observed for each conditioning. The highest values are for WET/HOT, the lowest for WET/RT, and the AR/RT values falls in between slightly above the WET/RT values.

Chapter 3 Hygrothermal effects on the translaminar fracture toughness: CP laminates

The size effect law that best fits for each case is plotted in Fig. 3.2. The R-curves of the laminate are shown in accordance with these size effect laws in Fig. 3.3. The highest fracture toughness value is obtained for the WET/HOT conditions and the lowest one for WET/RT case. On the other hand, differences between $l_{f_{pz}}$ can be observed: $l_{f_{pz}}$ are 3.88 mm, 4.09 mm and 4.39 mm for AR/RT, WET/RT and WET/HOT, respectively.

The size effect charts, shown in Fig. 3.4 are obtained to evaluate the location of the tested specimens. The approximation given by the strength criterion (horizontal line) is calculated using the unnotched tensile test (Table 3.3), which corresponds to very small specimens. The inclined straight line corresponds to the solution given by Linear Elastic Fracture Mechanics (LEFM). The sizes chosen for the specimens tested are in the central part of the chart. Nevertheless, a higher size (approaching the LEFM line) could have provided more experimental information around the \mathcal{G}_c , corresponding to the horizontal part of the R-curve.

3.3 Data reduction and results

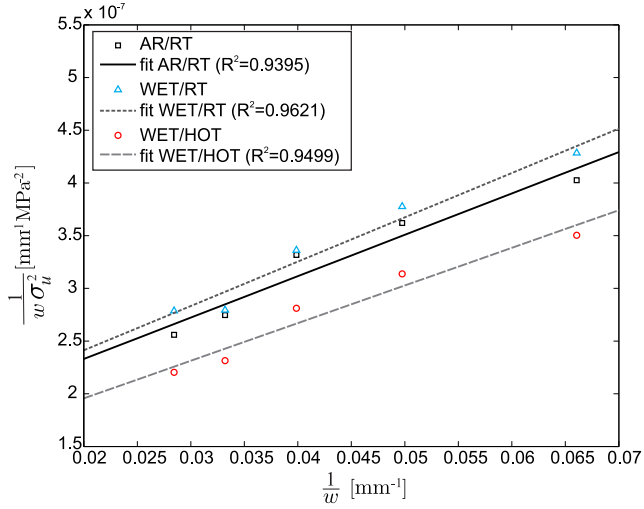


Figure 3.2: Linear regression II of the laminate for AR/RT ($\hat{A} = 3.926 \times 10^{-6} \text{ MPa}^{-2} \text{ mm}^{-1}$, $\hat{C} = 3.09 \times 10^{-7} \text{ MPa}^{-2}$), WET/RT ($\hat{A} = 4.206 \times 10^{-6} \text{ MPa}^{-2} \text{ mm}^{-1}$, $\hat{C} = 3.143 \times 10^{-7} \text{ MPa}^{-2}$) and WET/HOT ($\hat{A} = 3.571 \times 10^{-6} \text{ MPa}^{-2} \text{ mm}^{-1}$, $\hat{C} = 2.484 \times 10^{-7} \text{ MPa}^{-2}$) conditionings.

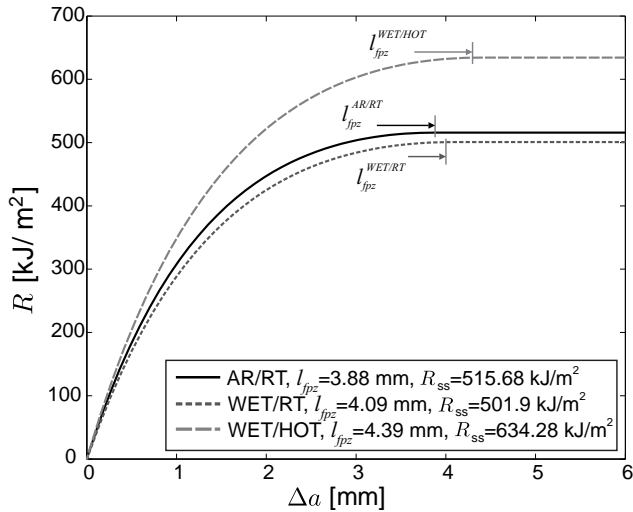
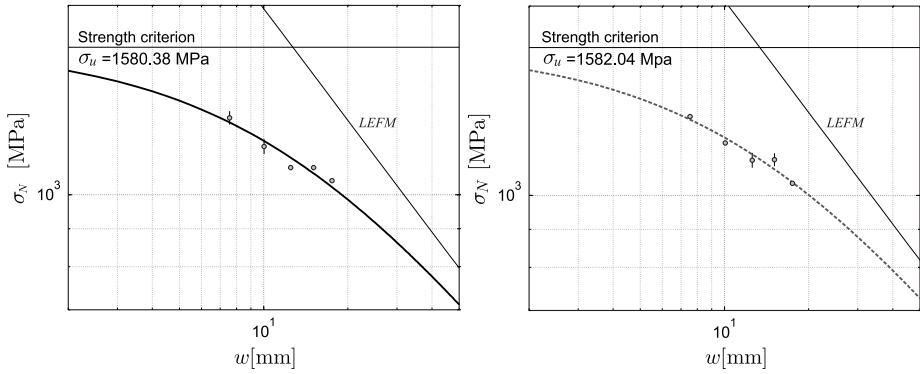
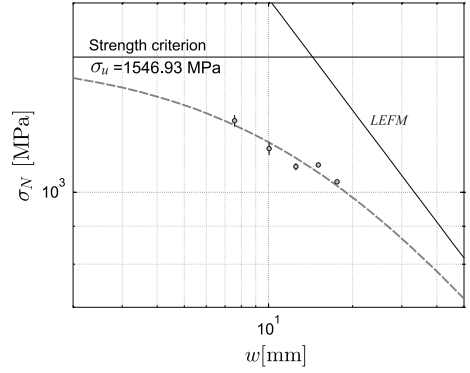


Figure 3.3: Fiber R-curve comparison.

Chapter 3 Hygrothermal effects on the translaminar fracture toughness: CP laminates



(a) Size effects for AR/RT specimens (b) Size effects for WET/RT specimens



(c) Size effects for WET/HOT specimens

Figure 3.4: Size effects graphics.

3.3.3 Fractography

SEM inspections on the fracture planes of broken specimens were performed, taking into account that the failure pattern was similar for each size. These inspections are shown in Fig. 3.5 and correspond to the same size specimens (label C, in Table 3.2) at different conditioning and magnification scales.

3.3 Data reduction and results

- Images from A.1 to C.1 (700 μm scale). Some bundles of fibers and a continuous failure plane are observed in image A.1 for AR/RT, whereas in B.1, WET/RT, the presence and the size of these bundles decreases significantly and that previous continuity of the failure plane has disappeared. For C.1, WET/HOT, these groups of fibers have disappeared completely and every fiber is bared of matrix.
- Images from A.2 to C.2 (100 μm scale). The fiber pull-out length can be analyzed. For instance, in A.2 the bundle of fibers maintains a solid block and no pull-out is observed. Nevertheless, an interlaminar step of length (l^{del}) between 0° and 90° plies is detected. On the other hand, some fiber pull-out are evidenced in B.2 with a stratified failure plane. Finally, in C.2, a broom-like failure is shown where part of the matrix has disappeared and the pull-out length has increased.
- Images from A.3 to C.3 (20 μm scale). In image A.3 the matrix is still bonded to the fiber, whereas in B.3 and C.3 fibers are almost clean, being the pull-out length higher for the last one. Small delaminations between plies were detected in image A.3.

The corresponding failure mechanisms have been sketched in the bottom row of Fig. 3.5. For the first AR/RT conditioning, shown in image A.4, the fiber debonding is small and the fracture is continuous in a plane. However, for WET/RT, the debonding length increases slightly, which is shown through a stratified failure plane. For WET/HOT, in image C.4 the matrix/fiber interface has been weakened and thereby debonding and pull-out lengths increase, which implies that fibers tend to break independently at different lengths.

Chapter 3 Hygrothermal effects on the translaminar fracture toughness: CP laminates

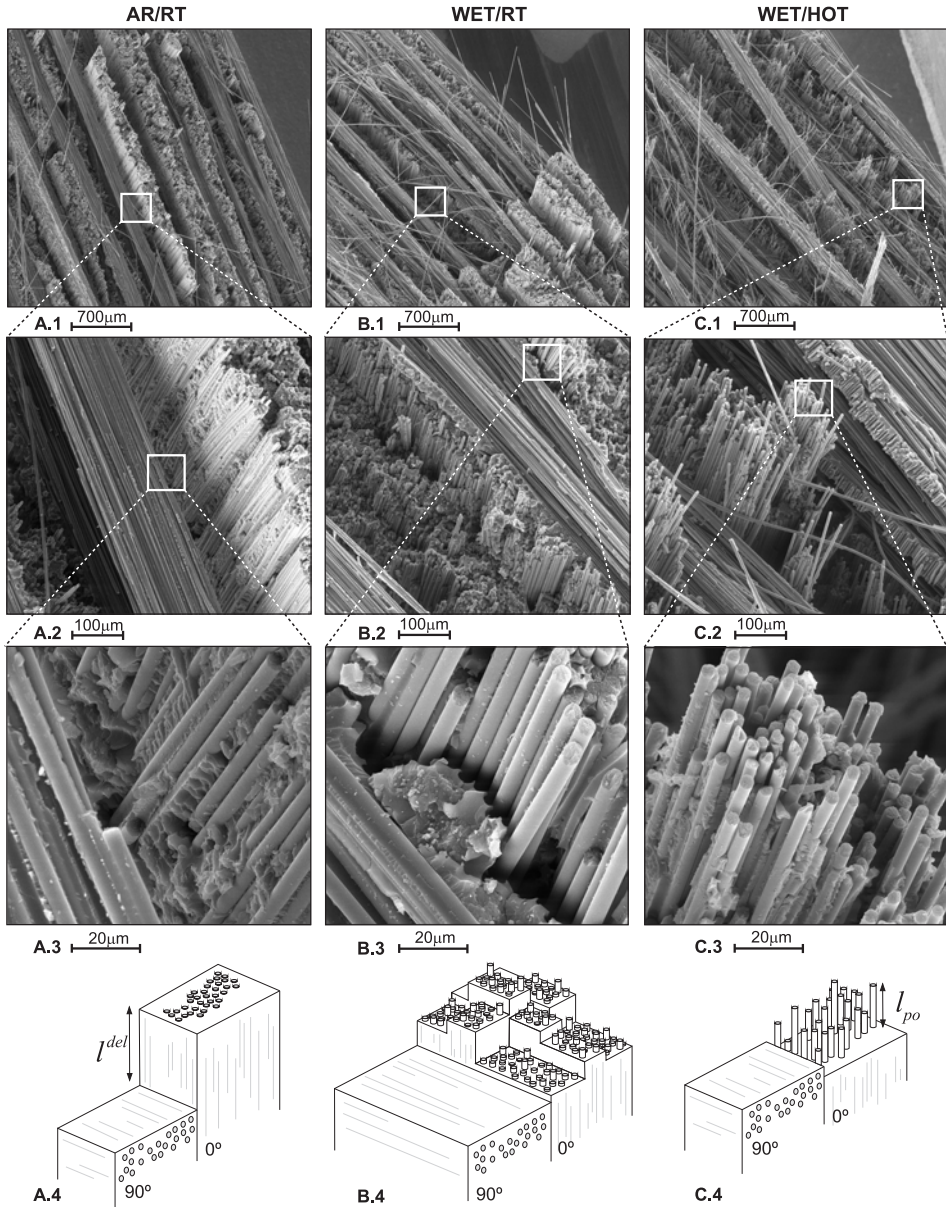


Figure 3.5: SEM fractography comparison between the three conditionings: AR/RT (A), WET/RT (B) and WET/HOT (C).

3.3 Data reduction and results

In Fig. 3.6, the three schematic processes are shown together with additional SEM images. The crack for the third conditioning, WET/HOT, is shown newly in C.5 and C.6. Particularly, in C.6 a high degree of fiber brooming is shown with all the fibers bare and with a wide range of pull-out lengths. In the case of AR/RT, an image taken in a plane perpendicular to fibers is shown in A.5, where no debonding can be appreciated, since fracture has happened in block. However, the image B.5 of a WET/RT specimen, multiple strata can be seen along several failure planes, but with small changes of height and with moderate pull-out lengths.

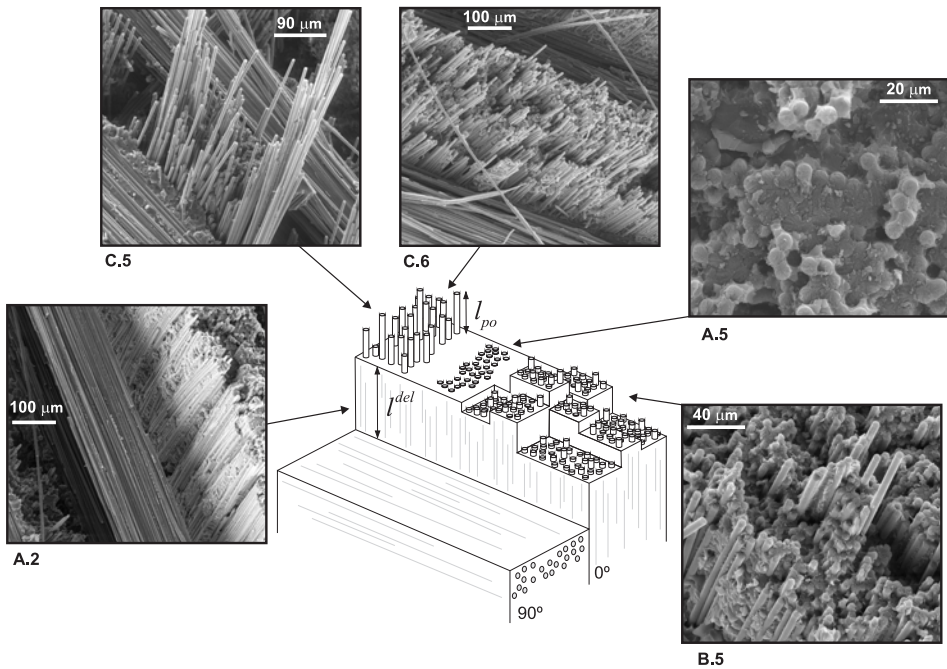


Figure 3.6: SEM fractography comparison between the three conditionings: AR/RT (A), WET/RT (B) and WET/HOT (C).

3.4 Discussion

For both unnotched and DEN-T specimens, the higher coefficient of variation for σ_u was of 5.72% for size C and WET/AR conditioning. This variation has been considered acceptable. Moreover, during the fractography inspection, no visual alteration was appreciated at the microscopic level.

The fracture toughness has shown a value of approximately twice the value obtained by Catalanotti et al. [16, 71] and Teixeira et al. [71] for the same T800S/M21 material, which could be attributed to the increment of the thickness [18, 69] (in [16, 71] the ply thickness is 0.125 mm instead of 0.184 mm). However, the ply properties cannot be considered equivalent, so the results cannot be compared. On the other hand, the T800S/M21 is much tougher than other materials from the literature, such as T300/913 (133 kJ/m²) [19], or T700/AR-2527 (254 kJ/m²) and IM7/8552 (205 kJ/m²) [16]. Teixeira et al. [71] attributed this higher value to the fracture in bundles and the high quantity of fiber pull-outs, where the last is in accordance with Underwood et al. [160] and the recent work developed by Bullegas et al. [70]. Underwood's work demonstrated the influence of the fiber pull-out by a comparison of the low toughness carbon/fiber pull-out with a high toughness carbon/bismaleimide which had a high amount of fiber pull-outs and Bullegas improved the translaminar toughness by triggering an increment of the energy dissipated by fiber pull-out and bundle of fibers. In the fractography inspection shown in Fig. 3.4(a) for AR/RT conditions, no single fiber pull-outs could be found but the fracture takes place in bundles of fibers.

3.4.1 Fractography

SEM fractography analysis has provided an understanding of the differences between the failure mechanisms for each conditioning. These differences are sketched in Fig. 3.7.

- For AR/RT, the small fiber debonding ($l_{d,(1)}$) indicates a strong matrix/fiber interface, which causes a proper stress transfer between fibers, and the distribution of forces are assumed to be more marked at the tip of the crack, as represented

in Fig. 3.7. In addition, a small quantity of energy is dissipated by an interfacial delamination process between plies.

- For WET/RT, the stresses are not transferred as perfectly as for AR/RT due to the weakness of the matrix/fiber interface. Some fiber pull-out ($l_{po(2)}$) and debonding ($l_{d(2)}$) appear. There is a redistribution of stresses, so that the failure plane begins to advance at different heights, in a stratified plane. This behavior causes crack propagation with a longer l_{fpz} than AR/RT and with broken fibers at different heights. Instead of increasing the energy dissipated by pull-out, the absolute energy decreases with respect to AR/RT, which can be explained by the reduction of the IFSS, through the frictional coefficient reduction in the presence of humidity, and the reduction of the energy dissipated by the interfacial delamination region.
- For WET/HOT, the pull-out ($l_{po(3)}$) and debonding lengths ($l_{d(3)}$) are the highest due to a weaker matrix/fiber interface. This weakening implies that the fibers tend to fracture independently at different lengths and, for this reason, the l_{fpz} is longer than WET/RT and AR/RT conditionings (see Fig. 3.7). In this case, the frictional coefficient will be similar to WET/RT, but conversely the l_{po} increases considerably, so the energy dissipated is the highest.

The debonding lengths have been represented in the sketch through the debonding angle (α_i) and the debonding line (D.L.). For the same opening increment (Δ), α_2 increases with moisture and α_3 with moisture and temperature. This angle is related to the quality of the interface.

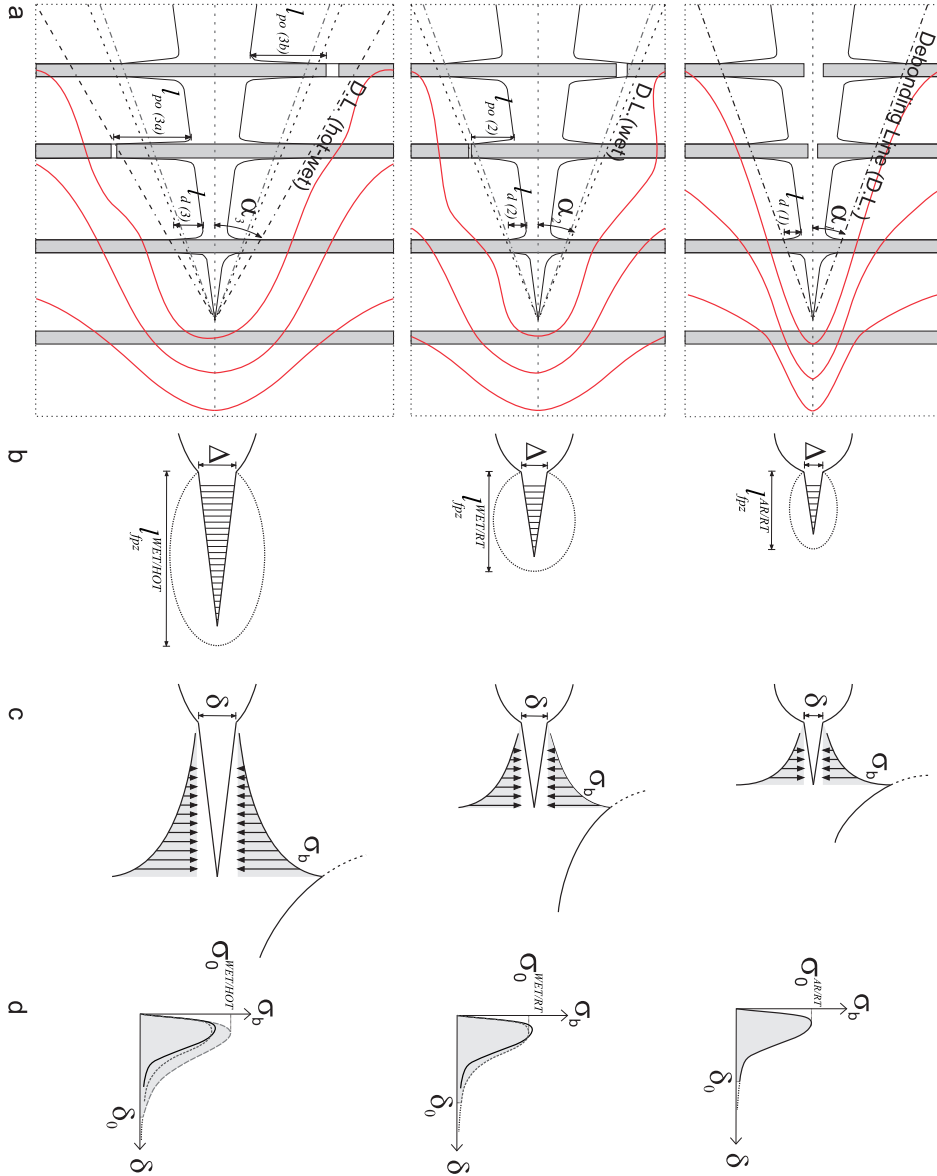


Figure 3.7: Comparison of failure mechanisms for AR/RT, WET/RT and WET/HOT. a) crack propagation sketches, b) fracture process zone, c) supposed stress distribution in l_{fpbz} , d) hypothetical bridging law.

3.4.2 Characterization of translaminar failure mechanisms

The dissipated energy, E_d , can be defined by means of the fracture toughness and the fracture area. That is:

$$E_d = t^{lam} \Delta a \mathcal{G}_c^{lam} = t^{90} \Delta a \mathcal{G}_c^{90} + t^0 \Delta a \mathcal{G}_c^0 + l^{del} \Delta a \mathcal{G}_c^{del} \quad (3.5)$$

where t^{lam} is the laminate thickness, and t^{90} and t^0 are the total thickness for 90° and 0° plies in the laminate. l^{del} is the interfacial length between plies and Δa is the variation of the crack length for the laminate. \mathcal{G}_c^0 is the critical fracture toughness for 0° plies and is defined by $\mathcal{G}_c^0 = \mathcal{G}_{po} + \mathcal{G}_f + \mathcal{G}_m$, where \mathcal{G}_f , \mathcal{G}_m and \mathcal{G}_{po} are the fracture toughness of the fiber, the matrix, and the fiber pull-out, respectively, and $\mathcal{G}_{po} = \mathcal{G}_{po}^{fric} + \mathcal{G}_{po}^{II}$, being \mathcal{G}_{po}^{fric} and \mathcal{G}_{po}^{II} the fracture toughness due to the friction and the mode II opening, respectively. The component \mathcal{G}_c^{90} is the critical fracture toughness for 90° plies. Both \mathcal{G}_c^{90} and \mathcal{G}_m are usually approached to the $\mathcal{G}_c^{del,I}$, which is practically negligible when compared to \mathcal{G}_c^{lam} [12]. Finally, \mathcal{G}_c^{del} is the interlaminar fracture toughness between plies, which will be important for mode II. Only for AR/RT seems relevant. This is in agreement with the results obtained by Asp [12], where $\mathcal{G}_c^{del,II}$ drops when temperature and/or moisture increase. However, as with \mathcal{G}_c^{90} , the values of $\mathcal{G}_c^{del,II}$ are around 1000 times smaller than values of \mathcal{G}_c^{lam} , so their influence is negligible.

The \mathcal{G}_{po}^{fric} for a fiber can be expressed as follows:

$$\begin{aligned} P(x) &= 2\pi r x \tau^{fric} \\ \mathcal{G}_{po}^{fric} &= \int_0^{l_{po}} P(x) dx = \pi r_f \tau^{fric} l_{po}^2 \end{aligned} \quad (3.6)$$

$$\mathcal{G}_{po}^{II} = l_{po} 2\pi r_f \mathcal{G}_{int}^{II} \quad (3.7)$$

where x defines the sliding in the fiber direction coordinate, l_{po} is the pull-out length, τ^{fric} is the IFSS, r_f is the fiber radius, and \mathcal{G}_{int}^{II} is the fracture energy stored by the

Chapter 3 Hygrothermal effects on the translaminar fracture toughness: CP laminates

matrix/fiber adhesion. For a group of fiber in a determined area, the fracture toughness due to the pull-out is:

$$\mathcal{G}_{po} = (\mathcal{G}_{po}^{fric} + \mathcal{G}_{po}^{II})N_f = \frac{V_f A}{r_f} l_{po} (l_{po} \tau^{fric} + 2\mathcal{G}_{int}^{II}) \quad (3.8)$$

where N_f is the number of fibers, so it can be defined as $N_f = V_f \frac{A}{A_f}$, being A the fracture area $A = t_0 \Delta a$, A_f the fiber area and V_f the fiber volume. N_f will be constant and $(\mathcal{G}_{po}^{fric} + \mathcal{G}_{po}^{II})$ will be variable.

From this relation, some questions can be analyzed: when moisture content is absorbed, the interface fiber-matrix is weaker, the frictional coefficient decreases and, then, the IFSS for WET/RT and WET/HOT is lower. This decrease in the frictional coefficient is in agreement with Biro et al [22], who obtained two values of τ^{fric} for two moisture contents, being τ^{fric} lower when moisture increases. Consequently, \mathcal{G}_{po}^{fric} decreases. Moreover, the adhesion between components has been deteriorated, so \mathcal{G}_{po}^{II} decreases as well. However, when temperature is introduced in the test, the absolute pull-out fracture toughness (\mathcal{G}_{po}) increases considerably, which can be explained through the highest value of l_{po} .

3.5 Conclusions

Hygrothermal effects on translaminar fracture toughness of the 0° ply for the T800S/M21 material have been evaluated by using the Double Edge Notched Tensile tests. Three different conditionings have been considered: AR/RT, WET/RT and WET/HOT.

The values of the translaminar fracture toughness are 515.68 kJ/m² for AR/RT, 501.90 kJ/m² for WET/RT, and 634.28 kJ/m² for WET/HOT conditions, with a good repeatability between the different specimens of each batch. The respective values of the fracture process zone are 3.88 mm, 4.09 mm, and 4.39 mm.

The fractography study has been essential to associate the different failure mechanisms for each conditioning and results, where the main observation has been the relevance of the fiber pull-out and the quality of the fiber/matrix interface and the fracture in bundles of fibers. The main differences for each conditioning are as follows:

3.5 Conclusions

- The fracture of the specimens with laboratory conditions showed a clean fracture in bundles of fibers, without pull-outs, which indicates a suitable transfer of stresses between fibers due to a good fiber/matrix adhesion.
- Moisture affect directly the fiber/matrix interface, causing a weakening adhesion and short fiber pull-outs appear, increasing the fracture process zone a 5.4%. Frictional coefficient between constituents decreases, which reduces a 2.7% the fracture toughness for the WET/RT conditioning.
- Interaction between moisture and temperature causes a strong weakening of the fiber/matrix interface. A broom-like fracture appeared with larger fiber pull-outs. This failure mechanisms increases a 23.0% the energy dissipated and a 13.1% the fracture process zone.

4 | Hygrothermal effects on the translaminar fracture toughness of quasi-isotropic carbon/epoxy laminates

Abstract. Double edge notched tensile specimens have been tested to analyze hygrothermal effects on the translaminar fracture toughness of three different quasi-isotropic laminates, which have been chosen to show the ply thickness and mismatch angle effects. A conventional laminate (L1-CV), a conventional with ply clustering (L2-CV-PC) and a non-conventional laminate (L4-nCV) were tested under as-received and room temperature (AR/RT), wet-room temperature (WET/RT) and wet-high temperature (WET/HOT). The L2-CV-PC and L4-nCV laminates did not obtain the translaminar fracture toughness because clustered plies induce delamination processes. However, for L1-CV, the WET/HOT conditioning had the highest fracture toughness value, WET/RT had the lowest, and the AR/RT value was slightly larger than the WET/RT value. As for the failure process zone length, WET/HOT had the longest and AR/RT, the shortest. Scanning electronic microscopy survey has allowed the failure mechanisms to be analyzed, which link the quality of the fiber/matrix interface with the results.

Part III

Concluding remarks

5 | Conclusions

The present thesis covers a study about how the hygrothermal conditions affect Carbon Fiber Reinforced Polymers (CFRP). In the first part of the work, hygrothermal loads are considered within an optimization procedure for stiffened panels, which is developed in Chapter 2. In the second part, an experimental test campaign to determine translaminal fracture toughness under several hygrothermal conditions is performed. The results of this test campaign have been analyzed and discussed in Chapter 3 and Chapter 4.

5.1 Optimization of stiffened panels

Mass reduction is a priority in aeronautical structures, which are generally subjected to a wide range of environmental conditions in spite of not being considered in the common optimization problems. The large amount of combinations between mechanical and hygrothermal loadings, which need to be considered, increase the computational cost in a procedure using FE analysis.

With the aim of reducing the mass together with failure considerations, the optimization procedure proposed in Chapter 2, which consists of the interaction between an Artificial Neural Network (ANN) system and a Genetic Algorithm (GA), is able to reduce the computational cost that the use of FE analysis could require for a group of subproblems, considering both mechanical and hygrothermal loads.

This system allows the optimum panel to be obtained under a compressive load, for a combination of seven subproblems characterized by different temperature ranges and

moisture presence. The principal advantage of this scheme is that the system decomposed in seven cases helps to analyze the hygrothermal effects with negative or positive thermal variations. This tool reduced the computational cost about 92.8 %, obtaining the optimal panel for three different objectives: mass of the panel, hygrothermal strain and tension between stringers and skin.

The Non-dominated Sorting Genetic Algorithm II has demonstrated to be a good and fast method to solve multi-objective problems.

The ANN system has been a useful approximation method, which allows different groups of subproblems to be included in a global optimization problem by using a training set extracted from FE analysis. The drawback of this kind of approximation techniques is the time required to design their internal architecture to obtain the suitable behavior.

5.2 Translaminar fracture toughness

A lack of the understanding of the failure behavior of the composite under hygrothermal effects has been detected, specially, in the field of translaminar fracture toughness. To analyze these effects, an experimental test campaign for a cross-ply laminate and three quasi-isotropic laminates have been conducted for the T800S/M21 material. These three quasi-isotropic laminates were chosen in order to compare the ply thickness effect and the mismatch angle on the translaminar fracture toughness, so each laminate is described as a conventional laminate, a conventional laminate with ply clustering and a non-conventional laminate with larger mismatch angles.

The test method used is based on the Double Edge Notched Tensile (DEN-T) specimen. The main conclusions obtained under laboratory conditions (AR/RT) are as follows:

- The resistance curve was obtained for the 0° plies by the cross-ply laminate, resulting a high fracture toughness of 515.68 kJ/m² and a fracture process zone of 3.88 mm.
- This kind of test is suitable to obtain the fracture toughness of tougher materials.

5.2 Translaminar fracture toughness

- The resistance curve was obtained for only one of the three quasi-isotropic laminates: the conventional laminate without ply clustering with a fracture toughness value of 247.46 kJ/m² and a length of fracture process zone of 7.88 mm.
- The resistance curve for laminates with thick plies or ply clustering and laminates with larger mismatch angles cannot be obtained using this method because these kind of laminates are prone to experience large delaminations during testing. These delaminations dissipate a considerable amount of energy which interferes with the energy to be measured in the test.
- A wider range of sizes of the specimens is recommended but often the testing machines do not allow to test larger sizes due to limitations on clamping widths.

Regarding the hygrothermal effects, a second conditioning with high relative humidity of 85% at room temperature (WET/RT) and a third conditioning with 85% RH at 120°C (WET/HOT) were considered and compared with the baseline AR/RT conditioning.

The resistance curve has been obtained for each conditioning for both cross-ply and conventional quasi-isotropic laminates, concluding the following observations:

- The shortest fracture toughness zone lengths were for the baseline conditioning.
- The presence of moisture reduces slightly the fracture toughness and enlarges the fracture process zone with respect to those values obtained with the baseline conditioning. The test performed revealed a decrease of the fracture toughness of 2.7% for the cross-ply laminate and 9.6% for the quasi-isotropic laminate and an increment of fracture process zone of 5.4% and 3.6%, respectively.
- Combination of moisture and temperature causes the highest values of fracture toughness and the largest fracture process zone lengths. The increment of the fracture toughness was of 23.0% for the cross-ply and 58.5% for the quasi-isotropic laminate while the fracture process zone length increased a 13.1% and a 18.0%, respectively.
- The behavior under hygrothermal conditions was similar in both cases, being the failure process zones longer for the quasi-isotropic laminate. Also, the dif-

Chapter 5 Conclusions

ferences between each conditioning were generally more accentuated for the quasi-isotropic laminate.

Scanning Electronic Microscopy analysis has been essential to describe the failure mechanisms and the characterization of translaminal failure mechanisms analytically by a hypothetical bridging law. The general remarks about this analysis and the characterization of translaminal fracture toughness can be summarized as follows:

- The quality of the matrix/fiber interface is decisive in the fracture toughness, the type of failure and the fracture process zone length. The weakening of this interface causes an unsuitable stress transfer between fibers.
- Hygrothermal conditions affect strongly the quality of the interface, which turns out to be a key factor in translaminal fracture. The effects have been analyzed by the frictional coefficient and the fiber pull-out:
 - The baseline AR/RT conditioning exhibited a clean fracture, where the fibers broke in block and no pull-outs appeared.
 - The frictional coefficient between matrix and fiber is reduced by the moisture, which weakens the adhesion between constituents. Additionally, the fracture is produced in several heights, showing a plane distributed by strata.
 - The interaction between moisture and temperature originates a fracture with longer fiber pull-outs, due to a larger weakening of the matrix/fiber interface.
 - The fiber pull-out length depends on the quality of the matrix/fiber interface and is a relevant factor of the fracture toughness and the length of the fracture process zone.

5.3 General conclusions

This work has been focused on two different levels of the building block approach: structural element and characterization of the material. The contributions previously noted are only a short part along the building block approach.

The cost of a complete experimental campaign increases considerably if several environmental conditions are considered, not only because of the cost of the material, but also because of the time required to the material conditioning. Much further work is needed about how the hygrothermal conditions affect the composite materials taking into account the zones which are more sensitive to these effects: matrix/fiber interface, surfaces between plies, surfaces between elements and the zones rich in matrix.

6 | Suggestions for future research

6.1 Translaminar fracture toughness characterization

Design of a suitable test and analytical tools

Certain limitations have been identified concerning the test method used to measure the translaminar fracture toughness, so further research could be conducted in the experimental investigation of a suitable procedure for this material property for any laminate.

- To define a suitable geometry for Compact Tension (CT) tests or modified CT tests. This kind of test has the advantage of propagating the crack in a stable form. However, there is no standard for composite materials, which accounts the corresponding laminate anisotropy. Some materials can be tested with the standard geometry for metallic materials, but for tougher materials and quasi-isotropic laminates this procedure is not suitable because of buckling instability. A thorough study of the buckling instability has to be analyzed in order to achieve an optimum geometry.
- To define a suitable test with stable crack propagation and develop a linked method to determine the cohesive law of the material or the laminate. DEN-T test method does not allow to obtain the cohesive law and its form could modify the resulting fracture toughness. Through DEN-T method, it is difficult to test wider specimens, which could contribute to define the horizontal part of the resistance curve.

Chapter 6 Suggestions for future research

Moreover, the changes of the detected failure mechanisms under hygrothermal conditions could alter the cohesive law of the material.

- An experimental study of DEN-T cross-ply specimens with different ply clustering is needed in order to analyze if this kind of test is suitable to thick plies.

Hygrothermal effects on translaminar fracture toughness

In order to improve the understanding about how hygrothermal effects can affect the translaminar fracture toughness and its associated failure mechanisms, some issues have to be analyzed, which are:

- The characterization of cold conditions (-55°) on translaminar fracture toughness for cross-ply and quasi-isotropic laminates. This temperature without moisture is also an extreme condition because of the high level of residual stresses between fiber and matrix. However, the interface could result less weakened without the presence of the moisture.
- The characterization of high temperature without moisture on translaminar fracture toughness for cross-ply and quasi-isotropic laminates. This condition could help to understand the interaction between moisture and temperature and how it affect the interface matrix/fiber.
- The characterization of ply thickness size effect with hygrothermal effects. Lafan et al. [18] reported an experimental study with AR/RT conditions about the influence of the thickness on the translaminar fracture toughness of the fiber using CT, obtaining an increment for thicker 0° ply laminates, which is attributed to an increment in fiber pull-out. A study of the ply thickness size effect with hygrothermal effects could be relevant to detect the failure mechanisms that cause the increment of the toughness with thicker plies.
- The characterization of the Interfacial Shear Strength by a single-experimental model system under hygrothermal loads.

6.2 Constitutive model for FE simulations

Until now, there is no tool able to account the hygrothermal loads because of the lack of understanding about this field, so the development of a constitutive model able to predict the behavior of a laminate under hygrothermal effects could be performed once the failure mechanisms are analyzed for all possible combinations of moisture and temperature.

6.3 Stiffened panels

Once the material is characterized under hygrothermal effects and virtual testing allows a validation of the first step in the building block approach, the study in the level of structural elements could be performed.

Firstly, an experimental study in order to analyze the hygrothermal effects on the joint between skin and stringers has to be tested. As explained the Chapter 1, residual stresses are very important between constituents (microscale), between plies (mesoscale) and between structural elements (macroscale) and in a future study of stiffened panels should be considered, over all, between skin and stringers.

Secondly, the tool developed in Chapter 2 could be used to obtain an optimum panel under any combination of hygrothermal and mechanical loadings. Moreover, the study could consider the following improvements:

- To include the hygrothermal effects on the study of buckling instability in stiffened panels.
- To consider other type of stringer and run-outs finishing. Topology optimization could be used for a first step of the procedure in order to choose the shape of the stringer.
- To contrast the ANN system with other approximation techniques.
- To use a GA to improve the ANN and consequently, to reduce the time required to train and design the ANN.

Chapter 6 Suggestions for future research

- To add the stacking sequence as design variable in the optimization problem, which requires a previous analysis of the influence of the temperature and moisture on the variation of the stacking sequence of the laminate.

Part IV

Bibliography

Bibliography

- [1] Gu Y, Liu H, Li M, Li Y, Zhang Z. Macro- and micro-interfacial properties of carbon fiber reinforced epoxy resin composite under hygrothermal treatments. *Journal of Reinforced Plastics and Composites* 2014;33(4):369–79.
- [2] Hu B GJ, G V. Effet d'environnement hygrothermique sur les comportements mécaniques des composites à matrice époxyde. In: *JNC; Proceedings of the 11th Conference of the French Society for Composite Materials*. Arcachon, France; 1998, p. 255–64.
- [3] Botelho E, Pardini L, Rezende M. Hygrothermal effects on the shear properties of carbon fiber/epoxy composites. *Journal of Materials Science* 2006;41(21):7111–8.
- [4] Mechanical properties and failure behaviour of carbon fibre-reinforced polymer composites under the influence of moisture. *Composites Part A: Applied Science and Manufacturing* 1997;28(6):595 – 604.
- [5] Ray B. Temperature effect during humid ageing on interfaces of glass and carbon fibers reinforced epoxy composites. *Journal of Colloid and Interface Science* 2006;298(1):111–7.
- [6] Cunha JAP, Costa ML, Rezende MC. Study of the hygrothermal effects on the compression strength of carbon tape/epoxy composites. *Lat Am J Solids Stru* 2008;:157–170.
- [7] Barbero EJ. *Introduction to composite materials design*. Second edition. CRC Press. Taylor & Francis Group; 2011.
- [8] Kollar LP, Springer GS. *Mechanics of Composite Structures*. Cambridge University Press; 2003.
- [9] Hobbiebrunken T, Fiedler B, Hojo M, Ochiai S, Schulte K. Microscopic yielding of CF/epoxy composites and the effect on the formation of thermal residual stresses. *Composites Science and Technology* 2005;65(10):1626 –35.
- [10] Garg A, Ishai O. Hygrothermal influence on delamination behavior of graphite/epoxy laminates. *Engineering Fracture Mechanics* 1985;22(3):413 –27.

BIBLIOGRAPHY

- [11] Wilkins DJ. A comparison of the delamination and environmental resistance of a graphite-epoxy and a graphite-bismaleimide. Naval Air System Command, NAV-GD-0037 1981;
- [12] Asp LE. The effects of moisture and temperature on the interlaminar delamination toughness of a carbon/epoxy composite. *Composites Science and Technology* 1998;58(6):967–77.
- [13] Corporation RKN. *Composite Failure Analysis Handbook. Vol II: Thecnical handbook. Part 2- Atlas of Fractographs.* 1992.
- [14] ASTM E1922-97, Standard Test Method for Translaminar Fracture Toughness of Laminated Polymer Matrix Composite Materials, ASTM International, West Conshohocken, PA, www.astm.org. 2015.
- [15] El-Hajjar R, Haj-Ali R. Mode-I fracture toughness testing of thick section FRP composites using the ESE(T) specimen. *Engineering Fracture Mechanics* 2005;72(4):631 –43.
- [16] Catalanotti G, Arteiro A, Hayati M, Camanho PP. Determination of the mode I crack resistance curve of polymer composites using the size-effect law. *Engineering Fracture Mechanics* 2014;118(0):49 – 65.
- [17] Laffan MJ, Pinho ST, Robinson P, Iannucci L. Measurement of the in situ ply fracture toughness associated with mode I fibre tensile failure in FRP Part I: Data reduction. *Composites Science and Technology* 2010;70(4):606–13.
- [18] Laffan MJ, Pinho ST, Robinson P, Iannucci L. Measurement of the in situ ply fracture toughness associated with mode I fibre tensile failure in FRP Part II: Size and lay-up effects. *Composites Science and Technology* 2010;70(4):614–21.
- [19] Pinho ST, Robinson P, Iannucci L. Fracture toughness of the tensile and compressive fibre failure modes in laminated composites. *Composites Science and Technology* 2006;66(13):2069–79.
- [20] Choi HS, Ahn KJ, Nam JD, Chun HJ. Hygroscopic aspects of epoxy/carbon fiber composite laminates in aircraft environments. *Composites Part A: Applied Science and Manufacturing* 2001;32(5):709–20.
- [21] Zhao S, Gaedke M. Moisture effects on mode ii delamination behavior of carbon/epoxy composites. *Advanced Composite Materials: The Official Journal of the Japan Society of Composite Materials* 1996;5(4):291–307.
- [22] Biro DA, Pleizier G, Deslandes Y. Application of the microbond technique: Effects of hygrothermal exposure on carbon-fiber/epoxy interfaces . *Composites Science and Technology* 1993;46(3):293 – 301.
- [23] ASTM D5229 / D5229M-14, Standard Test Method for Moisture Absorption Properties and Equilibrium Conditioning of Polymer Matrix Composite Materials, ASTM International, West Conshohocken, PA, www.astm.org. 2014.

- [24] Fick A. Über diffusion. Poggendorff's Annalen der Physik und Chemic. 1855.
- [25] Whitaker AF, Finckenor MM, Dursch HW, Tennyson R, Young PR. Environmental effects on composites. In: Peters S, editor. Handbook of Composites. Springer US; 1998, p. 810–21.
- [26] Berketis K, Tzetzis D, Hogg P. The influence of long term water immersion ageing on impact damage behaviour and residual compression strength of glass fibre reinforced polymer (gfrp). *Materials & Design* 2008;29(7):1300–10.
- [27] Bao LR, Yee AF. Effect of temperature on moisture absorption in a bismaleimide resin and its carbon fiber composites. *Polymer* 2002;43(14):3987–97.
- [28] Komorowski JP. National Aeronautical Establishment. 20974; National Research Council of Canada, Aeronautical Note NAE-AN-4, NRC; 1983.
- [29] Vinson JR. Advanced composite materials: environmental effects. ASTM STP 658 American Society for Testing and Materials; 1978.
- [30] MIL-HDBK-17-1F (Military Handbook). Composite Materials Handbook: Polymer Matrix Composites Guidelines for Characterization of Structural Materials; vol. 1. Department of Defense of USA; 2002.
- [31] Sateesh N, Rao PS, Ravishanker DV, Satyanarayana K. Effect of moisture on gfrp composite materials. *Materials Today: Proceedings* 2015;2(4-5):2902–8. 4th International Conference on Materials Processing and Characterization.
- [32] Weitsman Y. Anomalous fluid sorption in polymeric composites and its relation to fluid-induced damage. *Composites Part A: Applied Science and Manufacturing* 2006;37(4):617–23. Internal Stresses in Polymer Composites.
- [33] Ray B. Temperature effect during humid ageing on interfaces of glass and carbon fibers reinforced epoxy composites. *Journal of Colloid and Interface Science* 2006;298(1):111–7.
- [34] Greenhalgh ES. Failure analysis and fractography of polymwer composites. Woodhead publishing in materials; 2009.
- [35] Kellogg KG, Kallmeyer AR, Chinnam RB, Dutra PK. Influence of moisture and low temperature onnotched izod impact toughness in a pultruded reinforced composite. *Proceeding of the Annual International Offshore and Polar Engineering Conference* 1999;.
- [36] Friedrich K. Application of fracture mechanics to composite materials. *Composite Materials Series*, 6. ELSEVIER; 1989.
- [37] Bond DA, Smith PA. Modeling the transport of low-molecular-weight penetrants within polymer matrix composites. *Applied Mechanics Review* 2006;59(5):249–68.

BIBLIOGRAPHY

- [38] Sobrinho LL, Calado VMA, Bastian FL. Effects of rubber addition to an epoxy resin and its fiber glass-reinforced composite. *Polymer Composites* 2012;33(2):295–305.
- [39] Hexcel, editor. Hexply M21- Product Data. 2010.
- [40] Sigl LS, Evans AG. Effects of residual stress and frictional sliding on cracking and pull-out in brittle matrix composites. *Mechanics of Materials* 1989;(8):1–12.
- [41] Nair SV. Crack-wake debonding and toughness in fiber- or whisker-reinforced brittle-matrix composites. *J Am Ceram Soc* 1990;73(10):2839–47.
- [42] Charalambides PG, Evans AG. Debonding properties of residually stressed brittle-matrix composites. *J Am Ceram Soc* 1989;72(5):746–53.
- [43] Evans AG, He MY, Hutchinson JW. Interface debonding and fiber cracking in brittle matrix composites. *J Am Ceram Soc* 1989;72(12):2300–303.
- [44] Deng S, Ye L. Influence of fiber-matrix adhesion on mechanical properties of graphite/epoxy composites: II. interlaminar fracture and nplane shear behavior. *Journal of Reinforced Plastics and Composites* 1999;18:1041–57.
- [45] Deng S, Ye L. Influence of fiber-matrix adhesion on mechanical properties of graphite/epoxy composites: I. tensile, flexure and fatigue properties. *Journal of Reinforced Plastics and Composites* 1999;18:1021–40.
- [46] Roulin-Moloney AC. *Fractography and failure mechanisms of polymers and composites*. 1989.
- [47] May C. *Epoxy Resins: Chemistry and Technology*. 1988.
- [48] Riew CK, Guilham JK. Rubber modified thermoset resins. *Adv Cham Ser* 1984;208.
- [49] Zhang M. A review of the epoxy resin toughening. *Environmental Degradation of Insustrial Composites* 2003;.
- [50] Greenhalgh E, Lewis A, Bowen R, Grassi M. Evaluation of toughening concepts at structural features in CFRP-Part I: Stiffener pull-off. *Composites Part A: Applied Science and Manufacturing* 2006;37(10):1521–35.
- [51] Yee A, Pearson R. Toughening mechanisms in elastomer-modified epoxies - part 1 mechanical studies. *Journal of Materials Science* 1986;21(7):2462–74.
- [52] Lin Y, Chen X. Investigation of the effect of hygrothermal conditions on epoxy system by fractography and computer simulation. *Materials Letters* 2005;59(29-30):3831 –6.

BIBLIOGRAPHY

- [53] Telford R, Katnam KB, Young TM. The effect of moisture ingress on through-thickness residual stresses in unsymmetric composite laminates: A combined experimental-numerical analysis. *Composite Structures* 2014;107:502 –11.
- [54] White SR, Hahn HT. Cure cycle optimization for the reduction of processing-induced residual stresses in composite materials. *Journal of Composite Materials* 1993;27(14):1352–78.
- [55] Ogi K, Kim HS, Maruyama T, Takao Y. The influence of hygrothermal conditions on the damage processes in quasi-isotropic carbon/epoxy laminates. *Composites Science and Technology* 1999;59(16):2375 –82.
- [56] Greenhalgh E, Singh S. The effect of moisture, matrix and ply orientation on delamination resistance, failure criteria and fracture morphology in cfrp. *ASTM*; 2002, p. 221–34.
- [57] Boukhoulda BF, Adda-Bedia E, Madani K. The effect of fiber orientation angle in composite materials on moisture absorption and material degradation after hygrothermal ageing. *Composite Structures* 2006;74(4):406–18.
- [58] A. C. Orifici H. Abramovich IHAKTWRSTJB. Failure in CFRP L-stiffened panel sections under postbuckling loads. *COCOMAT. 2nd International Conference on Buckling and Postbuckling Behaviour of Composite Laminated and Shell Structures*; 2008,.
- [59] Adhesively bonded joints in composite materials: An overview. *Proceedings of the Institution of Mechanical Engineers Part L Journal of Materials Design and Applications*; 2009.
- [60] da Silva LF, Adams R. Joint strength predictions for adhesive joints to be used over a wide temperature range. *International Journal of Adhesion and Adhesives* 2007;27(5):362 –79.
- [61] Greenhalgh E, Hiley M. The assessment of novel materials and processes for the impact tolerant design of stiffened composite aerospace structures. *Composites Part A: Applied Science and Manufacturing* 2003;34:151 –61.
- [62] Tong L, Mouritz AP, Bannister MK. *3D Fibre Reinforced Polymer Composites*. Elsevier; 2002.
- [63] Kumari S, Sinha PK. Effect of transverse stitching and hygrothermal environment on composite wing T-Joints. *Journal of Reinforced Plastic and Composites* 2003;22(18):1705–28.
- [64] Partridge I, Cartie D. Delamination resistant laminates by z-fiber δ pinning: Part i manufacture and fracture performance. *Composites Part A: Applied Science and Manufacturing* 2005;36(1):55–64.
- [65] Laffan MJ, Pinho ST, Robinson P, McMillan AJ. Translaminar fracture toughness testing of composites: A review. *Polymer Testing* 2012;31(3):481–9.
- [66] Kessler M. *Advanced Topics in Characterization of Composites*. Trafford Publishing; 2004.

BIBLIOGRAPHY

- [67] Blanco N, Trias D, Pinho ST, Robinson P. Intralaminar fracture toughness characterisation of woven composite laminates. Part I: design and analysis of a compact tension (CT) specimen. *Engineering Fracture Mechanics* 2014;131:349–60.
- [68] Laffan MJ, Pinho ST, Robinson P, McMillan AJ. Translaminar fracture toughness: The critical notch tip radius of 0° plies in CFRP. *Composites Science and Technology* 2011;72(1):97–102.
- [69] Pinho ST, Teixeira R, Robinson P. Does the translaminar fracture toughness of a 0° ply-block depend on its thickness? 7th International Conference on Composites Testing and Model Identification, Comptest 2015; 2015,.
- [70] Bullegas G, Pinho ST, Pimenta S. Improving translaminar toughness of thin-ply laminates. 7th International Conference on Composites Testing and Model Identification, Comptest 2015; 2015,.
- [71] Teixeira RF, Pinho ST, Robinson P. Translaminar ply fracture toughness of advanced composites. 18th International Conference on Composite Materials (ICCM18); 2011,.
- [72] Laffan MJ, Pinho ST, Robinson P. Mixed-mode translaminar fracture of CFRP: Failure analysis and fractography. *Composite Structures* 2013;95(0):135–41.
- [73] Xu X, Wisnom MR, Mahadik Y, Hallett SR. Scaling of fracture response in over-height compact tension tests. *Composites Part A: Applied Science and Manufacturing* 2015;69:40 –8.
- [74] Anderson TL. *Fracture Mechanics: Fundamentals and Applications*. CRC Press. Taylor & Francis Group; 2005.
- [75] Clements LL. Fractography of unidirectional graphite-epoxy as a function of moisture, temperature and specimen quality. *Journal of Material Science* 1986;21:1853–62.
- [76] Jang-Kyo Kim and Yiu-wing Mai . High strength, high fracture toughness fibre composites with interface control: a review. *Composite science and technology* 1991;41:333–78.
- [77] Jose S, Kumar RR, Jana M, Rao GV. Intralaminar fracture toughness of a cross-ply laminate and its constituent sub-laminates. *Composites Science and Technology* 2001;61(8):1115 –22.
- [78] Li X, Hallett SR, Wisnom MR. Numerical investigation of progressive damage and the effect of layup in overheight compact tension tests. *Composites Part A: Applied Science and Manufacturing* 2012;43(11):2137–50.
- [79] Li X, Hallett SR, Wisnom MR, Zobeiry N, Vaziri R, Poursartip A. Experimental study of damage propagation in over-height compact tension tests. *Composites Part A: Applied Science and Manufacturing* 2009;40(12):1891–9.

BIBLIOGRAPHY

- [80] Mollenhauer D, Ward L, Larve E, Putthanarat S, Hoos K, Hallett S, et al. Simulation of discrete damage in composite Overheight Compact Tension specimens. *Composites Part A: Applied Science and Manufacturing* 2012;43(10):1667–79.
- [81] Erçin G. Stress gradient effects in laminated composites, PhD thesis. University of Porto. 2013.
- [82] Marín L, Trias D, Badalló P, Mayugo JA. On how tough testing toughness can be: fracture toughness of quasi-isotropic carbon/epoxy laminates. In: 17th International Conference on Composite Structures (ICCS17). Porto (Portugal). 2013.
- [83] Bažant ZP, Planas J. Fracture and size effect in concrete and other quasibrittle materials. CRC Press; 1998.
- [84] Bažant ZP, Kazemi MT. Determination of fracture energy, process zone length and brittleness number from size effect, with application to rock and concrete. *International Journal of Fracture* 1990;44(2):111–31.
- [85] Bažant ZP, Kazemi MT. Size effect in fracture of ceramics and its use to determine fracture energy and effective process zone length. *Journal of the American Ceramic Society* 1990;73(7):1841–53.
- [86] Orifici AC, Thomson RS, Herszberg I, Weller T, Degenhardt R, Bayandor J. An analysis methodology for failure in postbuckling skin-stiffener interfaces. *Composite Structures* 2008;86(1-3):186–93.
- [87] Orifici AC, Herszberg I, Thomson RS. Review of methodologies for composite material modelling incorporating failure. *Composite Structures* 2008;86(1-3):194–210.
- [88] Orifici AC, Shah SA, Herszberg I, Kotler A, Weller T. Failure analysis in postbuckled composite T-sections. *Composite Structures* 2008;86(1-3):146–53.
- [89] Ghiasi H, Pasini D, Lessard L. Optimum stacking sequence design of composite materials Part I: Constant stiffness design. *Composite Structures* 2009;90(1):1–11.
- [90] Dorigo M, Maniezzo V, Colomi A. The ant system: optimization by a colony of cooperating agents; vol. 26. 1996.
- [91] Goldberg DE. Genetic algorithms in search, optimization and machine learning. Addison-Wesley Pub. Co.; 1989.
- [92] Holland JH. Adaptation in natural and artificial systems: an introductory analysis with applications to biology, control, and artificial intelligence. MIT Press; 1975.
- [93] Herskovits J, editor. *Advances in Structural Optimization*. 1995.

BIBLIOGRAPHY

- [94] Xu Z, Huang Q, Zhao Z. Topology optimization of composite material plate with respect to sound radiation. *Engineering Analysis with Boundary Elements* 2011;35(1):61–7.
- [95] Querin OM, Toropov VV, Liu D, Lohse-Busch H, Hühne C, Niemann S, et al. Topology and parametric optimization of a lattice composite fuselage structure. 2014.
- [96] Badalló P, Trias D, Lindgaard E. Damage tolerance optimization of composite stringer run-out under tensile load. *Composite Structures* 2015;133:98–104.
- [97] Greenhalgh E, Garcia MH. Fracture mechanisms and failure processes at stiffener run-outs in polymer matrix composite stiffened elements. *Composites Part A: Applied Science and Manufacturing* 2004;35(12):1447–58.
- [98] Queipo N, Haftka R, Shyy W, Goel T, Vaidyanathan R, Kevin Tucker P. Surrogate-based analysis and optimization. *Progress in Aerospace Sciences* 2005;41(1):1–28. Cited By 740.
- [99] Müller B, Strickland MT, Reinhardt J. *Neural Networks. An Introduction*. Springer-Verlag Berlin Heidelberg New York; 1995.
- [100] Bisagni C, Lanzi L. Post-buckling optimisation of composite stiffened panels using neural networks. *Composite Structures* 2002;58(2):237–47.
- [101] Lanzi L, Bisagni C, Ricci S. Neural network systems to reproduce crash behavior of structural components. *Computers and Structures* 2004;82(1):93–108.
- [102] Lanzi L, Giavotto V. Post-buckling optimization of composite stiffened panels: Computations and experiments. *Composite Structures* 2006;73(2):208–20.
- [103] Todoroki A, Sekishiro M. Stacking sequence optimization to maximize the buckling load of blade-stiffened panels with strength constraints using the iterative fractal branch and bound method. *Composites Part B: Engineering* 2008;39(5):842–50.
- [104] Todoroki A, Sekishiro M. New iteration fractal branch and bound method for stacking sequence optimizations of multiple laminates. *Composite Structures* 2007;81(3):419–26.
- [105] Todoroki A, Ishikawa T. Design of experiments for stacking sequence optimization with genetic algorithm using response surface approximation. *Composite Structures* 2004;64(3-4):349–57.
- [106] Rikards R, Abramovich H, Auzins J, Korjakins A, Ozolinsh O, Kalnins K, et al. Surrogate models for optimum design of stiffened composite shells. *Composite Structures* 2004;63(2):243–51.
- [107] Rikards R, Abramovich H, Kalnins K, Auzins J. Surrogate modeling in design optimization of stiffened composite shells. *Composite Structures* 2006;73(2):244–51.

- [108] Badran SF, Nassef AO, Metwalli SM. Y-stiffened panel multi-objective optimization using genetic algorithm. *Thin -Walled Structures* 2009;47(11):1331–42.
- [109] Irisarri FX, Laurin F, Leroy FH, Maire JF. Computational strategy for multiobjective optimization of composite stiffened panels. *Composite Structures* 2011;93(3):1158–67.
- [110] Irisarri FX, Bassir DH, Carrere N, Maire JF. Multiobjective stacking sequence optimization for laminated composite structures. *Composites Science and Technology* 2009;69(7-8):983–90.
- [111] Herencia JE, Weaver PM, Friswell MI. Initial sizing optimisation of anisotropic composite panels with Tshaped stiffeners. *Thin-Walled Structures* 2008;46(4):399–412.
- [112] Ruijter W, Spallino R, Warnet L, de Boer A. Optimization of composite panels using neural networks and genetic algorithms. *Computational Fluid and Solid Mechanics 2003*; Oxford: Elsevier Science Ltd; 2003, p. 2359–63.
- [113] Liu JS, Hollaway L. Design optimisation of composite panel structures with stiffening ribs under multiple loading cases. *Computers and Structures* 2000;78(4):637–47.
- [114] Kaufmann M, Zenkert D, Mattei C. Cost optimization of composite aircraft structures including variable laminate qualities. *Composites Science and Technology* 2008;68(13):2748–54.
- [115] Wang W, Guo S, Chang N, Yang W. Optimum buckling design of composite stiffened panels using ant colony algorithm. *Composite Structures* 2010;92(3):712–9.
- [116] Gigliotti M, Riccio A, Iuspa L, Scaramuzzino F, Mormile L. Weight optimisation of damage resistant composite panels with a posteriori cost evaluation. *Composite Structures* 2009;88(2):312–22.
- [117] Iuspa L, Ruocco E. Optimum topological design of simply supported composite stiffened panels via genetic algorithms. *Computers and Structures* 2008;86(17-18):1718–37.
- [118] Corvino M, Iuspa L, Riccio A, Scaramuzzino F. Weight and cost oriented multi-objective optimisation of impact damage resistant stiffened composite panels. *Computers and Structures* 2009;87(15-16):1033–42.
- [119] Nagendra S, Jestin D, Gürdal Z, Haftka RT, Watson LT. Improved genetic algorithm for the design of stiffened composite panels. *Computers and Structures* 1996;58(3):543–55.
- [120] Marín L, Trias D, Badalló P, Rus G, Mayugo JA. Optimization of composite stiffened panels under mechanical and hygrothermal loads using neural networks and genetic algorithms. *Composite Structures* 2012;94(11):3321–6.
- [121] Marín L, Trias D, Rus G, Badalló P, Martín E. Optimización de paneles rigidizados de materiales compuestos sometidos a cargas termomecánicas. In: IX Congreso Nacional de Materiales Compuestos. Girona (Spain). 2011.

BIBLIOGRAPHY

- [122] Marín L, Trias D, Badalló P, Rus G, Mayugo JA. Optimization of composite stiffened panels under mechanical and hygrothermal loads using neural networks and genetic algorithms. In: SAMPE Student Conference. Paris (France). 2012,.
- [123] Marín L, Trias D, Maimí P, González EV, Guillaumet G. Efectos higrotérmicos en la tenacidad translaminar. In: XI Congreso Nacional de Materiales Compuestos, Móstoles-Madrid (Spain). 2015,.
- [124] Marín L, González EV, Maimí P, Trias D, Camanho PP. Hygrothermal effects on the translaminar fracture toughness of cross-ply carbon/epoxy laminates: failure mechanisms. Submitted to Composite Science and Technology 2015,.
- [125] Marín L, González EV, Maimí P, Trias D, Catalanotti G. Hygrothermal effects on the fracture toughness of quasi-isotropic carbon/epoxy laminates. Submitted to Composites Part A-Applied Science and Manufacturing 2015,.
- [126] de Faria AR, de Almeida SFM. Buckling optimization of plates with variable thickness subjected to nonuniform uncertain loads. *International Journal of Solids and Structures* 2003;40(15):3955 –66.
- [127] Topal U, Uzman U. Thermal buckling load optimization of laminated composite plates. *Thin-Walled Structures* 2008;46(6):667–75.
- [128] Young-Shin L, Yeol-Wha L., Myung-Seog Y, Bock-Sun P. . Optimal design of thick laminated for maximum thermal buckling load. *Journal of Thermal Stresses* 1999;22:3:259–73.
- [129] Ijsselmuiden ST, Abdalla M, Gürdal Z. Thermomechanical design optimization of variable stiffness composite panels for buckling. *Journal of Thermal Stresses* 2010;33(10):977–92.
- [130] Cho HK. Optimization of dynamic behaviors of an orthotropic composite shell subjected to hygrothermal environment. *Finite Elements in Analysis and Design* 2009;45(11):852–60.
- [131] He Y. In-situ characterization of moisture absorption-desorption and hygroscopic swelling behavior of an underfill material. In: Electronic components and technology conference. 2011, p. 375 –86.
- [132] Vaddadi P, Nakamura T, Singh R. Inverse analysis to determine hygrothermal properties in fiber reinforced composites. *Journal of Composite Materials* 2007;41:309–34.
- [133] Chang TW, Tsai CL, Yeh W, Chang JJ. Tracking the moisture expansion of carbon/epoxy composite exposed to varying humidity. *Journal of Composite Materials* 2008;42(2):431–43.
- [134] Valery V. Vasiliev & Evgeny V. Morozov . *Advanced mechanics of composite materials*. 2007.
- [135] Mayugo JA. Proyecto: Ensayo Virtual y Supervisión Estructural de Revestimientos reforzados con larguerillos de fibra de carbono EVISER IF01, ref: TRA2006-15718-C02-01/TAIR. AMADE. Universitat de Girona. 2006-2009.

BIBLIOGRAPHY

- [136] ABAQUS version 6.9: ABAQUS User's Manual. SIMULIA World Headquarters, 166 Valley Street, Providence, RI 02909, USA; 2009.
- [137] Dávila CG, Camanho PP, Rose CA. Failure criteria for FRP laminates. *Journal of Composite Materials* 2005;39:323–45.
- [138] MIL-HDBK-17-3F (Military Handbook). Composite Materials Handbook: Polymer Matrix Composites Materials Usage, Design, and Analysis; vol. 3. Department of Defense of USA; 2002.
- [139] MATLAB. Using MATLAB manual. The Math Works Inc. Natick, MA; 1999.
- [140] Dennis Jr. JE, Schnabel RB. Numerical Methods for Unconstrained Optimization and Nonlinear Equations. SIAM, Philadelphia; 1983, 1996.
- [141] Deb K. Multi-objective optimization using evolutionary algorithms. John Wiley & Sons; 2001.
- [142] Rokbi M, Osmani H, Benseddiq N, Imad A. On experimental investigation of failure process of woven-fabric composites. *Composites Science and Technology* 2011;71(11):1375–84.
- [143] Boukhoulda BF, Adda-Bedia E, Madani K. The effect of fiber orientation angle in composite materials on moisture absorption and material degradation after hygrothermal ageing. *Composite Structures* 2006;74(4):406–18.
- [144] Press TNA, editor. Going to Extremes. Meeting the Emerging Demand for Durable Polymer Matrix Composites. Tech. Rep.; National Research Council of the National Academies.; 2005.
- [145] Upadhyay PC, Lyons DW, Wayne WS. Hygrothermal effect on the compressive strength of uniaxial fiber-reinforced polymer matrix composites. *Journal of Reinforced Plastics and Composites* 2009;28(21):2655–64.
- [146] Adams RD, Singh MM. The dynamic properties of fibre-reinforced polymers exposed to hot, wet conditions. *Composites Science and Technology* 1996;56(8):977–97.
- [147] Adams RD, Singh MM. Low temperature transitions in fibre reinforced polymers. *Composites - Part A: Applied Science and Manufacturing* 2001;32(6):797–814.
- [148] Russell AJ, Street KN. Moisture and temperature effects on the mode I and mode II interlaminar fracture of graphite/epoxy composites. *Mechanical and corrosion properties* 1989;37:199–208.
- [149] Bradley WL, Grant TS. The effect of the moisture absorption on the interfacial strength of polymeric matrix composites. *Journal of Material Science* 1995;5537–42.
- [150] Mandell JF, Grande DH, Tsiang T, McGarry FJ. Modified microbonding test for direct in situ fiber/matrix bond strength determination in fiber composites. *Composite Materials: Testing and Design* 1986;87–108.

BIBLIOGRAPHY

- [151] Hallett SR, Green BG, Jiang WG, Wisnom MR. An experimental and numerical investigation into the damage mechanisms in notched composites. *Composites Part A: Applied Science and Manufacturing* 2009;40(5):613–24.
- [152] ASTM E399-90, Standard Test Method for Plane-Strain Fracture Toughness of Metallic Materials, ASTM International, West Conshohocken, PA, www.astm.org. 1997.
- [153] Carbon fibre reinforced plastic; Unidirectional laminate tensile test perpendicular to the fibre direction, BS EN 2597:1998. 1998.
- [154] ASTM D3039 / D3039M-14, Standard Test Method for Tensile Properties of Polymer Matrix Composite Materials, ASTM International, West Conshohocken, PA, www.astm.org. 2014.
- [155] prEN 2823. Determination of the effect of exposure to humid atmosphere on physical and mechanical characteristics. Aerospace series. Fibre reinforced plastics. 1998.
- [156] Suo Z, Bao G, Fan B, Wang TC. Orthotropy rescaling and implications for fracture in composites. *International Journal of Solids and Structures* 1991;28(2):235–48.
- [157] Bao G, Ho S, Suo Z, Fan B. The role of material orthotropy in fracture specimens for composites. *International Journal of Solids and Structures* 1992;29(9):1105–16.
- [158] Bažant ZP, Kazemi MT. Size dependence of concrete fracture energy determined by RILEM work-of-fracture method. *International Journal of Fracture* 1991;51(2):121–38.
- [159] Bažant ZP, Gettu R, Kazemi MT. Identification of nonlinear fracture properties from size effect tests and structural analysis based on geometry-dependent R-curves. *International Journal of Rock Mechanics and Mining Sciences & Geomechanics Abstracts* 1991;28(1):43 – 51.
- [160] Underwood JH, Burch IA, Bandyopadhyay S. Effects of notched geometry and moisture on fracture strength of carbon/epoxy and carbon/bismaleimide laminates. US Army Amament Research. A development and engineering center; 1990.
- [161] Parvizi A, Garrett KW, Bailey JE. Constrained cracking in glass fibre-reinforced epoxy cross-ply laminates. *Journal of Materials Science* 1978;13(1):195–201.
- [162] Dvorak GJ, Laws N. Analysis of progressive matrix cracking in composite laminates-II. First Ply Failure. *Journal of Composite Materials* 1987;21(4):309–29.
- [163] EL-Dessouky HM, Lawrence CA. Ultra-lightweight carbon fibre/thermoplastic composite material using spread tow technology. *Composites Part B: Engineering* 2013;50(0):91 –7.
- [164] Baker A, Dutton S, Kelly D. *Composite materials for aircraft structures (2nd ed.)* American Institute of Aeronautics and Astronautics AIAA Inc., Roston, VA, USA. 2004.

BIBLIOGRAPHY

- [165] Camanho PP, Erçin GH, Catalanotti G, Mahdi S, Linde P. A finite fracture mechanics model for the prediction of the open-hole strength of composite laminates. *Composites Part A: Applied Science and Manufacturing* 2012;43(8):1219 –25.
- [166] Tada H, Paris PC, Irwin GR. *Stress analysis of cracks handbook*. Del Research Corporation; 1973.
- [167] Crossman FW, Wang ASD. The dependence of transverse cracking and delamination on ply thickness in graphite/epoxy laminates; vol. 775. *Damage Compos Mater, ASTM STP*; 1982.
- [168] Hallett SR, Jiang WG, Khan B, Wisnom MR. Modelling the interaction between matrix cracks and delamination damage in scaled quasi-isotropic specimens. *Composites Science and Technology* 2008;68(1):80 –9.
- [169] OBrien . *Analysis of local delaminations and their influence on composite laminate behaviour*. NASA Technical Memorandum. 1984.
- [170] Maimí P, Camanho PP, Mayugo JA, Turon A. Matrix cracking and delamination in laminated composites. Part II: Evolution of crack density and delamination. *Mechanics of Materials* 2011;43(4):194–211.
- [171] Zubillaga L, Turon A, Maimí P, Costa J, Mahdi S, Linde P. An energy based failure criterion for matrix crack induced delamination in laminated composite structures. *Composite Structures* 2014;112:339 –44.
- [172] Maimí P, Rodríguez H, Blanco N, Mayugo J. 7 - numerical modeling of matrix cracking and intralaminar failure in advanced composite materials. In: Hallett PPCR, editor. *Numerical Modelling of Failure in Advanced Composite Materials*. Woodhead Publishing Series in Composites Science and Engineering; Woodhead Publishing. ISBN 978-0-08-100332-9; 2015, p. 175 –92.

Part V

Appendices

A | Appendix

Published paper



Optimization of composite stiffened panels under mechanical and hygrothermal loads using neural networks and genetic algorithms

L. Marín^a, D. Trias^{a,*}, P. Badalló^a, G. Rus^b, J.A. Mayugo^a

^aAMADE, Dept. of Mechanical Engineering and Industrial Construction, Universitat de Girona, Campus Montilivi s/n, E-17071 Girona, Spain
^bDept. of Structural Mechanics, Universidad de Granada, Politécnico de Fuentenueva, E-18071 Granada, Spain

ARTICLE INFO

Article history:
 Available online 23 May 2012

Keywords:
 Multi-objective optimization
 Hygrothermal effects
 Stiffened panels
 Neural networks
 Genetic algorithms
 Finite element method

ABSTRACT

The present work develops an optimization procedure for a geometric design of a composite material stiffened panel with conventional stacking sequence using static analysis and hygrothermal effects. The procedure is based on a global approach strategy, composed by two steps: first, the response of the panel is obtained by a neural network system using the results of finite element analyses and, in a second step, a multi-objective optimization problem is solved using a genetic algorithm. The neural network implemented in the first step uses a sub-problem approach which allows to consider different temperature ranges. The compression load and relative humidity of the air are assumed to be constants throughout the considered temperature range.

The mass, the hygrothermal expansion and the stresses between the skin and the stiffeners are defined as the optimality criteria. The presented optimization procedure is shown to yield the optimal structure design without compromising the computational efficiency.

©2012 Elsevier Ltd. All rights reserved.

1. Introduction

Fibre reinforced polymer (FRP) composite materials have been used in the aerospace industry because of their high strength-to-weight and stiffness-to-weight ratios, and good behavior under elevated temperature environments. However, the major drawback of these materials is its high cost, so a suitable design and optimization process is essential in order to improve their structural behavior to cost ratio.

This has led several authors to study the optimization of composite panels, considering frequently as an objective the minimum mass, by geometric [1–3] and stacking sequence design [4–11]. On the other hand, these studies have focused on buckling or post-buckling dynamic analysis, without considering environmental effects. Nevertheless, these structures are exposed to extreme environmental conditions and some researchers have studied optimization problems of laminated composite plates with thermal effects to maximize the critical temperature capacity with uniform [12,13] or nonuniform temperature distribution [14]. In addition, Ijsselmuiden et al. [15] carried out a thermomechanical design optimization of composite panels and Cho [16] studied the hygrothermal effects in optimization problems of dynamic behavior, where temperature and moisture are assumed to be uniform once they have reached equilibrium.

Moisture and temperature changes affect the stiffness and strength of composites, and generate tensions between bonded sub-components. Their static and dynamic behaviors can depend significantly on such hygrothermal conditions. The combination of both phenomena is usually known as hot-wet (H/W) conditions. This state is characterized by moisture absorption by the matrix due its exposure to humid air and high temperature, which reduces the mechanical properties of the laminate. Additionally, this absorption causes a volume increase and consequently internal tensions between elements and interfaces. Experimental results show the influence of the temperature in moisture absorption [17–20], so this phenomenon should be analyzed for different thermal load cases and hygrothermal effects should be considered in any design and optimization process. On the other hand, Orifici et al. [21,22] analyzed the post-buckling failure of T-shaped stringers classifying in four failure modes: bend, blade, flange and core failure. The authors also found that delamination arises under the edges of stiffeners and the triangular resin-rich area.

The solution of the optimization problem is generally obtained with genetic algorithms (GAs) which have become one of the most employed solution method in engineering problems since they can handle integer, zero-one, discrete and continuous variables and are effective with nonlinear functions and non-convex design spaces. Due to this, both geometric and stacking sequence variables can be introduced. These methods are based on Darwin's theory of natural adaptation and biological evolution [23,24], which is translated into algorithmic terms through the computational

* Corresponding author.
 E-mail address: dani.trias@udg.edu (D. Trias).

operators of selection, crossover and mutation. In engineering applications, the evaluation of the objective function may be performed by means of an analytical function or, frequently, a numerical model (a finite element model, for instance). Since a large number of evaluations is generally required to obtain the optimal solution, the whole solution process implies a high computational cost. Some authors have used global approximation techniques to reduce function evaluation computational time by using data previously obtained with analytical or numerical methods. In this direction, Bisagni and Lanzi [25] developed an optimization procedure with a global approximation strategy based on obtaining the structure response by means of a system of artificial neural networks (ANNs) and GA. Lanzi et al. [26] performed a comparative study between three different global approximation techniques: ANN, kriging method and radial basis functions. All the techniques showed a similar behavior that the dynamic finite element (FE) analysis and computational time was satisfactorily reduced.

The aim of the present work is the definition of a fast multi-objective optimization procedure for the geometric design of stiffened panels under mechanical and hygrothermal loads, which minimizes the mass, the stresses between elements and the strain due to hygrothermal effects. The optimization problem is subject, in turn, to the corresponding constraints of tensions between stiffener-skin, provided by a failure criterion. The optimization procedure is carried out under different thermal load cases. A global approximation technique based on ANN is used to reduce computational cost.

This paper is structured as follows: firstly, in Section 2, a standard panel is analyzed to set up the model that will compute the objective functions and to define suitable constraints; the optimization process is described in Section 3; next, results are shown in Section 4 and finally, conclusions are presented in Section 5.

2. Definition of the multi-objective problem

2.1. Stiffened panel design

The considered structure is a compression loaded stiffened composite panel with three stringers, as shown in Fig. 1. This kind of panels represents a flat and partial idealization of the wings and fuselage structures of commercial aircrafts and so is frequently used in analysis and testing as a subcomponent. It is made of carbon fiber reinforced polymer (CFRP) and is symmetric in x-z and y-z planes. The stiffener sections are double-L shaped showing rounded corners with a mean radius of 4 mm for construction reasons. No run-outs are present. The different stacking sequences corresponding to each part of the geometry are shown in Fig. 1. Ply thickness is 0.184 mm. The specimen studied in this work is made with Hexcel T800/M21 prepreg ribbon of epoxy matrix rein-

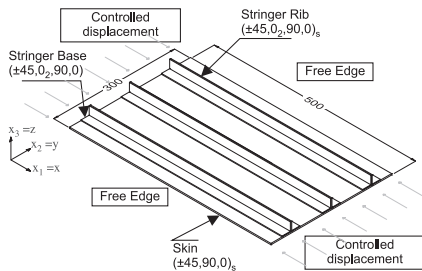


Fig. 1. Stiffened panel (dimensions in mm).

Table 1 T800/M21 UD CFRP properties[29].

Property	Value	Description
E_{xx} (GPa)	134.7	Young's modulus
$E_{yy} = E_{zz}$ (GPa)	7.7	
$\nu_{xy} = \nu_{xz}$	0.369	Poisson's ratio
ν_{yz}	0.5	
$G_{xy} = G_{xz}$ (GPa)	4.2	Shear modulus
G_{yz} (GPa)	2.5	
α_{xx} ($^{\circ}\text{C}^{-1}$)	-3.08×10^{-7}	Coefficient of thermal expansion ^a
$\alpha_{yy} = \alpha_{zz}$ ($^{\circ}\text{C}^{-1}$)	3.18×10^{-5}	
ρ (kg/m ³)	1590	Density
X_T (MPa)	2290.5	Longitudinal tensile strength
X_C (MPa)	1051	Longitudinal compression strength
Y_T (MPa)	41.43	Transverse tensile strength
Y_C (MPa)	210	Transverse compression strength
S_U (MPa)	69.4	Shear strength
S_{IS} (MPa)	106.48	Shear strength <i>in situ</i>
α ($^{\circ}$)	53.5	Transverse compression fracture angle
β	$5.10 \cdot 10^{-8}$	Shear response factor
g	0.5769	Toughness ratio (G_I/G_{II})

^a Values obtained using the relations described in [36].

Table 2 Geometric variables domain (mm).

Geometric variables: x	Lower bound: x ^(l)	Upper bound: x ^(u)
	20	30
	20	30
	70	110

forced with unidirectional carbon fibers. Its properties are shown in Table 1. The parametric analysis of the stiffened panel is performed in function of three geometric design variables $\mathbf{x} = (x_1, x_2, x_3)$ where x_1 is the stringer base width, x_2 is the stringer rib and x_3 is the distance between stringers with domains set forth in Table 2 and $\mathbf{x} \in \Omega_d$, where Ω_d is the decision space.

2.2. Model of the panel: finite element modeling

For the automatic parametric generation of panels, a python code is used together with the commercial software ABAQUS [27]. The stiffened panels are modeled by 4-node shells S4R, with six degree of freedom at each node, three integration points along the thickness for each ply. A compressive controlled displacement is applied to each transverse edge, while the longitudinal edges are free, as shown in Fig. 1. On the other hand, different temperature states are considered with a constant moisture.

The temperature and moisture are assumed to be in equilibrium state. The thermal strain is defined as $\epsilon^T = \alpha \Delta T$ and the moisture strain has been computed by the formulation proposed by Chang et al. [20] which considers the influence that temperature has in moisture strain for HTA1200A/ACD8801 material:

$$\epsilon^H = \frac{0.591R}{T+273} \tag{1}$$

where T is considered as the final temperature of the ΔT and R is the relative humidity. This approach is used for transverse and out-of-

Table 3
Loading conditions for each subproblem.

Subproblem (n)	Loading conditions	Thermal (T[°C])			
		Mechanical: compression controlled displacement	Moisture content (H[%])	T ₁ (y ₁) ^a	
				T _F ^b	ΔT(y ₂) ^c
SP1	1.9 mm	70	-55	120	175
SP2			20	120	100
SP3			70	90	20
SP4			20	-55	-75
SP5			70	20	-50
SP6			90	-55	-145
SP7			120	-70	-50

^a Initial temperature.
^b Final temperature.
^c Temperature variation.

plane direction, while the longitudinal moisture strain is considered negligible[28]. So the general form of stress–strain relationship for a transversely isotropic ply in which temperature and moisture effects are considered is $\epsilon^{Tot} = \epsilon^T + \epsilon^H + \epsilon$, where the components are:

$$\begin{Bmatrix} \epsilon_{xx}^{Tot} \\ \epsilon_{yy}^{Tot} \\ \epsilon_{zz}^{Tot} \end{Bmatrix} = \begin{Bmatrix} \alpha_{xx} \\ \alpha_{yy} \\ \alpha_{zz} \end{Bmatrix} \Delta T + \begin{Bmatrix} \approx 0 \\ \frac{0.591R}{T+273} \\ \frac{0.591R}{T+273} \end{Bmatrix} + \begin{Bmatrix} \epsilon_{xx} \\ \epsilon_{yy} \\ \epsilon_{zz} \end{Bmatrix} \quad (2)$$

A standard stiffened-panel, analyzed in a previous project [29], is taken as the reference panel with the following dimensions: $x_1 = 24$ mm, $x_2 = 24$ mm and $x_3 = 100$ mm. The behavior of the reference panel under different compressive and hygrothermal loads is studied in depth, using LaRC-03 failure criterion [30], which defines the following variables: failure indexes for transverse tensile failure (F_{TT}), transverse compressive failure (F_{TC}), longitudinal tensile failure (F_{LT}), and longitudinal compression failure (F_{LC}).

For temperature rising cases, the strains in the perpendicular direction are higher than the temperature decreasing cases, and localized in the stiffener bases, so the tensions between stringers and skin also increase. However, F_{TC} and F_{LC} indicate that the panel is capable of supporting larger temperature increases without breaking up to 1.45 mm compressive controlled displacement.

For decreasing thermal variations, the panel shows lower tensions, breaking with variations between -50° and -125° and compressive moderated displacement, depending on the final temperature. In these cases, F_{TT} and F_{LC} are the most important failure indexes. The interaction between moisture and thermal effects helps to the behavior of the panel but the matrix is damaged after the moisture absorption. Different environmental conditions with decreasing and rising thermal variations have been considered in the optimization problem.

2.3. Definition of subproblems

The behavior of the panel under a wide range of temperatures leading to different failure modes is analyzed. For this purpose, the initial problem has been decomposed into seven sub-problems so that, for each one, different ranges of temperature are considered. Initial temperatures correspond to the most significant values used in experimental analysis (generally -55° C, ambient temperature, 70° C, 90° C and 120° C) and temperature variations are chosen by the most important cases within the considered temperature range from -55° to 120° [31], where the minimum and the maximum service temperature commercial transport aircraft are considered as -54° C and 71° C respectively and the design ultimate loads at temperature up during takeoff and landing is 93° C; the temperatures higher than 100° C are considered only for special cases, such as supersonic transport, fighter, and bomber

aircraft. So the different subproblems described in Table 3 were considered. The variables T_1 (initial temperature) and ΔT (temperature variation) form the vectors $\mathbf{y}_n = (y_{1n}, y_{2n})$ whereas n is the number of each subproblem.

2.4. Formulation of the multi-objective optimization problem

A multi-objective problem is established, which seeks to minimize the weight of the panel $f_1(\mathbf{x}, \mathbf{y}_n)$, the local strain in direction perpendicular $f_2(\mathbf{x}, \mathbf{y}_n)$ and the tension between skin and stiffeners $f_3(\mathbf{x}, \mathbf{y}_n)$. All three objective functions are considered to be equally important.

In this way, the optimization problem can be formulated as:

$$\begin{aligned} &\text{Minimize } Y(f_1(\mathbf{x}, \mathbf{y}_n), f_2(\mathbf{x}, \mathbf{y}_n), f_3(\mathbf{x}, \mathbf{y}_n)) \quad Y \in \Omega_o \\ &\text{Subject to } \quad g_k(\mathbf{x}, \mathbf{y}_n) > 0 \quad k=1,2 \\ &\quad \quad \quad x_j^{(l)} \leq x_j \leq x_j^{(u)} \quad (3) \\ &\text{where } \quad \mathbf{y}_n = (y_{1n}, y_{2n}) \\ &\quad \quad \quad \mathbf{x} = (x_1, x_2, x_3) \end{aligned}$$

where Ω_o is the objective space. The constraints $g_k(\mathbf{x}, \mathbf{y}_n)$ are defined as:

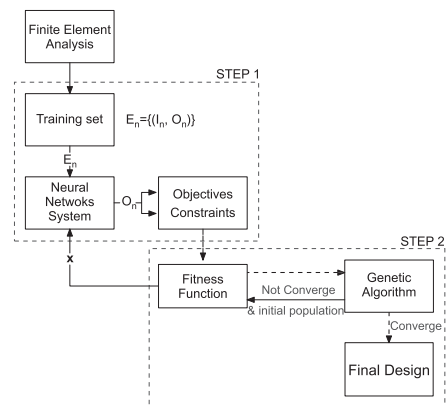


Fig. 2. Optimization scheme.

$$\begin{aligned}
 g_1(\mathbf{x}, \mathbf{y}_n) &= 1 - Fl_{TC}(\mathbf{x}, \mathbf{y}_n) \quad \text{if } \Delta T > 0, & g_1(\mathbf{x}, \mathbf{y}_n) &= 1 - Fl_{TT}(\mathbf{x}, \mathbf{y}_n) \quad \text{if } \Delta T < 0 \\
 g_2(\mathbf{x}, \mathbf{y}_n) &= 1 - Fl_{LC}(\mathbf{x}, \mathbf{y}_n) & g_2(\mathbf{x}, \mathbf{y}_n) &= 1 - Fl_{LC}(\mathbf{x}, \mathbf{y}_n)
 \end{aligned}
 \tag{4}$$

3. Optimization procedure

The solution of the problem, displayed in Eqs. (3) and (4), implies a high computational cost for the optimization process since the values of the objective functions and the constraints are obtained from a parametrized FE model. For this reason, the procedure shown in Fig. 2 based on a global approximation technique is used to reduce the computational time. This procedure is composed by two steps:

1. A system of ANN that is partially capable to reproduce the solution of the FE model is developed. To the seven inputs corresponding to each subproblem $E_n(I_n)$ it delivers the different outputs composed of the objectives and constraints $E_n(O_n)$.
2. A GA obtains to get the optimal value for the design variables previously described.

3.1. Model of the panel: neural network modeling

An ANN is a system used for information processing whose basic unit is inspired by the fundamental cell of the human nervous system: the neuron. This system is capable of acquiring knowledge and resolve situations that cannot be expressed mathematically by the experience [32].

The ANN needs a learning process and a training set, composed of input–output patterns, as known examples. The input signals of an artificial neuron are continuous variables instead of discrete pulses, as presented in a biological neuron. Each input signal passes through a *weight* or *gain*, known as *synaptic weight* or strength of the connection whose function is analogous to the *synaptic function* of the biological neuron. An other term, called *bias*, supposes a reinforcement of these connections. The summation node accumulates all input signals multiplied by the weights and bias and output passes through a *transfer function* or, where appropriate, *activation function*. The result of this sum is known as *propagation function*, which obtains the output vector.

A commercial software, MATLAB [33], was applied for developing an ANN procedure that includes the following process:

- (a) *Choice of data set.* The training data set is composed by seven subsets that correspond to the different sub-problems displayed in Table 3. The set consists of an input–output

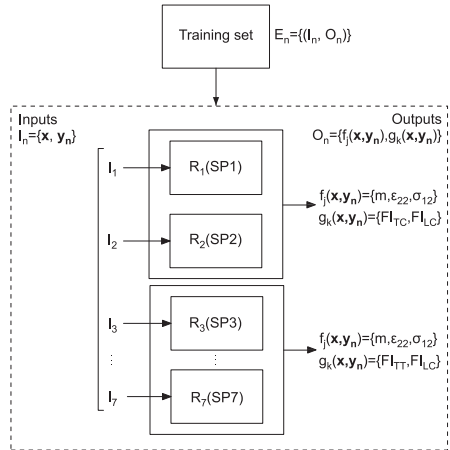


Fig. 3. Neural network scheme.

pattern-pairs obtained through FE analysis. The input pattern forms a vector I_n , composed of the geometrical parameters x and the vector y_n , and the output pattern O_n , composed of the corresponding responses of the panel for each sub-problem (objectives and constraints).

- (b) *Architecture of the ANN.* The complexity of the problem is solved by using by a suitable architecture to implement the information of the input–output pattern for each sub-problems discussed that, once inside the network will be merged.

This architecture, shown in Fig. 3, is defined by multilayer perceptron (MLP) that consists of an input layer with a vector dimensions I_n , two hidden layers with *competantansig* functions as *activation* and *transfer functions* respectively, and Levenberg–Marquardt [34] backpropagation learning rule and an output layer, with *tansig* function, that obtains the vector O_n , calculated from the bias and weights are adapted after training in the network.

- (c) *Training of the ANN.* The ANN is taught to form the relationship between input and output variables by the training data set of known input–output patterns. This set is composed by

Table 4 Objectives and constraints values for each subproblem. Bold values denote relevant results discussed in the text and Table 5.

	Method	SP1	SP2	SP3	SP4	SP5	SP6	SP7
Objectives	m (g)	378	378	378	378	378	378	378
	σ_{xy} (MPa)	FE Analysis 32.84	28.79	25.43	24.85	23.90	22.08	22.49
	NN System	33.15	29.89	26.50	24.66	24.16	21.80	22.05
	Error (%)	0.9	3.1	4.2	0.7	1.1	1.2	1.9
	ϵ_{yy}	FE Analysis 4.76	4.46	4.24	4.23	4.22	4.22	4.21
	NN System	4.78	4.57	4.16	4.17	4.17	4.35	4.23
	Error (%)	0.4	2.5	1.9	1.4	1.2	3.0	0.5
Constraints	Fl_{TT}	FE Analysis –	–	–	0.32	0.42	0.948	0.784
	NN System	–	–	–	0.31	0.45	0.93	0.81
	Error (%)	–	–	–	6	7.1	1.9	3.3
	Fl_{LC}	FE Analysis 0.996	0.64	0.61	0.58	0.47	0.996	0.87
	NN System	0.97	0.68	0.65	0.54	0.49	0.98	0.89
	Error (%)	2.6	6.2	6.5	6.9	4.2	1.6	2.3
	Fl_{TC}	FE Analysis 0.978	0.80	0.36	–	–	–	–
	NN System	0.98	0.82	0.38	–	–	–	–
	Error (%)	0.2	2.5	5.6	–	–	–	–

Table 5
Comparison of the reference and optimal panels for the most restrictive subproblems.

Objectives		Panel	SP1	SP3	SP6
m (g)	Reference panel		379	379	379
	Optimum panel		378	378	378
	Reduction (%)		0.54	0.54	0.54
σ_{xy} (MPa)	Reference panel		35.52	27.06	23.24
	Optimum panel		32.84	25.43	22.08
	Reduction (%)		7.55	6.02	4.99
ϵ_{yy}	Reference panel		5.09	4.46	4.37
	Optimum panel		4.76	4.24	4.22
	Reduction (%)		6.48	4.93	3.43

the response of 120 FE analysis for each sub-problem to achieve a good performance of the system. A data processing MSE of about 10^{-4} is obtained.

3.2. Genetic algorithm

A variant of the algorithm Non-dominated Sorting Genetic Algorithm II (NSGA-II) [35] is used to solve the formulated problem by the Toolbox for Matlab (Global Optimization). It is one of the results of the evolution of the GA and is based on the application of elitism preserving the use of Pareto front. This elitism is controlled by two options: the *Pareto fraction* and *crowding distance measure* functions. The first, limits the number of individuals on the Pareto front and the distance function helps to maintain diversity on a front by favoring individuals that are relatively far away on the front.

The fitness function, which measures the genetic informations of each individual, is composed of the different objectives and the constraints. A penalty method is used to describe the

constraints, reported in Eq. (4). The individuals with better characteristics survive during the evaluation process.

The genetic search is performed with a population size of 75 members, generated randomly, with a 'genotype' function as crowding distance measure and the value of the Pareto fraction is set as 0.5.

4. Results and discussion

The GA converged after 33 generations and required 1701 fitness function evaluations. A considerable reduction of the computational cost is achieved with the optimization procedure proposed. In fact, to obtain the optimal configuration, 120 FE analysis for each subproblem were performed in a total computational time of about 35 h. The used computer is a DELL Precision T1500 with an Intel® Core™ i5 CPU with 2.67 GHz, 4 GB of RAM, Windows 7 x64 Edition. The CPU time required by the ANN training process was approximately 25 min, while the computational cost for optimization was about 8 min. However, a direct optimization using GA coupled with FE analysis supposes about 1701 different simulations for each subproblem, which means roughly 500 h of computational time.

The optimal panel has been selected between all those solutions of the Pareto front such as each objective function has the same weight. This panel is characterized by a mass of 378 g and the following dimensions: $x_1 = 26.397$ mm, $x_2 = 21.404$ mm and $x_3 = 90.23$ mm.

The solution obtained using the ANN modeling is compared with the FE modeling for each subproblem as shown in Table 4.

In turn, all the failure indexes of LaRC criterion are verified to be lower than 1. For this parameters, the most restrictive problems have been the SP1 for temperature increase and SP3 and SP6 for temperature decrease. In comparison with the reference panel,

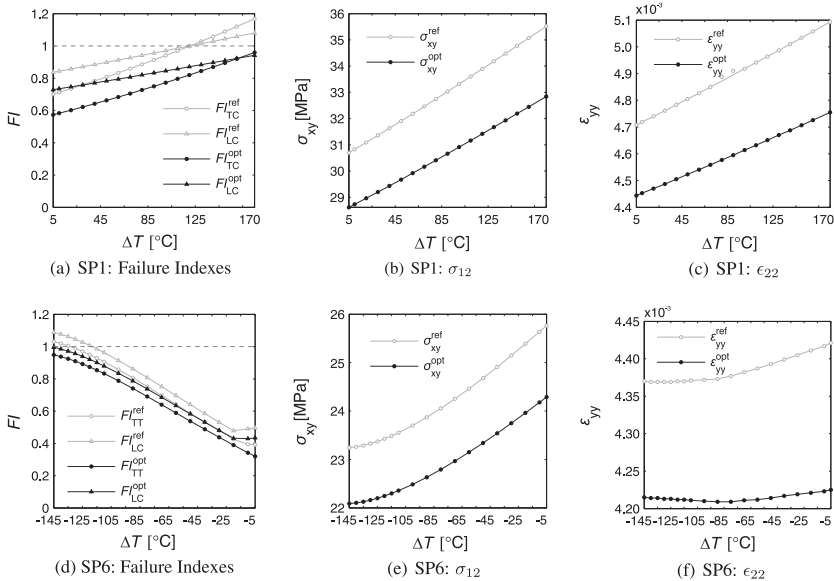


Fig. 4. Comparison between reference and optimal panels.

the reduction in mass is 0.54%, and the hygrothermal strain and the tensions between the stiffeners and the skin are reduced about 6.48–3.43% and 7.55–4.99% respectively depending on the sub-problem (Table 5).

Positive and negative temperature increments of five degrees are considered for each interval in Fig. 4, where the comparison between these panels is shown for the extreme temperature cases. In both cases, the reference panel breaks as failure indexes values indicate in Fig. 4a and d while the optimal panel shows a good performance and the strain and the tension between the stiffeners and the skin are considerably reduced.

5. Conclusions

An optimization procedure for stiffened panels under mechanical and hygrothermal loads has been developed. This procedure consists of the interaction between an ANN system and a GA with the purpose of reducing the computational cost that could reach a direct optimization using FE analysis to obtain the response of the panel. For the correct definition of the optimization problem, the behavior of a reference panel has been analyzed by means of FE with the aim of selecting the most significant objectives and constraints for the possible load states.

A set of seven subproblems characterized by different temperature ranges and moisture presence was considered in the optimization procedure. This decomposition of the initial problem in several subproblems helps to analyze the hygrothermal effects with negative or positive thermal variations and to find the optimal panel for the maximum number of load cases at which these structural elements can be subject. However, the implementation of different subproblems increases the computational cost in the optimization problem.

The use of ANN systems can increase the speed of the optimization processes, reducing the computational cost about 92.8%. The drawback of these tools is the time required to design its architecture to obtain the suitable learning, which can be higher in specific terms and affect the optimization results. However, comparing the optimal panel behavior calculated with FE analysis and ANN system, it can be observed that is suitable for all subproblems and is able to reduce the several objectives satisfying the considered constraints. Comparing the optimal and reference panels, the mass is reduced about 0.54% and the hygrothermal strain and tension between stringers and skin are decreased until 6.48% and 7.55% respectively in specific load cases.

In conclusion, ANN and GA reduce the computational cost with suitable accuracy and can help to implement several load states to minimize the global problem. These tools can be used in engineering applications with a unique or various ANN systems. On the other hand, to reduce the time required to train the ANN and replace the problematic trial-and-error approach, a GA system could be used to find the optimal internal architecture.

Acknowledgments

The authors acknowledge the financial support of the Spanish Government under the Project DPI2009-08048. The first author would like to thank Spanish Government for the FPI pre-doctoral Grant BES-2010-042387.

References

- [1] Kaufmann M, Zenkert D, Mattei C. Cost optimization of composite aircraft structures including variable laminate qualities. *Compos Sci Technol* 2008;68(13):2748–54.
- [2] Rikards R, Abramovich H, Kalnins K, Auzins J. Surrogate modeling in design optimization of stiffened composite shells. *Compos Struct* 2006;73(2):244–51.
- [3] Badran SF, Nassef AO, Metwalli SM. Y-stiffened panel multi-objective optimization using genetic algorithm. *Thin Wall Struct* 2009;47(11):1331–42.
- [4] Irisarri FX, Bassir DH, Carrere N, Maire JF. Multiobjective stacking sequence optimization for laminated composite structures. *Compos Sci Technol* 2009;69(7–8):983–90.
- [5] Irisarri FX, Laurin F, Leroy FH, Maire JF. Computational strategy for multiobjective optimization of composite stiffened panels. *Compos Struct* 2011;93(3):1158–67.
- [6] Todoroki A, Ishikawa T. Design of experiments for stacking sequence optimizations with genetic algorithm using response surface approximation. *Compos Struct* 2004;64(3–4):349–57.
- [7] Todoroki A, Sekishiro M. Stacking sequence optimization to maximize the buckling load of blade-stiffened panels with strength constraints using the iterative fractal branch and bound method. *Compos Part B: Eng* 2008;39(5):842–50.
- [8] Todoroki A, Sekishiro M. New iteration fractal branch and bound method for stacking sequence optimizations of multiple laminates. *Compos Struct* 2007;81(3):419–26.
- [9] Wang W, Guo S, Chang N, Yang W. Optimum buckling design of composite stiffened panels using ant colony algorithm. *Compos Struct* 2010;92(3):712–9.
- [10] Gigliotti M, Riccio A, Tuspa L, Scaramuzzino F, Mormile L. Weight optimisation of damage resistant composite panels with a posteriori cost evaluation. *Compos Struct* 2009;88(2):312–22.
- [11] Nagendra S, Jestin D, Gürdal Z, Hafika RT, Watson LT. Improved genetic algorithm for the design of stiffened composite panels. *Comput Struct* 1996;58(3):543–55.
- [12] de Faria A, de Almeida S. Buckling optimization of plates with variable thickness subjected to nonuniform uncertain loads. *Int J Solids Struct* 2003;40(15):3955–66.
- [13] Topal U, Uzman U. Thermal buckling load optimization of laminated composite plates. *Thin Wall Struct* 2008;46(6):667–75.
- [14] Young-Shin L, Yeol-Wha L, Myung-Seog Y, Bock-Sun P. Optimal design of thick laminated for maximum thermal buckling load. *J Therm Stresses* 1999;22(3):259–73.
- [15] Jisselmuiden ST, Abdalla M, Gürdal Z. Thermomechanical design optimization of variable stiffness composite panels for buckling. *J Therm Stresses* 2010;33(10):977–92.
- [16] Cho HK. Optimization of dynamic behaviors of an orthotropic composite shell subjected to hygrothermal environment. *Finite Elem Anal Des* 2009;45(11):852–60.
- [17] Boukhoulda BF, Adfa-Bedia E, Madani K. The effect of fiber orientation angle in composite materials on moisture absorption and material degradation after hygrothermal ageing. *Compos Struct* 2006;74(4):406–18.
- [18] He Y. In-situ characterization of moisture absorption-desorption and hygroscopic swelling behavior of an underfill material. In: *Electronic components and technology conference*; 2011. p. 375–86.
- [19] Vaddadi P, Nakamura T, Singh R. Inverse analysis to determine hygrothermal properties in fiber reinforced composites. *J Compos Mater* 2007;41:309–34.
- [20] Chang TW, Tsai CL, Yeh W, Chang JJ. Tracking the moisture expansion of carbon/epoxy composite exposed to varying humidity. *J Compos Mater* 2008;42(2):431–43.
- [21] Orifici AC, Thomson RS, Herszberg I, Weller T, Degenhardt R, Bayandor J. An analysis methodology for failure in postbuckling skin-stiffener interfaces. *Compos Struct* 2008;86(1–3):186–93.
- [22] Orifici AC, Shah SA, Herszberg I, Kotler A, Weller T. Failure analysis in postbuckled composite T-sections. *Compos Struct* 2008;86(1–3):146–53.
- [23] Holland J. *Adaptation in natural and artificial systems: an introductory analysis with applications to biology, control, and artificial intelligence*. MIT Press; 1975.
- [24] Goldberg DE. *Genetic algorithms in search, optimization and machine learning*. Addison-Wesley Pub. Co.; 1989.
- [25] Bisagni C, Lanzi L. Post-buckling optimisation of composite stiffened panels using neural networks. *Compos Struct* 2002;58(2):237–47.
- [26] Lanzi L, Bisagni C, Ricci S. Neural network systems to reproduce crash behavior of structural components. *Comput Struct* 2004;82(1):93–108.
- [27] ABAQUS version 6.9: ABAQUS User's manual. SIMULIA World Headquarters, 166 Valley Street, Providence, RI 02909, USA; 2009.
- [28] Barbero EJ. *Introduction to composite materials design*. 2nd ed. CRC Press. Taylor & Francis Group; 2011.
- [29] Mayugo JA. Proyecto: ensayo virtual y supervisión estructural de revestimientos reforzados con largueros de fibra de carbono EVISER FT-01, ref: TRA2006-15718-CO2-01/TAIR. AMADE. Universitat de Girona; 2006–2009.
- [30] Dávila CG, Camanho PP, Rose CA. Failure criteria for FRP laminates. *J Compos Mater* 2005;39:323–45.
- [31] MIL-HDBK-17-3F (Military Handbook). Composite materials handbook: polymer matrix composites materials usage, design, and analysis, vol. 3. Department of Defense of USA; 2002.
- [32] Müller B, Reinhardt J. *Neural networks. An introduction*. Berlin Heidelberg New York: Springer-Verlag; 1995.
- [33] MATLAB. *Using MATLAB manual*. The Math Works Inc. Natick, MA; 1999.
- [34] Dennis Jr JE, Schnabel RB. *Numerical methods for unconstrained optimization and nonlinear equations*. SIAM, Philadelphia; 1983.
- [35] Deb K. *Multi-objective optimization using evolutionary algorithms*. John Wiley & Sons; 2001.
- [36] Valery V Vasiliev, Evgeny V Morozov. *Advanced mechanics of composite materials*; 2007.